REPORT No. 51

ASYMMETRIC INLET FLOW IN AXIAL TURBO MACHINES

BARRY S. SEIDEL

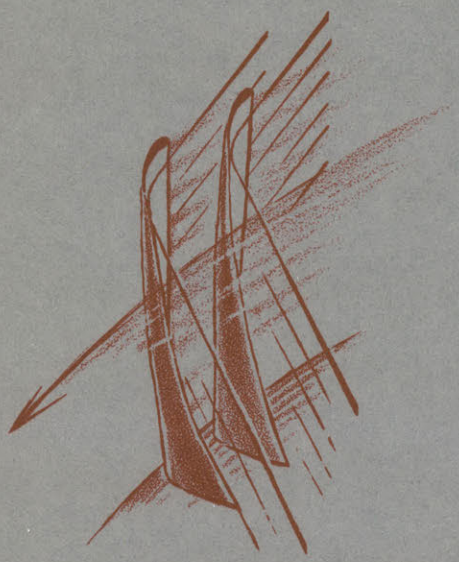

May 1959

GAS TURBINE LABORATORY
MASSACHUSETTS INSTITUTE OF TECHNOLOGY
CAMBRIDGE · 39 · MASSACHUSETTS

ASYMMETRIC INLET FLOW IN AXIAL TURBOMACHINES

by

BARRY S. SEIDEL

Under the Sponsorship of:

General Electric Company
Westinghouse Electric Corporation
Allison Division of General Motors Corporation

Gas Turbine Laboratory
Report Number 51

May 1959

Massachusetts Institute of Technology

TABLE OF CONTENTS

ACKNOWLEDGMENTS

The author expresses his gratitude to the staff of the Gas Turbine Laboratory. Professor E. S. Taylor, Director, continually brought the major issues into focus. Professor Alan H. Stenning served as thesis supervisor and guided the early part of the work until his departure to the Nuclear Engineering Department. Professor Yasutoshi Senoo then became thesis supervisor. Professors James W. Daily and Alve J. Erickson served on the thesis committee. Their continual guidance and suggestions are indeed appreciated. Also, helpful discussions on the problem were held with Dr. F. Ehrich (General Electric Co.) and with Professors H. Emmons and C. C. Lin.

For providing experimental information on this problem, the author thanks Lieut. (U.S.N.) Frank Carter, Joseph Jennings and Captain (U.S.M.C.) Marvin S. Shinbaum, who also lent valuable assistance in other phases of the report. Messrs. Dalton Baugh, Basil Kean and Paul Wassmouth aided in the use of the laboratory equipment and provided precision mechanisms and probes. In computation and graph preparation the author was aided by Messrs. James Brown, Charles Haspel, and James Hurley.

This work was done in part at the M. I. T. Computation Center, Cambridge, Massachusetts. The author is grateful for the use of the IBM 704 Electronic Data Processing Machine.

Typing was ably performed by Natalie Appleton.

Finally the author is grateful to his family and especially his wife for providing assistance of every description.

ABSTRACT

A modified actuator disc analysis is made which, through an improved prediction of the blade forces, attempts to give closer correspondence with experiment than the previous theory. The fluid is assumed inviscid and incompressible. Perturbations to the two-dimensional flow through an isolated blade row are considered. The steady flow equations of motion and continuity are linearized.

According to experiments conducted on an isolated compressor rotor, the present theory offers an improvement, compared to previous theory, in the prediction of distortion attenuation, effects of flow rate, and effects of varying chord/spacing ratio.

ASYMMETRIC INLET FLOW IN AXIAL TURBOMACHINES

1. INTRODUCTION

The problem of asymmetric inlet flow, or circumferential distortion, in axial turbomachines is quite simply stated. The velocity of the flow far upstream of any blade row may in general vary with the radius r, the angle θ, and even with time t. Because in the 'normal' (classical potential flow through cascades) situation the velocity far upstream is r-θ-t independent, the flow in problems in which one of these variables assumes a non-trivial role is spoken of as 'distorted'. In the asymmetric inlet flow problem here considered, θ-dependency alone is studied. The problem is thus: given the properties of the inlet flow (as a function of θ) and the characteristics of the blade row (s), to determine the properties of the fluid everywhere in space.

In the actual turbomachine these distortions may occur when the engine is operated at an off-design condition, when the aircraft is flown at high angles of attack, or when the flow is turned or diffused too rapidly within the intake duct.

In the solution to the problem one would also like to know the perturbations in blade force from their mean value (and how to minimize them), the attenuation of the distortion through the blade row (and how to maximize this quantity) and the overall effects on compressor performance.

Linearized actuator disc solutions to this problem have been presented by Ehrich (1) and by Rannie and Marble (6). Ehrich has assumed that

the relative angle of the flow leaving the rotor is constant and that there are no losses in the flow relative to the rotor. Rannie and Marble have generalized to allow both of these quantities to be functions of the relative inlet angle to the blade row. Ehrich's theory is for an isolated cascade; Rannie and Marble also treat finitely spaced blade rows. Although these two theories utilize completely different mathematical techniques they do give the same result for the conditions of isolated cascade, no losses, constant relative leaving angle. Indeed they must give the same result, by the uniqueness principle. Since the conditions mentioned are used throughout this report in computing the predictions of the previous theory, in this sense we have only to acknowledge the existence of a single previous theory. The mathematical technique of Rannie-Marble has been used throughout and hence the previous theory is labelled "Rannie-Marble". It is understood that Ehrich gives the same prediction.

2. ANALYSIS

2.1 Description of the Flow Field and Governing Equations

Let x, y be rectangular coordinates with the axis of y parallel to the plane of the cascade, Figure 1. The average velocity components and pressure of the undisturbed uniform flow are U, V and P, constant upstream and downstream respectively. The circumferentially distorted flow is represented by superposing a disturbance flow on the uniform flow. The disturbance velocity components and the disturbance pressure are u, v, p, all with space average values zero. The disturbance is assumed to be periodic in y direction. The disturbance flow treated here is due to non-uniform upstream flow and its interaction with the cascade as a whole; local disturbances due to individual blades are not considered. Thus, as will subsequently be seen, one may consider this to be a "modified" actuator disc analysis. The fluid is assumed inviscid and incompressible; the flow field is considered two-dimensional.

Under these circumstances, the equations of motion and continuity in linearized form are

$$U\frac{\partial u}{\partial x} + V\frac{\partial u}{\partial y} = -\frac{1}{\rho}\frac{\partial p}{\partial x} \qquad 1$$

$$U\frac{\partial v}{\partial x} + V\frac{\partial v}{\partial y} = -\frac{1}{\rho}\frac{\partial p}{\partial y} \qquad 2$$

$$\frac{\partial u}{\partial x} + \frac{\partial v}{\partial y} = 0 \qquad 3$$

In the place of these familiar equations we choose to use the following three, completely equivalent equations:

$$\left(U\frac{\partial}{\partial x}+V\frac{\partial}{\partial y}\right)\left(\frac{p}{\rho}+Uu+Vv\right)=0 \qquad 4$$

$$\frac{\partial}{\partial y}(Uv-Vu)=\frac{\partial}{\partial x}\left(\frac{p}{\rho}\right) \qquad 5$$

$$\frac{\partial}{\partial x}(Uv-Vu)=-\frac{\partial}{\partial y}\left(\frac{p}{\rho}\right) \qquad 6$$

Equation 4 is simply the condition that the perturbation in total pressure is constant along the mean streamlines. Equations (5) and (6) show that the combination Uv - Vu (proportional to flow angle perturbation) and the static pressure divided by density satisfy the Cauchy-Riemann conditions. It is convenient to introduce the definitions

$$H=p/\rho+Uu+Vv \qquad 7$$

$$\Theta=Uv-Vu \qquad 8$$

$$P=p/\rho \qquad 9$$

the following relations then hold

$$H(x,y)=H\left(0,y-\frac{V}{U}x\right) \qquad 10$$

$$\frac{\partial\Theta}{\partial y}=\frac{\partial P}{\partial x} \qquad 11$$

$$\frac{\partial\Theta}{\partial x}=-\frac{\partial P}{\partial y} \qquad 12$$

The establishment of equations (11) and (12) constitute a major step toward the solution, for now, all of the power of potential theory can be brought to bear, at least on Θ and Φ . We are able to use potential theory, not on u and v (since the flow is not irrotational), but on two other functions (Θ , Φ) of the physical variables, u, v, p.

A particularly useful example of the functional relationship between Θ and Φ is developed in Appendix I*. Consistent with our assumption of an isolated blade row lying along the y axis, it is there shown that for $\Theta(0, y)$ given, $\Phi(0, y)$ can then be found from

$$\Phi(0+,y) = \int_0^1 \Theta(0+,\eta)\cot\pi(y-\eta)\,d\eta = \Theta^*(0+,y) \qquad 13$$

$$\Phi(0-,y) = -\int_0^1 \Theta(0-,\eta)\cot\pi(y-\eta)\,d\eta = -\Theta^*(0-,y) \qquad 14$$

similarly

$$\Theta(0+,y) = -\Phi^*(0+,y)$$

$$\Theta(0-,y) = \Phi^*(0-,y)$$

---

*The correspondence between this appendix and the main body of the text is as follows:

Text	Appendix
Θ	u
Φ	v
x	x
y	y

Since Θ and Φ satisfy the Cauchy-Riemann conditions, they may be found for all values of x and y if the boundary values $\Theta(o, y)$ or $\Phi(o, y)$ along the blade row are given. Finally, in order to relate Θ or Φ to u and v, $H(x, y) = H(o, y - \frac{V}{U} x)$ must be known.

2.2 Boundary Conditions at the Blade Row

(a) Axial Velocity Match Condition

Since we are neglecting any change in density through the blade row, and the annulus area is constant, the axial velocity entering the blade row must equal the axial velocity leaving the blade row. Letting station 1 represent the line x = 0-(just upstream of the cascade) and station 2 the line x = 0+(just downstream of the cascade) we have then that

$$U_1 + u_1 = U_2 + u_2$$

Obviously, the average axial velocities are the same upstream and downstream and so we have simply that

$$u(0-, y) = u(0+, y)$$

or

$$u_1 = u_2 \qquad 15$$

(b) Quasi-Steady Bernoulli Equation; Relative to the Rotor

We define a loss coefficient $C_D(\beta_1)$ such that the Bernoulli equation for the mean flow may be written

$$P_1 + \tfrac{1}{2}\rho[U^2 + (V_1 - \Omega r)^2] = P_2 + \tfrac{1}{2}\rho[U^2 + (V_2 - \Omega r)^2] + \tfrac{1}{2}\rho \frac{U^2 C_D}{\cos^2 \beta_{mean}}$$

Then the condition for the perturbed flow, obtained by taking the differential of the previous equation,

$$p_1 + \rho U u_1 + \rho(V_1 - \Omega r) v_1 = p_2 + \rho U u_2 + \rho(V_2 - \Omega r) v_2 + \frac{\rho U C_D u_1}{\cos^2 \beta_m} + \rho \frac{U^2}{2} \sec^2 \beta_1 \frac{C_D'}{\cos^2 \beta_m} \Delta \beta_1 \qquad 16$$

Also, since $\tan A - \tan B = \dfrac{\sin(A-B)}{\cos A \cos B}$

$$\Delta \tan\beta = \frac{\Delta\beta}{\cos^2\beta}$$

Alternatively,

$$\Delta \tan\beta = \Delta\left(\frac{\Omega r - V}{U}\right) = \frac{U(-v) - (\Omega r - V)\mu}{U^2} = -\frac{\textcircled{H} + \Omega r \mu}{U^2}$$

$$\therefore \Delta\beta = -\frac{\cos^2\beta}{U^2}(\textcircled{H} + \Omega r \mu)$$

Now we may rewrite (16),

$$\frac{p_1}{\rho} + (V_1 - \Omega r)v_1 = \frac{p_2}{\rho} + (V_2 - \Omega r)v_2 + U\mu_1 \frac{C_D}{\cos^2\beta_m} - \frac{C_D'}{2}(\textcircled{H}_1 + \Omega r \mu_1)\frac{1}{\cos^2\beta_m} \qquad 16a$$

(c) Prescription of the Blade Force

The force parallel to the blade row corresponding to the mean flow is

$$-\mathcal{F}_y = \rho S U (V_1 - V_2) \qquad 17$$

when the inlet flow has a distortion, this force is composed of a mean value $-\mathcal{F}_y$ plus a variable component, $-\Delta\mathcal{F}_y$. The variable component, obtained by taking the differential of the previous equation is

$$-\frac{\Delta\mathcal{F}_y}{\rho S} = U(v_1 - v_2) + \mu(V_1 - V_2) \qquad 18$$

2.3 Translation of Boundary Condition to Relations in H, β, Θ

We now require these matching conditions in terms of the functions Θ, β, H

Equation (15) becomes (Appendix II)

$$\zeta_1^\rho (H_2 - \beta_2) - \zeta_2^\rho \Theta_2 = \zeta_3^\rho (H_1 - \beta_1) - \zeta_4^\rho \Theta_1 \qquad 19$$

The ζ^ρ's are known constants.

Equation (16a) becomes

$$\beta_1 + \zeta_{26}^\rho (H_1 - \beta_1) + \zeta_{27}^\rho \Theta_1 = \beta_2 + \zeta_7^\rho (H_2 - \beta_2) + \zeta_8^\rho \Theta_2 \qquad 20$$

Again, the ζ^ρ's are known constants.

Equation (18) becomes

$$-\frac{\Delta \mathcal{F}_Y}{\rho S} = \Theta_1 - \Theta_2 + 2\cos^2\theta_1 (\tan\theta_1 - \tan\theta_2)(H_1 - \beta_1 - \Theta_1 \tan\theta_1) \qquad 21$$

or letting

$$\zeta_9^\rho = 2\cos^2\theta_1 (\tan\theta_1 - \tan\theta_2)$$

$$\zeta_{10}^\rho = 2\cos^2\theta_1 (\tan\theta_1 - \tan\theta_2)\tan\theta_1$$

(21) becomes

$$-\frac{\Delta \mathcal{F}_Y}{\rho S} = \Theta_1 - \Theta_2 + \zeta_9^\rho (H_1 - \beta_1) - \zeta_{10}^\rho \Theta_1 = \Theta_1 (1 - \zeta_{10}^\rho) - \Theta_2 + \zeta_9^\rho (H_1 - \beta_1) \qquad 22$$

We now choose to eliminate the H_2 in equation (20). From (19)

$$H_2 = \left[\zeta_3^\rho (H_1 - \beta_1) - \zeta_4^\rho \Theta_1 + \zeta_2^\rho \Theta_2\right] \frac{1}{\zeta_1^\rho} + \beta_2 \qquad 23$$

letting

$$\zeta_{11}^{\rho} = \zeta_3^{\rho} / \zeta_1^{\rho}$$
$$\zeta_{12}^{\rho} = \zeta_4^{\rho} / \zeta_1^{\rho}$$
$$\zeta_{13}^{\rho} = \zeta_2^{\rho} / \zeta_1^{\rho}$$

(23) becomes

$$H_2 = \zeta_{11}^{\rho}(H_1 - \theta_1) - \zeta_{12}^{\rho}\,\textcircled{H}_1 + \zeta_{13}^{\rho}\,\textcircled{H}_2 + \theta_2 \qquad 23a$$

Substituting this value of H_2 into (20), we obtain

$$\theta_1 + \zeta_{26}^{\rho}(H_1 - \theta_1) + \zeta_{27}^{\rho}\,\textcircled{H}_1 = \theta_2 + \zeta_7^{\rho}\left[\zeta_{11}^{\rho}(H_1 - \theta_1) - \zeta_{12}^{\rho}\,\textcircled{H}_1 + \zeta_{13}^{\rho}\,\textcircled{H}_2 + \theta_2 - \theta_2\right] + \zeta_8^{\rho}\,\textcircled{H}_2 \qquad 24$$

letting

$$\zeta_{14}^{\rho} = \zeta_7^{\rho}\,\zeta_{11}^{\rho}$$
$$\zeta_{15}^{\rho} = \zeta_7^{\rho}\,\zeta_{12}^{\rho}$$
$$\zeta_{16}^{\rho} = \zeta_7^{\rho}\,\zeta_{13}^{\rho}$$

(24) becomes

$$\theta_1 + \zeta_{26}^{\rho}(H_1 - \theta_1) + \zeta_{27}^{\rho}\,\textcircled{H}_1 = \theta_2 + \zeta_{14}^{\rho}(H_1 - \theta_1) - \zeta_{15}^{\rho}\,\textcircled{H}_1 + \zeta_8^{\rho}\,\textcircled{H}_2 + \zeta_{16}^{\rho}\,\textcircled{H}_2$$

$$\theta_1(1 - \zeta_{26}^{\rho} + \zeta_{14}^{\rho}) - \theta_2 + \textcircled{H}_1(\zeta_{27}^{\rho} + \zeta_{15}^{\rho}) - (\zeta_8^{\rho} + \zeta_{16}^{\rho})\,\textcircled{H}_2 = H_1(\zeta_{14}^{\rho} - \zeta_{26}^{\rho})$$

$$\textcircled{H}_1(\zeta_{27}^{\rho} + \zeta_{15}^{\rho}) - (\zeta_8^{\rho} + \zeta_{16}^{\rho})\,\textcircled{H}_2 + \theta_1(1 - \zeta_{26}^{\rho} + \zeta_{14}^{\rho}) - \theta_2 = H_1(\zeta_{14}^{\rho} - \zeta_{26}^{\rho}) \qquad 25$$

letting

$$\zeta_{17}^{\rho} = \zeta_{27}^{\rho} + \zeta_{15}^{\rho}$$
$$\zeta_{18}^{\rho} = 1 - \zeta_{26}^{\rho} + \zeta_{14}^{\rho} \quad ; \quad \zeta_{18}^{\rho} - 1 = \zeta_{14}^{\rho} - \zeta_{26}^{\rho} = \zeta_{19}^{\rho}$$
$$\zeta_{19}^{\rho} = \zeta_{14}^{\rho} - \zeta_{26}^{\rho}$$
$$\zeta_{28}^{\rho} = \zeta_8^{\rho} + \zeta_{16}^{\rho}$$

(25) becomes

$$\zeta_{17}^{p}\,\Theta_1 - \zeta_{28}^{p}\,\Theta_2 + \zeta_{18}^{p}\,\beta_1 - \beta_2 = \zeta_{19}^{p}\,H_1 \qquad 26$$

(22) may be rearranged to give

$$\Theta_1(1-\zeta_{10}^{p}) - \Theta_2 - \zeta_9^{p}\,\beta_1 = -\frac{\Delta\hat{F}_Y}{\rho S} - \zeta_9^{p}\,H_1 \qquad 27$$

letting

$$\zeta_{20}^{p} = 1 - \zeta_{10}^{p}$$

(27) becomes

$$\zeta_{20}^{p}\,\Theta_1 - \Theta_2 - \zeta_9^{p}\,\beta_1 = -\frac{\Delta\hat{F}_Y}{\rho S} - \zeta_9^{p}\,H_1 \qquad 28$$

For reference we recall (26)

$$\zeta_{17}^{p}\,\Theta_1 - \zeta_{28}^{p}\,\Theta_2 + \zeta_{18}^{p}\,\beta_1 - \beta_2 = \zeta_{19}^{p}\,H_1 \qquad 26$$

We now operate on equations (28) and (26), using the previously developed notion of complementary functions to obtain

$$-\zeta_{20}^{p}\,\beta_1 - \beta_2 - \zeta_9^{p}\,\Theta_1 = \left(-\frac{\Delta\hat{F}_Y}{\rho S} - \zeta_9^{p}\,H_1\right)^{*} \qquad 29$$

$$-\zeta_{17}^{p}\,\beta_1 - \zeta_{28}^{p}\,\beta_2 + \zeta_{18}^{p}\,\Theta_1 + \Theta_2 = \zeta_{19}^{p}\,H_1^{*} \qquad 30$$

The four linear equations (28), (26), (29), (30) are sufficient to determine $\Theta_1, \Theta_2, \beta_1, \beta_2$ in terms of the functions H_1, H_1^{*}, $\frac{\Delta\hat{F}_Y}{\rho S}$, $\frac{\Delta\hat{F}_Y^{*}}{\rho S}$. H_2 may now be determined from equation (23a), completing the solution.

In this entire section the blade force has been treated as a known quantity. The manner in which blade force is actually obtained is discussed in the subsequent section.

2.4 Determination of the Blade Forces

As we have seen, as the blade passes through the distortion, it incurs a perturbation in force directly related to the mean flow and to the perturbations in the mean flow. At any instant (or y location) a given airfoil is subject to a perturbation in velocity. The velocity perturbations which affect the airfoil lift are u_{o+}, u_{o-}, v_{o+} and v_{o-}. Specifically as has been discussed in Reference 18, the lift is affected by $\bar{u} = (u_{o+} + u_{o-})/2$ and by $\bar{v} = (v_{o+} + v_{o-})/2$. Thus the total velocity perturbation is given by $\bar{u} + \bar{v}$, as shown by the dashed line in Figure 2. The lift in uniform flow, as is well known, is determined by the mean relative velocity vector w_o.

It is both natural and fruitful to resolve the total velocity perturbation along and normal to w_o. As is shown in Figure 2, we have called u_r, the component along w_o and v_r, the component normal to w_o. In the Figure as drawn, v_r is inducing a negative perturbation in force on the blade, hence the minus sign.

As is obvious by inspection, by simple resolution of vectors,

$$u_r = \bar{u}\cos\beta_m - \bar{v}\sin\beta_m$$

$$-v_r = \bar{u}\sin\beta_m + \bar{v}\cos\beta_m$$

Conversely

$$\bar{u} = u_r\cos\beta_m - v_r\sin\beta_m$$

$$\bar{v} = -u_r\sin\beta_m - v_r\cos\beta_m$$

Here $\bar{u}$ and $\bar{v}$ may be found, as a first approximation, from the previous theory (Rannie-Marble).

Thus a given airfoil in cascade is subject to both a time varying v_r and a time varying u_r, both of course periodic of period equal to the period of the distortion. The determination of the time varying lift of an airfoil in cascade under the influence of either of these velocity perturbations has not been solved.* Therefore, the author suggests the somewhat simpler model of a single uncambered flat plate airfoil subject to time varying u_r and v_r; the influence of other airfoils would then be treated by the lattice coefficient (Ref. 28) notion or its equivalent. Each velocity component would be treated separately and the resultant blade forces added algebraically.

A solution to the fluctuating u_r problem has been obtained by Isaacs, Ref. 17. A solution to the fluctuating v_r problem has been obtained by Sears, Ref. 10. Both solutions are subsequently described.

2.4.1 Blade Force Caused by Velocity Perturbations Normal to the Mean Relative Velocity Vector (Sears Force)

The calculation of the nonsteady aerodynamic lift induced at a thin airfoil by a relative upwash, such as is shown in Figure 3, can be obtained from the results of a paper by Sears, Ref. 10. In this theory, both the impulsive pressure (virtual mass) and the influence of the shed vorticity are accounted for in computing the lift. Sears has shown that if a thin airfoil experiences a nonsteady upwash of the form

$$v_r = v_0 e^{i\omega\left(t - \frac{x}{U_0}\right)}$$

*A solution to the closely related problem of an oscillating cascade is given in Ref. 20.

the time dependent lift is given by

$$L(t) = 2\pi\rho b w_0 v_0 S(k) e^{i\omega t}$$

where k is the reduced frequency $\frac{\omega b}{w_0}$ and S is the Sears function shown in Figure 4. In this figure note that the magnitude of lift is represented by the modulus of the vector from the origin to the frequency in question. The phase, with respect to the zero frequency lift, is given by the angle between this vector and the positive real axis. Note that

$\lim_{k \to \infty} L = 0.$

For a distortion of period 2π, the appropriate trigonometric form for the primary wave is clearly $e^{i\Omega t}$. More generally, for a periodic distortion of primary wave length λ (radians) the appropriate form is

$$e^{i\frac{2\pi}{\lambda}\Omega t}$$

Thus, in general, the fundamental circular frequency is

$$\omega_r = \frac{2\pi}{\lambda}\Omega$$

Since the lift is determined by the relative velocity, we may find the lift whether the airfoil is sationary and the wave is moving, or vice versa. In our case, the distortion is, of course, fixed in space (stationary) and the airfoil is moving. There is, therefore, a simple relation between the variables of time t and distance λ_{ry}, specifically

$$\lambda_{ry} = \Omega r t$$

The time required for a blade to pass through a complete cycle is

$$t_c = \frac{\lambda_r \gamma_c}{\Omega r} = \frac{\lambda}{\Omega}$$

since, according to our definition of y, $y_{cycle} = 1$.

Now we can represent a periodic gust of arbitrary shape as

$$v_r(y) = \sum a_n e^{in\omega_r(t-\frac{r\xi}{w_o})} = * \sum a_n e^{i2\pi ny}$$

and expect to find the lift as

$$L(t) = 2\pi\rho b w_o \sum a_n S(nk_r) e^{in\omega_r t}$$

The tangential blade force deviation may now be found from

$$\Delta \tilde{F}_{y_{v_r}} = L \cos\beta_{mean}$$

β_{mean} is defined by the relation

$$\tan\beta_m = \frac{\frac{1}{2}[(\Omega r - V_1) + (\Omega r - V_2)]}{U}$$

Therefore

$$\Delta \tilde{F}_{y_{v_r}} = 2\pi\rho b w_o \cos\beta_m \sum a_n S(nk_r) e^{in\omega_r t}$$

Now that we have $\Delta \tilde{F}_{y_{v_r}}$ as a function of time, it is clear that we may find $\Delta \tilde{F}_{y_{v_r}}(y)$ from the relation $\lambda r y = \Omega r t$ or $t = \frac{\lambda}{\Omega} y$

---

* The relation between y, t and ξ can best be demonstrated by referring to Figure 5.

The wave phenomenon under discussion occurs along the $r\xi$ axis as shown. $r\xi$ is in the direction of w_o. The time required for the blade to travel from peak to peak along the y axis is

$$t_c = \lambda r y_c / \Omega r = \lambda y_c / \Omega$$

If the observer now moves from $r\xi = 0$ to the point $r\xi_1$ with the wave velocity w_o, an additional time of $r\xi_1 / w_o$ will be required before the expected peak reaches the observer. Thus in general

$$t_c = \frac{\lambda y_c}{\Omega} + \frac{r\xi_1}{w_o}$$

and since this is true for arbitrary t, y, ξ we have

$$y = \frac{\Omega}{\lambda}\left(t - \frac{r\xi}{w_o}\right)$$

2.4.2 Blade Force Caused by Velocity Perturbation in the Direction of the Mean Relative Velocity Vector (Isaacs Force)

As previously discussed, the blade is subject to time varying u_r. The time varying lift for such a blade has been given in a paper "Airfoil Theory for Flows of Variable Velocity", by Rufus Isaacs, Ref. 17. This problem and the Sears problem previously discussed are not trivial problems to solve chiefly for one reason: in each solution, the Kutta condition is maintained, airfoil circulation is continuously changing (circulation is continuously shed) and the effects of the shed circulation must be taken into account in determining the lift.

The problem is easily represented with the aid of the diagram in Fig. 6-1. As previously, w_o is the mean relative velocity vector; a sinusoidal perturbation $\sigma w_o \sin \omega t$ occurs. k is again the non-dimensional frequency, defined exactly as in the Sears force discussion. L_o is the lift corresponding to w_o; the expression for L_o is as shown in this diagram.

Thus the ratio of the instantaneous lift L to the lift L_o is a function of σ, k and t. Graphs of L/L_o versus time t with σ and k as independent variables are given in Figure 6. These graphs have been computed using the formulae given by Isaacs. These formulae are next described.

For the case in which

$$w = w_o (1 + \sigma \sin \omega t)$$

$$= w_o \left(1 + \frac{u_r}{w_o} \sin \omega t\right)$$

the lift is found to be

$$L = L_0\left[1+\frac{\sigma^2}{2}+\sigma\left(\ell_1+\frac{k}{2}\right)\cos\omega t+\sigma\left(\ell_1'+1+\frac{\sigma^2}{2}\right)\sin\omega t+\sigma\sum_{2}^{\infty}\left(\ell_m\cos m\omega t+\ell_m'\sin m\omega t\right)\right]$$

where

$$\ell_m+i\ell_m' = -m(-i)^m\sum_{n=1}^{\infty}\left\{F_n\left[J_{n+m}(n\sigma)-J_{n-m}(n\sigma)\right]+iG_n\left(J_{n+m}(n\sigma)+J_{n-m}(n\sigma)\right)\right\}$$

$$F_n = \frac{J_{n+1}(n\sigma)-J_{n-1}(n\sigma)}{n^2}\,F(nk)$$

$$G_n = \frac{J_{n+1}(n\sigma)-J_{n-1}(n\sigma)}{n^2}\,G(nk)$$

F and G are the real and imaginary parts respectively of the Theodorsen function shown in Figure 7.

What we want to have is

$$\Delta\mathcal{F}_{\mu_r} = (L-L_0)\cos\beta_m = L_0\left(\frac{L}{L_0}-1\right)\cos\beta_m$$

or

$$\Delta\mathcal{F}_{\mu_r} = \frac{1}{2}\,2\pi\sin i_m\,\rho\omega_0^2(2b)\cos\beta_m\left\{\frac{\sigma^2}{2}+\sigma\left(\ell_1+\frac{k}{2}\right)\cos\omega t+\sigma\left(\ell_1'+1+\frac{\sigma^2}{2}\right)\sin\omega t+\sigma\sum_{2}^{\infty}\left(\ell_m\cos m\omega t+\ell_m'\sin m\omega t\right)\right\}$$

Fourier generalizing in the usual manner, we find that if the disturbance can be represented as

$$\omega-\omega_0=\mu_r=\sum_{n=1}^{\infty}D_n\sin n\omega_r t=\sum_{n=1}^{\infty}D_n\sin 2\pi n\frac{\Omega}{\lambda}t=\sum_{n=1}^{\infty}D_n\sin 2\pi n\gamma$$

then the perturbation in force is given by

$$\Delta \hat{F}_{y_{\mu_r}} = \pi \sin i_m \rho \omega_0^2 (2b) \cos\beta_m \sum_{n=1}^{\infty} \left\{ \left(\frac{D_n}{\omega_0}\right)^2/2 + \frac{D_n}{\omega_0}\left(\ell_{1n} + \frac{nk_r}{2}\right)\cos n\omega_r t + \right.$$

$$\frac{D_n}{\omega_0}\left(\ell'_{1n} + 1 + \frac{1}{2}\left(\frac{D_n}{\omega_0}\right)^2\right)\sin n\omega_r t + \frac{D_n}{\omega_0} \sum_{m=2}^{\infty} \left(\ell_{mn} \cos mn\omega_r t + \right.$$

$$\left. \left. \ell'_{mn} \sin mn\omega_r t \right) \right\}$$

And again, $t = \frac{\lambda}{\Omega} Y$.

Fortunately, the series for $\ell_m + i^\circ \ell'_m$ converges very rapidly (because of the rapid convergence of the Bessel functions) both in n and in m. For example taking m = 2 and n = 5 seems to insure that L/L_0 calculated on this basis will not differ from the value implied by the infinite series by more than 2%.,

As has been discussed, the Sears force and the Isaacs force are finally added algebraically, giving a continuous function of y:

$$\left(\frac{\Delta \hat{F}_{y_{\sigma_r}}}{\rho 2bU^2} + \frac{\Delta \hat{F}_{y_{\mu_r}}}{\rho 2bU^2} \right) \frac{2b}{S} A = \frac{\Delta \hat{F}_y}{\rho S U^2}$$

A is the lattice coefficient, the determination of which is discussed in Appendix V. Also discussed in this appendix is the determination of the mean incidence i_m, required in the Isaacs force computation.

Thus we have found the blade force required in the Analysis, 2.1.

3. EXPERIMENTAL INVESTIGATION

The experiments were conducted on an isolated compressor rotor. Fig. 8 is a schematic diagram of the machine; Fig. 9 is a photograph of the rotor with 2b/s = .525. Also shown here is the pressure measuring equipment to be described subsequently.

The essential dimensions of the compressor are:

Hub-tip ratio	0.75
Tip radius	11.63 inches
Blade chord	1.51 inches (no taper)
Linear twist, root to tip	9.7°
No. of blades	44, at 2b/s = 1.05 22, at 2b/s = 0.525
Blade section	NACA 65-(12)10
Mean radius stagger, measured from the axial direction	52.7°
Tip clearance	approx. .035 inches

The constant area annulus extended 29.8 inches upstream and 36.5 inches downstream of the rotor. Radial air flow entrance was through screens. In all tests, the rotor was operated at 1000 rpm. U was of the order of 50 ft/sec; w_o was of the order of 100 ft/sec. A tabulation of Reynolds numbers based on blade chord together with other significant parameters is given in Table I.

TABLE I

2b/s = 1.05			2b/s = .525		
$U/\Omega r$	i_m	Re_{2b}	$U/\Omega r$	i_m	Re_{2b}
.562	9.30°	40,500	.514	8.80°	36,500
.460	15.30°	32,100	.391	16.10°	27,400

Two flow rates were studied at each of two solidities. The lower flow rate was, in each case, just above the point of inception of propagating stall. Before any distortion producing screens were inserted, it was determined that the flow in this case, to the accuracy of the measuring instruments, was axisymmetric. Relative position of screen and measuring instruments was obtained by rotating the screen, in stepwise fashion, using the reel and cord arrangement shown in Fig. 10. The fact that three screens are shown in this figure is discussed subsequently. The relative location of screen, probes, and rotor is shown in Fig. 11.

As has been mentioned, the distortions were produced by screens, the choice of which is to be described. A photograph of these screens and their frame holder is shown in Fig. 12. Early in the investigation it was found that one had to make a rather careful choice in the screen or screens to be used. Screens of too high solidity diverted the flow around them so that the requirements of the theory (flow uniform in direction at upstream infinity) could not be met. Any screen, of course, does this to a certain extent. However, the screens ultimately chosen produced uniformly axial flow generally to within 5°. The second problem concerned the generation of vortices at the edges of the screen. This problem, discussed more

completely in References 21 and 24 was solved, at least to a large extent, by reducing the effective solidity toward the edge of the screen. Finally, the screen had to produce a measurable perturbation that could be considered within the bounds of a linearized analysis. A trial and error process resulted in the following description, applicable to each of the three segments shown in Fig. 12.

a) 45° (circumferential extent) screen or mesh 4 x 4, wire size 23

b) symmetrically place 36° screen of mesh 6 x 6, wire size 25.

The choice of the 3 blockage segments shown in Fig. 12 is now discussed. The problem is essentially that of choosing a screen-to-rotor distance that can be considered 'infinite'. As is shown in Ref. 1, and in the present theory, disturbances occuring at the rotor die away as $e^{-2\pi x}$. We recall that $x = \frac{\text{(physical distance in x direction)}}{r\,\lambda}$. Thus, of course, larger values of x correspond to closer approximations to infinity. Once can increase the physical distance from the screen to the rotor and/or one can reduce the fundamental wave length of the distortion. The latter alternative, of course, corresponds to the use of 3 screens. Thus, the wave length chosen for the experiments was $\lambda = 120° = \frac{2}{3}\pi$. For the final arrangement then, $e^{-2\pi x}$ was equal to 0.001.

The type of probe used in all the measurements is shown in Fig. 13. The probe is first yawed, using the two extreme holes, in the normal fashion. The stagnation pressure may then be read from the center tap. At the same time one may read the pressure indicated by either of the extreme holes. This measurement, p_i, when the probe has been properly calibrated, can be easily related to the stream static pressure. In fact

$\frac{p - p_i}{p_o - p}$ = an experimentally determined constant. This type of probe is described in Ref. 25. The effects of turbulence on the readings were in all cases neglected.

These pressures were measured on null reading type transducer equipment manufactured by the Dynamic Instrument Co. of Cambridge, Massachusetts.

RPM was measured with an electrical strobotac.

All measurements were taken at the mean geometric radius of the flow annulus.

The size of the perturbations may be represented by the ratio $(\frac{u - \infty}{U})_{max}$. This value was of the order of .35 for the present series of tests. The theory essentially neglects the third term in the expansion of

$$(1 + \frac{u}{U})^2 = 1 + 2\frac{u}{U} + (\frac{u}{U})^2$$

The first term represents the mean condition; the theory treats the second term. The ratio of the term neglected to the term retained is thus at most $\frac{(.35)^2}{2(.35)} = .175$.

4. COMPARISON OF THEORY AND EXPERIMENT

As explained previously, a knowledge of the upstream flow (H_1/U^2), the mean flow, and the rotor characteristics enables one to solve for the perturbations everywhere. As the theory indicates, the important perturbations are B_1/U^2, B_2/U^2, Φ_1/U^2, Φ_2/U^2 and H_2/U^2. All of these quantities were determined experimentally and the comparison with the present theory and that of Rannie-Marble are presented in Section 4.2.

Another means of comparing the theory of Rannie-Marble with the present theory is through their respective predictions of the perturbations in force on the blades. The present theory attempts to correct the previous work by means of a more adequate prediction of the blade loading. As has been noted one may compute the Rannie-Marble prediction of blade force, using equation 22.

As has been discussed, in the present theory one first finds u_r and v_r, using the Rannie-Marble solution as a first approximation. The respective Isaacs and Sears forces are calculated for this disturbance flow. Then, applying these forces in the present theory the second approximation of the flow is obtained.

The above mentioned forces were computed for each of the experiments conducted and the results are shown in Fig. 14-1 through 14-4.

It is also interesting to investigate by experiment the validity of the assumption $\tan\beta_2$ = constant. This was done for a single case ($2b/s = 1.05$, $U/\Omega r = .460$) and the result is shown in Fig. 17.

4.1 Comparison of Blade Force Predictions

The perturbation in y-component force on the blade, as discussed in Section 4, is shown in Fig. 14-1 through 14-4. The conditions of the experiment are indicated in the caption. No experimental data concerning blade forces were taken. The non-dimensional values of the Sears and Isaacs "forces per chord length" per unit span are shown as the two bottom curves. The next higher curve is simply an algebraic addition of the two aforementioned curves, hence it is also a non-dimensional graph of "force per chord length" per unit span. All of these three previously mentioned curves apply to a single airfoil passing through the distortion. If we multiply the middle curve by the chord pitch ratio, 2b/s, we find the non-dimensional "force per pitch" per unit span and if we then multiply by A, the lattice coefficient (Appendix V), we finally find the non-dimensional "force per pitch" per unit span of an airfoil in cascade. Thus we achieve the solid curve at the top of the figure, which is compared with the Rannie-Marble prediction ($2b/s = \infty$), dashed curve, for this quantity. Note that the relative size of the Sears and Isaacs forces is related to the mean incidence, i_m. From the theory, the Isaacs force = 0 if i_m is zero. This is of course not true for the Sears force.

In general, the present theory predicts lower maxima and higher minima than the previous theory.

4.2 Comparison of Θ, G, H

The perturbations upstream and downstream of the rotor as obtained from the experiments and as predicted from the previous theory

and the present theory are presented in Fig. 15-1 through 15-4. The H_1/U^2 curve presented is of course part of the input information for both theories. The 51 points enclosed by triangles on this curve are either data points or points interpolated from the data, as explained in Appendix IV.

The present theory corresponds more closely to the experimental data for all of the downstream perturbations ($\mathcal{B}_2/U^2$, $\mathcal{H}_2/U^2$ and H_2/U^2) in each of the four experiments. The theory of Rannie-Marble apparently offers a closer correspondence for the upstream quantities, $\mathcal{B}_1/U^2$ and $\mathcal{H}_1/U^2$. One should bear in mind several points, however, when comparing theory and experiment.

One factor is the ease with which $\pm\ \infty$ are "located" on the compressor, compared with the difficulty of establishing the points ± 0. This stems, of course, from the manner ($e^{-2\pi x}$) in which the fundamental harmonic of $\mathcal{H}$ and $\mathcal{B}$ decay with distance from the rotor. Thus x-mislocation of a given amount has a larger effect on this factor for small x than for large x. Actually, if one places the actuator disc at the half chord position this exponential factor for either the +0 probe or the -0 probe becomes $e^{-\frac{2\pi\ 1.5}{10.27\ (\frac{2}{3}\pi)}} = .645$. That is, on this basis, the theoretical curves for $\mathcal{H}_1/U^2$, $\mathcal{H}_2/U^2$, $\mathcal{B}_1/U^2$ and $\mathcal{B}_2/U^2$ are to be multiplied by .645 for a somewhat fairer comparison with experiment. As may be seen, this tends to improve the correspondence between experiment and both theories.

One would thus perhaps look to H_2/U^2 as the most genuine comparison quantity for theory and experiment. It may well be, but again one point must be considered. In either theory, it is shown that, since

the fluid is assumed inviscid, the perturbation in stagnation pressure is carried undiminished by the main flow. The experiments are, of course, conducted with a fluid of finite viscosity and the gradients are all diminished by viscous decay. This is perhaps the reason for the "underestimation" of the attenuation of H by both theories. As is noted in the theory then, $H_{-\infty}/U^2 = H_{-0}/U^2$. Also $H_{+0}/U^2 = H_{+\infty}/U^2$. A comparison of these quantities is made in Fig. 16. The downstream data tend to verify the above discussion, though the upstream measurements do not allow one to make this conclusion.

Another point is that in the computation of both theories relative stagnation pressure loss through the blade row was taken to be zero. Both theories do allow for finite losses and, as shown in Ref. 26, the inclusion of this factor does in fact bring theory and experiment into closer correspondence.

4.3 Effects of Flow Rate and Solidity

The effect of flow rate on the attenuation is shown in Fig. 18. The experiment strongly indicates, for this case, larger attenuation at the lower flow rate. The theory of Rannie-Marble clearly indicates the opposite trend. The present theory agrees with experiment at least in several y intervals and clearly must be considered as predicting the experimental results more adequately. Perhaps the agreement would have been further improved if an appropriate non-zero loss coefficient had been assumed for each flow rate. The lower flow rate curve could be associated with a higher C_D, perhaps giving more attenuation (Ref. 26) than that resulting from the application of the smaller C_D to the high flow rate

curve.*

The effect of varying solidity on the attenuation is shown in Fig. 19. Experiment indicates increasing attenuation with increasing chord/pitch. This trend is also predicted by the present theory, though the effect is underestimated. In this respect note that, since the blades are unstalled, increasing solidity implies a higher loss coefficient C_D for the higher solidity case. Referring again to Ref. 26, we infer then that if an appropriate C_D is used in each case, the higher solidity curve will receive more attenuation than the lower solidity curve, improving the prediction of the effect of solidity. The Rannie-Marble theory of course can offer no information on this effect since their theory treats only the single solidity $2b/s = \infty$. Note that, because in the experiment, the attempt to keep flow rate constant at each solidity was not successful (there being no convenient means to control this parameter for the distorted flow except by measuring a representative velocity), one had to interpolate between flow rates, as indicated on this Figure.

---

* It should be noted that, as is to be expected, the curves of H_1/U^2 are very nearly the same in each case.

5. CONCLUSION

A theory for asymmetric inlet flow in an isolated blade row has been developed. This theory gives a prediction for distortion attenuation, effect of flow rate, and effect of solidity variation which agrees more closely with the present experiments than does the previous theory. For the cases tested, attenuation was increased by reducing the flow rate and by increasing the chord-pitch ratio.

The attempt to improve the prediction of blade forces thus appears to have been a fruitful approach to the problem of asymmetric inlet flow. In particular, the effect of velocity perturbations in the direction of the mean relative velocity vector, often ignored, is seen to be the dominating influence at the larger values of mean incidence.

APPENDIX I

A Boundary Relationship Between Two Cauchy-Riemann Variables

Since the two velocity components (u, v) in plane potential flow satisfy the Cauchy-Riemann conditions ($\frac{\partial u}{\partial x} + \frac{\partial v}{\partial y} = 0$, $\frac{\partial v}{\partial x} - \frac{\partial u}{\partial y} = 0$) it will be convenient to derive the following in terms of these variables. It is understood, however, that the following is true for <u>any</u> pair of Cauchy-Riemann variables.

Let u be periodic along the y axis of period 1, and let this velocity distribution be the result of a source distribution along the y axis, also of period 1, Figure A - 1. That the introduction of the sources does not make the following less general follows from the second fundamental theorem of potential theory: if continuous boundary values are assigned, on the surface of a regular region, to the normal derivatives, not more than one function, apart from an additive constant, harmonic in the region, can have normal derivatives with these values. For infinite regions, we require that our harmonic function (in this case the velocity potential φ) be regular at infinity. That is, $r\varphi$, $r^2 \frac{\partial \varphi}{\partial x}$, $r^2 \frac{\partial \varphi}{\partial y}$ shall be bounded in absolute value for all sufficiently large r, where r is the distance from any fixed point. That is, thus far all we have assumed is that u is periodic along x = 0, period = 1, and that the velocity potential φ is regular at infinity. Our results will hold whether this periodic distribution of u is caused by a periodic distribution of sources or not.

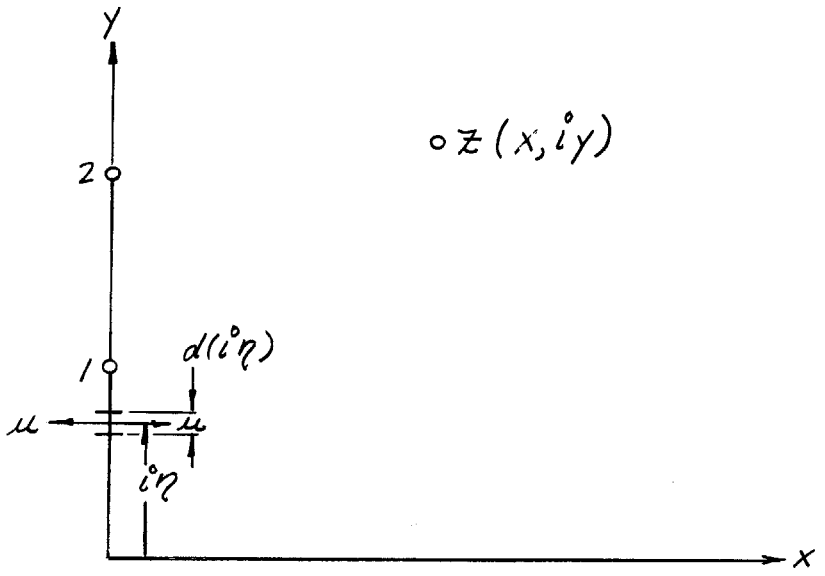

FIGURE A - 1

The source strength dQ of an element is clearly $2u\,d\eta$.

In the following, η, n, x, y are all real. Consider the element shown in Figure A - 1 and the elements at $i^\circ(\eta+1), i^\circ(\eta+2), \ldots i^\circ(\eta+n), -i^\circ(1-\eta), i^\circ[-(1-\eta)-1], \ldots i^\circ[-(1-\eta)-n]$ that is, corresponding elements in the wave length.

Let $d\Omega$ be the complex potential at z due to the sources at these locations.

$$d\Omega = \frac{dQ}{2\pi}\ln(z-i^\circ\eta) + \frac{dQ}{2\pi}\ln[z-i^\circ(\eta+1)] + \ldots + \frac{dQ}{2\pi}\ln[z-i^\circ(\eta+n)] + \frac{dQ}{2\pi}\{z-[-i^\circ(1-\eta)]\} + \ldots \frac{dQ}{2\pi}\ln\{z-i^\circ[-(1-\eta)-n]\}$$

$$= \frac{dQ}{2\pi}\left\{\ln(z-i^\circ\eta) + \ln\prod_{1}^{\infty}(z-i^\circ\eta+i^\circ\eta)(z-i^\circ\eta-i^\circ\eta)\right\}$$

$$= \frac{dQ}{2\pi}\left\{\ln(z-i^\circ\eta) + \ln\pi n^2\left(1+\frac{z-i^\circ\eta}{i^\circ\eta}\right)\left(1-\frac{z-i^\circ\eta}{i^\circ\eta}\right)\right\}$$

$$= \frac{dQ}{2\pi}\left\{\ln(z-i^\circ\eta) + \ln\pi n^2\,\pi\left[1-\left(\frac{(z-i^\circ\eta)/i^\circ}{n}\right)^2\right]\right\}$$

$$= \frac{dQ}{2\pi}\left\{\ln(z-i^\circ\eta) + \ln\pi\left[1-\left(\frac{(z-i^\circ\eta)/i^\circ}{n}\right)^2\right] + \ln\pi n^2\right\}$$

The last term, $\ln \prod_{1}^{\infty} n^2$, is a constant and will disappear in the subsequent differentiation; it is henceforth ignored.

$$d\Phi = \frac{dQ}{2\pi}\left\{\ln(z-i\eta)\prod_{1}^{\infty}\left[1-\left(\frac{(z-i\eta)/i}{n}\right)^2\right]\right\}$$

The infinite product has a special form*:

$$\prod_{1}^{\infty}\left[1-\left(\frac{(z-i\eta)/i}{n}\right)^2\right] = \frac{\sin\pi(z-i\eta)/i}{\pi(z-i\eta)/i}$$

$$d\Phi = \frac{dQ}{2\pi}\ln(z-i\eta)\frac{\sin\pi(z-i\eta)/i}{\pi(z-i\eta)/i} = \frac{dQ}{2\pi}\left[\ln\sin\pi(z-i\eta)/i - \ln\pi/i\right]$$

Log $\frac{\pi}{i}$ disappears in subsequent differentiation.

Now, to find the influence of all the sources, we must integrate from 0 to 1.

$$\Phi = \int_0^1 \frac{dQ}{2\pi}\ln\sin\pi(z-i\eta)/i$$

And finally we find

$$\frac{d\Phi}{dz} = \int_0^1 -i\cot-i\pi(z-i\eta)\frac{dQ}{2} = u - iv$$

Specializing to z on the y axis

$$v(0,y) = -\Re\left\{\int_0^1 -i\cot\pi(y-\eta)\frac{dQ(0,\eta)}{2}\right\} = \int_0^1 \cot\pi(y-\eta)\frac{dQ(0,\eta)}{2}$$

Suppose that x = 0 is a line of discontinuity (as, for example, in actuator disc theory). Now we consider properties at x = 0+ and at x = 0-. For the region x > 0, since we have assumed that dQ is a source, and hence $\geq$ 0, $dQ = 2\mu d\eta$, $v(0+,y) = \int_0^1 \cot\pi(y-\eta)\mu(0+,\eta)d\eta$ and since u $\leq$ 0 for x = 0-, Figure A-1, for the region x < 0 we have $dQ = -2\mu d\eta$. Note that, from symmetry, $v(-x,y_0) = v(x,y_0)$

$$v(0-,y) = -\int_0^1 \cot\pi(y-\eta)\mu(0-,\eta)d\eta$$

*Whittaker and Watson, Modern Analysis, Cambridge University Press, Page 33.

A similar derivation yields

$$u(0,y) = \mp \int_0^1 \cot \pi(y-\eta)\, v(0,\eta)\, d\eta \quad , \quad x = 0^{\pm}$$

Example

Given u(0+, y) = C, a constant

Then $v(0+,y) = C \int_0^1 \cot \pi(y-\eta)\, d\eta = -\frac{C}{\pi}\left\{ \ln|\sin \pi(y-1)| - \ln|\sin \pi y| \right\}$

Then $v(0+,y) \equiv 0$

APPENDIX II

$\{u, v, p\}$ - $\{H, \mathcal{G}, \Theta\}$ Equivalence; Translation of the Boundary Conditions to Relations in $H, \mathcal{G}, \Theta$.

The defining equations for $H, \mathcal{G}, \Theta$ are

$$p/\rho + Uu + Vv = H$$
$$-Vu + Uv = \Theta$$
$$p/\rho = \mathcal{G}$$

Regarding this as a set of three linear algebraic equations, may solve for u, v, and p successively. One then finds that

$$u = \frac{U(H-\mathcal{G}) - \Theta V}{U^2+V^2} \qquad \text{A2-1}$$

$$v = \frac{V(H-\mathcal{G}) + U\Theta}{U^2+V^2} \qquad \text{A2-2}$$

$$p/\rho = \mathcal{G} \qquad \text{A2-3}$$

Then, whenever u, v or p/ρ appears in a boundary condition we substitute the expressions given above. This operation and the resulting simplifications are set forth as is shown.

The matching condition $u_2 = u_1$ becomes

$$\frac{U(H_2-\mathcal{G}_2) - \Theta_2 V_2}{U^2+V_2^2} = \frac{U(H_1-\mathcal{G}_1) - \Theta_1 V_1}{U^2+V_1^2} \qquad \text{A2-4}$$

letting

$$\varphi_1 = \frac{U}{U^2 + V_2^2}$$

$$\varphi_2 = \frac{V_2}{U^2 + V_2^2}$$

$$\varphi_3 = \frac{U}{U^2 + V_1^2}$$

$$\varphi_4 = \frac{V_1}{U^2 + V_1^2}$$

A2-4 becomes

$$\varphi_1 (H_2 - \beta_2) - \varphi_2 \Theta_2 = \varphi_3 (H_1 - \beta_1) - \varphi_4 \Theta_1 \qquad \text{A2-5}$$

For the Bernoulli equation with losses, we have

$$p_1/\rho + v_1 (V_1 - \Omega r) = p_2/\rho + v_2 (V_2 - \Omega r) + U\mu_1 \frac{C_D}{\cos^2 \beta_m} - \frac{C_D'}{2} \frac{(\Theta_1 + \Omega r \mu_1)}{\cos^2 \beta_m}$$

Translating into Θ, β, H notation

$$\beta_1 + \frac{V_1 (H_1 - \beta_1) + U\Theta_1}{U^2 + V_1^2} (V_1 - \Omega r) = \beta_2 + \frac{V_2 (H_2 - \beta_2) + U\Theta_2}{U^2 + V_2^2} (V_2 - \Omega r) +$$

$$\frac{U(H_1 - \beta_1) - \Theta_1 V_1}{U^2 + V_1^2} \frac{UC_D}{\cos^2 \beta_m} - \left[\Theta_1 + \frac{U(H_1 - \beta_1) - \Theta_1 V_1}{U^2 + V_1^2} \Omega r \right] \frac{C_D'}{2 \cos^2 \beta_m}$$

letting

$$\varphi_5 = \frac{V_1(V_1-\Omega r)}{U^2+V_1^2}$$

$$\varphi_6 = \frac{U(V_1-\Omega r)}{U^2+V_1^2}$$

$$\varphi_7 = \frac{V_2(V_2-\Omega r)}{U^2+V_2^2}$$

$$\varphi_8 = \frac{U(V_2-\Omega r)}{U^2+V_2^2}$$

$$\varphi_{21} = \frac{U^2}{U^2+V_1^2}\,\frac{C_D}{\cos^2\beta_m} \qquad \varphi_{24} = \frac{U\Omega r}{U^2+V_1^2}\,\frac{C_D'}{2\cos^2\beta_m}$$

$$\varphi_{22} = \frac{V_1 U}{U^2+V_1^2}\,\frac{C_D}{\cos^2\beta_m} \qquad \varphi_{25} = \frac{V_1\Omega r}{U^2+V_1^2}\,\frac{C_D'}{2\cos^2\beta_m}$$

$$\varphi_{23} = \frac{1}{2}\,\frac{C_D'}{\cos^2\beta_m}$$

We then have

$$\beta_1+\varphi_6(H_1-\beta_1)+\varphi_6\textcircled{H}_1=\beta_2+\varphi_7(H_2-\beta_2)+\varphi_8\textcircled{H}_2+\varphi_{21}(H_1-\beta_1)-\varphi_{22}\textcircled{H}_1-$$

$$\varphi_{23}\textcircled{H}_1-\varphi_{24}(H_1-\beta_1)+\varphi_{25}\textcircled{H}_1$$

$$\beta_1+(\varphi_5-\varphi_{21}+\varphi_{24})(H_1-\beta_1)+(\varphi_6+\varphi_{22}+\varphi_{23}-\varphi_{25})\textcircled{H}_1=$$

$$\beta_2+\varphi_7(H_2-\beta_2)+\varphi_8\textcircled{H}_2$$

letting

$$\zeta_{26}^{\varphi} = \zeta_5^{\varphi} - \zeta_{21}^{\varphi} + \zeta_{24}^{\varphi}$$

$$\zeta_{27}^{\varphi} = \zeta_6^{\varphi} + \zeta_{22}^{\varphi} + \zeta_{23}^{\varphi} - \zeta_{25}^{\varphi}$$

we finally obtain

$$\Theta_1 + \zeta_{26}^{\varphi}(H_1 - \Theta_1) + \zeta_{27}^{\varphi}\textcircled{H}_1 = \Theta_2 + \zeta_7^{\varphi}(H_2 - \Theta_2) + \zeta_8^{\varphi}\textcircled{H}_2 \qquad \text{A2-6}$$

For the tangential momentum boundary equation, we have

$$-\frac{\Delta \mathcal{F}_Y}{\rho S} = U(v_1 - v_2) + \mu(V_1 - V_2)$$

$$= U(v_1 - v_2) + \mu(V_2 - V_1) + 2\mu(V_1 - V_2)$$

$$= U(v_1 - v_2) + \mu(V_2 - V_1) + 2\frac{U(V_1 - V_2)}{U^2 + V_1^2}\frac{\mu}{U}(U^2 + V_1^2)$$

$$= U(v_1 - v_2) + \mu(V_2 - V_1) + 2\frac{U(V_1 - V_2)}{U^2 + V_1^2}\mu(U + V_1^2/U)$$

$$= U(v_1 - v_2) + \mu(V_2 - V_1) + 2\frac{U(V_1 - V_2)}{U^2 + V_1^2}\left[U\mu + V_1 v_1 - v_1 V_1 + \mu\frac{V_1^2}{U}\right]$$

$$= Uv_1 - V_1\mu - (Uv_2 - V_2\mu) + 2\frac{U^2}{U^2 + V_1^2}\left(\frac{V_1}{U} - \frac{V_2}{U}\right)\left[p_1/\rho + U\mu + V_1 v_1 - p_1/\rho - (Uv_1 - V_1\mu)\frac{V_1}{U}\right]$$

$$-\frac{\Delta \mathcal{F}_Y}{\rho S} = \textcircled{H}_1 - \textcircled{H}_2 + 2\cos^2\theta_1(\tan\theta_1 - \tan\theta_2)(H_1 - \Theta_1 - \textcircled{H}_1\tan\theta_1) \qquad \text{A2-7}$$

APPENDIX III

Tabulation of the φ's.

$$\varphi_1 = \frac{U}{U^2+V_2^2} \qquad \varphi_2 = \frac{V_2}{U^2+V_2^2} \qquad \varphi_3 = \frac{U}{U^2+V_1^2}$$

$$\varphi_4 = \frac{V_1}{U^2+V_1^2} \qquad \varphi_5 = \frac{V_1(V_1-\Omega r)}{U^2+V_1^2} \qquad \varphi_6 = \frac{U(V_1-\Omega r)}{U^2+V_1^2}$$

$$\varphi_7 = \frac{V_2(V_2-\Omega r)}{U^2+V_2^2} \qquad \varphi_8 = \frac{U(V_2-\Omega r)}{U^2+V_2^2}$$

$$\varphi_9 = 2\cos^2\theta_1(\tan\theta_1-\tan\theta_2) \qquad \varphi_{10} = 2\cos^2\theta_1(\tan\theta_1-\tan\theta_2)\tan\theta_1$$

$$\varphi_{11} = \frac{U^2+V_2^2}{U^2+V_1^2} \qquad \varphi_{12} = \frac{V_1/(U^2+V_1^2)}{U/(U^2+V_2^2)} \qquad \varphi_{13} = \frac{V_2}{U}$$

$$\varphi_{14} = \frac{V_2(V_2-\Omega r)}{U^2+V_1^2} \qquad \varphi_{15} = \frac{V_1V_2}{U}\,\frac{V_2-\Omega r}{U^2+V_1^2} \qquad \varphi_{16} = \frac{V_2^2}{U}\,\frac{V_2-\Omega r}{U^2+V_2^2}$$

$$\varphi_{17} = \frac{U(V_1-\Omega r)}{U^2+V_1^2} + \frac{V_1U}{U^2+V_1^2}\,\frac{C_D}{\cos^2\beta_m} + \frac{1}{2}\,\frac{C_D'}{\cos^2\beta_m} - \frac{V_1\Omega r}{U^2+V_1^2}\,\frac{C_D'/\cos^2\beta_m}{2} + \frac{V_1V_2}{U}\,\frac{V_2-\Omega r}{U^2+V_1^2}$$

$$\varphi_{18} = 1 - \frac{V_1(V_1-\Omega r)}{U^2+V_1^2} + \frac{U^2}{U^2+V_1^2}\,\frac{C_D}{\cos^2\beta_m} - \frac{U\Omega r}{U^2+V_1^2}\,\frac{C_D'/\cos^2\beta_m}{2} + \frac{V_2(V_2-\Omega r)}{U^2+V_1^2}$$

$$\varphi_{19} = \varphi_{18} - 1 \qquad \varphi_{20} = 1 - 2\cos^2\theta_1(\tan\theta_1-\tan\theta_2)\tan\theta_1$$

$$\varphi_{S21} = \frac{U^2}{U^2+V_1^2}\,\frac{C_D}{\cos^2\beta_m} \qquad \varphi_{S22} = \frac{V_1 U}{U^2+V_1^2}\,\frac{C_D}{\cos^2\beta_m}$$

$$\varphi_{S23} = \frac{1}{2}\,\frac{C_D'}{\cos^2\beta_m} \qquad \varphi_{S24} = \frac{U\Omega r}{U^2+V_1^2}\,\frac{C_D'/\cos^2\beta_m}{2}$$

$$\varphi_{S25} = \frac{V_1\Omega r}{U^2+V_1^2}\,\frac{C_D'/\cos^2\beta_m}{2}$$

$$\varphi_{S26} = \frac{V_1(V_1-\Omega r)}{U^2+V_1^2} - \frac{U^2}{U^2+V_1^2}\,\frac{C_D}{\cos^2\beta_m} + \frac{U\Omega r}{U^2+V_1^2}\,\frac{C_D'/\cos^2\beta_m}{2}$$

$$\varphi_{S27} = \frac{U(V_1-\Omega r)}{U^2+V_1^2} + \frac{V_1 U}{U^2+V_1^2}\,\frac{C_D}{\cos^2\beta_m} + \frac{1}{2}\,\frac{C_D'}{\cos^2\beta_m} - \frac{V_1\Omega r}{U^2+V_1^2}\,\frac{C_D'/\cos^2\beta_m}{2}$$

$$\varphi_{S28} = \frac{U(V_2-\Omega r)}{U^2+V_2^2} + \frac{V_2^2}{U}\,\frac{V_2-\Omega r}{U^2+V_2^2}$$

APPENDIX IV

Description of the Computation (Programming)

The present theory was programmed, not as a unit, but rather as a main program and two auxiliary programs. The division exactly follows the development in the text. That is, the main body of the theory, consisting of the operations indicated in Section 2.3 exists as the main program. Both the Sears force and the Isaacs force occur as separate programs whose output, when operated on in the manner described in the test, serves as partial input for the main program. A description of these programs, together with sample or 'test' solutions appears as subsections of this appendix.

The computer was the M.I.T. Computation Center IBM 704 Electronic Data-Processing Machine.

A4.1 Main Body of the Present Theory

The block diagram for the computation is shown in Fig. 20. Each instruction is of course not listed but rather the general manner in which the computation proceeds is indicated.

The input information for this program is:

a) 51 y-equispaced values of H_1

b) 51 y-equispaced values of $-\frac{\Delta \tilde{f}_y}{\delta^0 s} - \delta^0_9 H_1$

c) 9 constants $\delta^0_9, \delta^0_{11}, \delta^0_{12}, \delta^0_{13}, \delta^0_{17}, \delta^0_{18}, \delta^0_{19}, \delta^0_{20}, \delta^0_{28}$

The output information is 51 y equispaced values of each of $\textcircled{H}_1$, $\textcircled{H}_2, \beta_1, \beta_2$ and H_2. Since the theory involves essentially only the finding of the complementary functions (integration) and the solving of linear

algebraic equations, it is easy to see that an alternate set of input information is

a) 51 y-equispaced values of H_1/U^2

b) 51 y-equispaced values of $-\frac{\Delta \mathcal{F}_Y}{\rho S U^2} - \varsigma_9^{\rho} \frac{H_1}{U^2}$

c) 9 constants $\varsigma_9^{\rho}, \varsigma_{11}^{\rho}, \varsigma_{12}^{\rho}, \varsigma_{13}^{\rho}, \varsigma_{17}^{\rho}, \varsigma_{18}^{\rho}, \varsigma_{19}^{\rho}, \varsigma_{20}^{\rho}, \varsigma_{28}^{\rho}$

With this input, the output information is 51 y-equispaced values of $\mathcal{H}_1/U^2$, $\mathcal{H}_2/U^2$, $\mathcal{P}_1/U^2$, $\mathcal{P}_2/U^2$ and H_2/U^2. The latter method was actually used. As indicated, the program stops after the last (y = 1.0) set of output is printed.

As is customary in machine computation, one checks to see that the programming is correct by using the program on a non-trivial problem whose answer is known, from hand computation or elsewhere. For this program the test solution was exactly the case illustrated in Fig. 26. The required blade force information, labelled (b) above was artificially supplied from a previous Rannie-Marble solution:

$$-\frac{\Delta \mathcal{F}_Y}{\rho S U^2} = \frac{\mathcal{H}_1}{U^2}\left(1-\varsigma_{10}^{\rho}\right) - \frac{\mathcal{H}_2}{U^2} + \varsigma_9^{\rho}\left(\frac{H_1}{U^2} - \frac{\mathcal{P}_1}{U^2}\right)$$

Therefore the test solution should be exactly that given in Fig. 26. This was the solution achieved.

A4.2 Sears Force

$v_r(y)$ is first determined from Rannie-Marble solution as follows:

$$-v_r = \tfrac{1}{2}\left[(\mu_{+0}\sin\beta_m + v_{+0}\cos\beta_m) + (\mu_{-0}\sin\beta_m + v_{-0}\cos\beta_m)\right]$$

$$= \tfrac{1}{2}\left[2\mu\sin\beta_m + (v_{+0} + v_{-0})\cos\beta_m\right]$$

$$= \tfrac{1}{2}\left[2\,\frac{U(H_2-\beta_2) - \Theta_2 V_2}{U^2+V_2^2}\sin\beta_m + \left(\frac{V_2(H_2-\beta_2)+U\Theta_2}{U^2+V_2^2} + \frac{V_1(H_1-\beta_1)+U\Theta_1}{U^2+V_1^2}\right)\cos\beta_m\right]$$

The mathematical statement of the problem may then be written

$$v_r(y) = \sum_{n=0}^{\infty} a_n \cos 2\pi n y \qquad \text{A4.2-1}$$

Then

$$\frac{\Delta F_{y v_r}}{\rho 2b\pi\omega_0\cos\beta_m} = \mathcal{R}\sum_{n=0}^{\infty} a_n S(nk_r) e^{in\omega_r t} \qquad \text{A4.2-2}$$

Let us let

$$S(nk_r) = A_n e^{iB_n}$$

Recalling that $\omega_r = \frac{2\pi}{\lambda}\Omega$ we then have, from A4.2-2,

$$\frac{\Delta F_{y v_r}}{\rho 2b\pi\omega_0\cos\beta_m} = \mathcal{R}\sum_{n=0}^{\infty} a_n A_n e^{i\left(2\pi\frac{\Omega}{\lambda}nt + B_n\right)}$$

$$= \mathcal{R}\sum_{n=0}^{\infty} a_n A_n e^{i(2\pi n y + B_n)}$$

$$= \sum_{n=0}^{\infty} a_n A_n \cos(2\pi n y + B_n)$$

However, it is not possible to represent by a cosine series such as A4.2-1 which has common period 1, a general function whose period is 1. Rather, to represent a function of period 1, we need cosines of common wave length 2.

Therefore, if we represent $v_r(y)$ as

$$v_r(y) = \sum_{n=0}^{\infty} C_n \cos n\pi y \qquad \text{A4.2-3}$$

the force expression will be given by

$$\frac{\Delta \bar{f}_{y_{v_r}}}{\rho 2b\pi w_0 \cos\beta_m} = \sum_{n=0}^{\infty} C_n S(n k_r) e^{i^\circ 2\pi n y} \qquad \text{A4.2-4}$$

Again, letting $S(k) = Ae^{iB}$, A4.2-4 becomes

$$\frac{\Delta \bar{f}_{y_{v_r}}}{\rho 2b\pi w_0 \cos\beta_m} = \sum_{n=0}^{\infty} C_n A_n \cos(\pi n y + B_n) \qquad \text{A4.2-5}$$

W_r is in general $\frac{2\pi}{\lambda}\Omega$. The fundamental non-dimensional frequency is

$$k_r = \frac{\omega_r b}{w_0} = \frac{2\pi\Omega(b/\lambda)}{w_0}$$

In the present experiments, the physical fundamental wave length was $\frac{2}{3}\pi$. However as previously discussed, the computation is carried out with twice this fundamental period. Therefore, for computation purposes,

$$k_r = \frac{2\pi\Omega\left(\frac{b}{4\pi/3}\right)}{w_0} = \frac{1.5\Omega b}{w_0}$$

The input for this program was thus

a) 51 y-equispaced values of $v_r(y)(v_r(o)....v_r(1))$

b) $\frac{2\pi\Omega(b/\lambda)}{w_o}$

c) $\pi w_o \cos\beta_m$

The output information was 51 y-equispaced values of $\frac{\Delta f_{y_{v_r}}}{\rho 2b}$. The test solution for this program is shown in Fig. 22. Twenty harmonics are used in the computation. As indicated in the block diagram, the values of A_n and B_n, indicated in A4.2-5, and characterizing the Sears function, were stored in memory and located, according to the frequency of the particular harmonic; by a table interpolation subroutine.

A4.3 Isaacs Force

$u_r(y)$ is first determined from the Rannie-Marble solution as follows:

$$u_r = \tfrac{1}{2}\left[(u_{+o}\cos\beta_m - v_{+o}\sin\beta_m) + (u_{-o}\cos\beta_m - v_{-o}\sin\beta_m)\right]$$

$$= \tfrac{1}{2}\left[2u\cos\beta_m - (v_{+o} + v_{-o})\sin\beta_m\right]$$

$$= \tfrac{1}{2}\left[2\,\frac{U(H_2-\beta_2) - \textcircled{H}_2 V_2}{U^2+V_2^2}\cos\beta_m - \left(\frac{V_2(H_2-\beta_2)+U\textcircled{H}_2}{U^2+V_2^2} + \frac{V_1(H_1-\beta_1)+U\textcircled{H}_1}{U^2+V_1^2}\right)\sin\beta_m\right]$$

We have seen that for $u_r = \sum_{n=1}^{\infty} D_n \sin 2\pi n y$

$$\frac{\Delta \mathcal{F}_y/\mu_r}{\rho\, 2b} = \pi \sin i_m \omega_0^2 \cos\beta_m \sum_{n=1}^{\infty} \left\{ \frac{1}{2}\left(\frac{D_n}{\omega_0}\right)^2 + \frac{D_n}{\omega_0}\left(\ell_{1n} + \frac{n}{2}\frac{2\pi\Omega b}{\omega_0}\right)\cos 2\pi n y + \right.$$

$$\left. \frac{D_n}{\omega_0}\left(\ell'_{1n} + 1 + \frac{1}{2}\left(\frac{D_n}{\omega_0}\right)^2\right)\sin 2\pi n y + \frac{D_n}{\omega_0}\ell_{2n}\cos 4\pi n y + \frac{D_n}{\omega_0}\ell'_{2n}\sin 4\pi n y \right\}$$

If, on the other hand, u_r is represented as

$$u_r = \sum_{n=1}^{\infty} E_n \cos n\omega_r t$$

then the force could be written

$$\frac{\Delta \mathcal{F}_y/\mu_r}{\rho\, 2b} = \pi \sin i_m \omega_0^2 \cos\beta_m \sum_{n=1}^{\infty} \left\{ \frac{1}{2}\left(\frac{E_n}{\omega_0}\right)^2 - \frac{E_n}{\omega_0}\left(\ell_{1n} + \frac{nk_r}{2}\right)\sin n\omega_r t + \right.$$

$$\left. \frac{E_n}{\omega_0}\left(\ell'_{1n} + 1 + \frac{1}{2}\left(\frac{E_n}{\omega_0}\right)^2\right)\cos n\omega_r t - \frac{E_n}{\omega_0}\ell_{2n}\sin 2n\omega_r t + \frac{E_n}{\omega_0}\ell'_{2n}\cos 2n\omega_r t \right\}$$

For present purposes, $k_r = \frac{\omega_r b}{\omega_0} = \frac{2\pi\Omega(b/\lambda)}{\omega_0} = \frac{2\pi\Omega\left(\frac{b}{2\pi/3}\right)}{\omega_0} = \frac{3\Omega b}{\omega_0}$

$$u_r = \sum_{n=1}^{\infty} E_n \cos 2\pi n y$$

$$\frac{\Delta \mathcal{F}_y/\mu_r}{\rho\, 2b} = \pi \sin i_m \omega_0^2 \cos\beta_m \sum_{n=1}^{\infty} \left\{ \frac{1}{2}\left(\frac{E_n}{\omega_0}\right)^2 - \frac{E_n}{\omega_0}\left(\ell_{1n} + \frac{n}{2}k_r\right)\sin 2\pi n y + \right.$$

$$\left. \frac{E_n}{\omega_0}\left(\ell'_{1n} + 1 + \frac{1}{2}\left(\frac{E_n}{\omega_0}\right)^2\right)\cos 2\pi n y - \frac{E_n}{\omega_0}\ell_{2n}\sin 4\pi n y + \frac{E_n}{\omega_0}\ell'_{2n}\cos 4\pi n y \right\}$$

Then if the u_r representation is

$$u_r = \sum_{n=1}^{\infty} \left(D_n \sin 2\pi n y + E_n \cos 2\pi n y \right)$$

with

$$\begin{cases} D_n = 2 \int_0^1 u_r \sin 2\pi n y \, dy \\ E_n = 2 \int_0^1 u_r \cos 2\pi n y \, dy \\ E_0 = \int_0^1 u_r \, dy = 0 \end{cases}$$

the force perturbation will be

$$\frac{\Delta \bar{f}_{y u_r}}{\rho 2b} = \pi \sin i_m^o \omega_0^2 \cos \beta_m \sum_{n=1}^{\infty} \left\{ \frac{1}{2} \left[\left(\frac{D_n}{\omega_0} \right)^2 + \left(\frac{E_n}{\omega_0} \right)^2 \right] + \right.$$

$$\frac{D_n}{\omega_0} \left(\bar{\ell}_{1n} + \frac{n}{2} \frac{2\pi\Omega b}{\omega_0} \right) \cos 2\pi n y - \frac{E_n}{\omega_0} \left(\ell_{1n} + \frac{n}{2} \frac{2\pi\Omega b}{\omega_0} \right) \sin 2\pi n y +$$

$$\frac{D_n}{\omega_0} \left(\bar{\ell}'_{1n} + 1 + \frac{1}{2} \left(\frac{D_n}{\omega_0} \right)^2 \right) \sin 2\pi n y + \frac{E_n}{\omega_0} \left(\ell'_{1n} + 1 + \frac{1}{2} \left(\frac{E_n}{\omega_0} \right)^2 \right) \cos 2\pi n y +$$

$$\left. \frac{D_n}{\omega_0} \bar{\ell}_{2n} \cos 4\pi n y - \frac{E_n}{\omega_0} \ell_{2n} \sin 4\pi n y + \frac{D_n}{\omega_0} \bar{\ell}'_{2n} \sin 4\pi n y + \frac{E_n}{\omega_0} \ell'_{2n} \cos 4\pi n y \right\}$$

Thus the input information for this program is

a) 51 y-equispaced values of u_r ($u_r(o)....u_r(1)$)

b) $2/w_o$

c) $\frac{2\pi\Omega(b/\lambda)}{w_o}$

d) $\pi \sin i_m w_o^2 \cos\beta_m$

The output information is 51 y-equispaced values of $\frac{\Delta f_{y/\mu_r}}{\rho^2 b}$

The block diagram of the computation is shown in Fig. 23. As the reader may suspect, this presented a formidable programming effort, even compared to the other three programs in this report. Part of the complication, as may be seen from the governing equations is that the size of the perturbation u_r here enters in a much more complicated fashion than does the corresponding quantity v_r in the Sears force computation. In the latter computation we could characterize both size of lift and phase by k_r (with v_r entering as a simple multiplicative factor); in the Isaacs force computation, k_r and u_r together determine size of lift and phase. Therefore, whereas in the Sears force computation we needed only a single interpolation at a time, now we need a double interpolation for <u>each</u> lmn. The use of the double interpolation subroutine is indicated in the block diagram. Since this subroutine takes about 1 second for the order of interpolation used (first order) in each of the primary and secondary variables*, it was decided to economize on computer time by taking only 10 harmonics, compared with 20 in the Sears force computation. This is apparent in the test solution, Fig. 24.

The l_m's and l'_m's indicated in equation 33 were all computed by hand, stored in memory and extracted, as discussed, by the double

*Compare with the time required to find a sin or cos, using sin, cos subroutine UAS+C1: 3 milliseconds.

interpolation subroutine according to the u_r and k_r in question.

A4.4 Rannie-Marble Theory

The complete theory of Rannie and Marble is given in Ref. 6. In that theory, as mentioned elsewhere, the boundary condition β_2 = constant or a variation thereof is used. Therefore the theory is much like that presented in Section 2.1. The programming therefore is also quite similar. The block diagram is shown in Fig. 25; the test solution appears in Fig. 26.

The input information for this program is

a) 51 y-equispaced values of H_1

b) 5 constants:

$$A_r = -\frac{\Omega r - V_1}{U} + P_r'$$

$$B_r = -\frac{(\Omega r - V_1)^2 + (\Omega r - V_2)^2}{U \Omega r} + \frac{\Omega r - V_1}{U} + 2\frac{U P_r}{\Omega r} - P_r'$$

$$\alpha_r = \frac{V_1}{U}$$

$$\beta_r = -\frac{U^2 + V_1^2}{U \Omega r}$$

$$\gamma_r = -\frac{U^2 + V_2^2 - \Omega r V_2}{U \Omega r}$$

P is here a known function of $\tan\beta_1$, which describes the total pressure loss as defined by

$$\Delta P_T = \rho (U+\mu)^2 P(\tan\beta_1)$$

$$P_r' = \frac{dP_r}{d\tan\beta_1}$$

In both the Rannie-Marble theory and the present theory, losses were always taken to be zero. Some idea of the effect of assuming finite losses may be implied from Ref. 26.

The output information is 51 y-equispaced values of $\beta_1, \beta_2, \Theta_1, \Theta_2,$ and H_2.

For the same reasons set forth in A4.1 it is permissible to use H_1/U^2 instead of H_1 in the input. Then the output will be $\beta_1/U^2, \beta_2/U^2, \Theta_1/U^2, \Theta_2/U^2, H_2/U^2$.

APPENDIX V

Determination of i_m and A

The theory has been written for an uncambered flat plate airfoil; the experiments were conducted using airfoils of considerable camber: NACA 65-(12)10 airfoils.

In accounting for this effect, the effect of airfoil thickness, and also the effect of neighboring blades, the lift of the cascade has been represented by

$$\frac{C_L}{2\pi} = A \sin(\alpha_m - \phi) = A \sin i_m^\circ$$

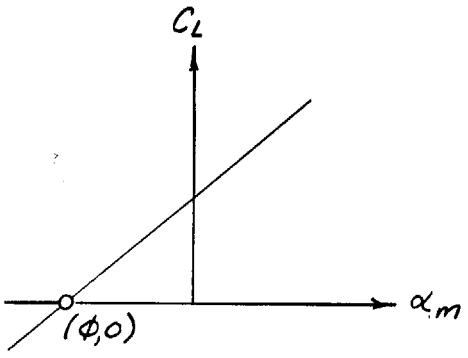

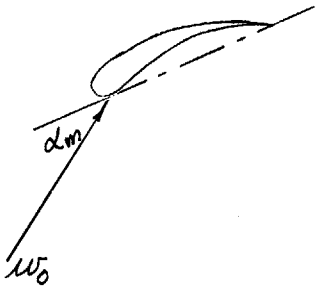

The value of ϕ may be found from linearly interpolating the results of tests of the present airfoils, described in Ref. 29, at the appropriate solidity and stagger.

For the case 2b/s = 1.05, $\lambda = 52.7^\circ$, ϕ was found to be -8°. For the case 2b/s = 0.525, $\lambda = 52.7^\circ$, ϕ was found to be -5.5°.

The value of A may be determined from the mean flow as follows:

$$\mathcal{F}_y = \rho S U (V_2 - V_1) = L \cos \beta_m$$

$$C_L = 2\pi \sin(\alpha_m - \phi) = \frac{L}{\frac{1}{2}\rho (2b) w_0^2}$$

Then

$$A = \frac{U(V_2 - V_1)}{\left(\frac{2b}{S}\right) \pi \sin(\alpha_m - \phi) w_0^2 \cos \beta_m}$$

The value of A in each experiment conducted is shown in Fig. 14.

LIST OF SYMBOLS

x	(distance normal to the plane of the cascade)/$r\lambda$
y	(distance measured in the direction of the wheel speed vector)/$r\lambda$
r	radial coordinate
U	x direction component of mean velocity
V	y direction component of mean velocity
P	mean pressure
u	x direction velocity perturbation
v	y direction velocity perturbation
p	perturbation in pressure
ρ	density
θ	direction of flow, absolute coordinate system
β	direction of flow, relative coordinate system
Ωr	rotor speed
λ	primary wave length (radians) of the distortion
s	blade spacing
$2b$	length of the blade chord
t	time
ζ	a constant
H	$p/\rho + Uu + Vv$
$\mathcal{P}$	p/ρ
$\mathcal{H}$	$Uv - Vu$
i	incidence
w_o	mean relative flow velocity

$\bar{u}$	$\frac{1}{2}(u_{+o} + u_{-o})$
$\bar{v}$	$\frac{1}{2}(v_{+o} + v_{-o})$
u_r	perturbation in velocity in the direction of the mean relative velocity vector
v_r	perturbation in velocity normal to the mean relative velocity vector
ω	circular frequency, radians/sec
ω_r	fundamental circular frequency
k	non-dimensional frequency = $\frac{\omega b}{w_o}$
k_r	fundamental non-dimensional frequency = $\frac{\omega_r b}{w_o}$
C_D	drag coefficient = $\frac{\text{drag loss}}{1/2\rho w_o^2}$
$\mathcal{F}_y$	mean value of the force acting on the blade in the y direction
$\Delta \mathcal{F}_y$	perturbation to $\mathcal{F}_y$
L	lift
L_o	lift corresponding to w_o
L_E	'elementary' lift (virtual mass and wake effects are neglected)
σ	u_r/w_o
C(k)	Theodorsen function; $C(k) = F(k) + iG(k) = \frac{K_1(ik)}{K_o(ik) + K_1(ik)}$
F(k)	$\mathcal{R}\, C(k)$
G(k)	$\mathcal{I}\, C(k)$
$\mathcal{R}$	real part
$\mathcal{I}$	imaginary part
K_o, K_1	modified Bessel functions of the second kind
S(k)	Sears function = $\frac{1}{ik[K_o(ik) + K_1(ik)]}$
i	$\sqrt{-1}$
n	index

A_n	modulus of S(nkr), $A_n = \|S(nkr)\|$
B_n	angular coordinate of S(nkr), $S(nkr) = A_{ne}^{iBn}$
$\bar{l}_m$, $\bar{l}'_m$	coefficients in the Isaacs force, associated with sin Fourier terms
l_m, l'_m	coefficients in the Isaacs force, associated with cos Fourier terms
m	index
ϕ	velocity potential, also angle defined in Appendix V
Φ	complex potential
z	complex coordinate, z = x + iy
Π	infinite product
η	auxiliary variable
Re_{2b}	Reynolds number based on blade chord
A	lattice coefficient

Subscripts

1	just upstream of the cascade, (o-, y)
2	just downstream of the cascade, (o+, y)
$-\infty$	$(-\infty, y)$
$+\infty$	$(+\infty, y)$
$(\ )^*$	complementary function
c	cycle
m	mean

BIBLIOGRAPHY

1.) Ehrich, Fredric F.
"Circumferential Inlet Distortions in Axial Flow Turbomachinery", Journal of the Aeronautical Sciences, June 1957.

2.) Ashby, George C. Jr.
"Investigation of the Effect of Velocity Diagram on Inlet Total-Pressure Distortions through Single Stage Subsonic Axial Flow Compressors", NACA RML57A03, April 17, 1957.

3.) English, Robert E. and Yohner, Peggy L.
"Theoretical Analysis of One-Stage Windmills for Reducing Flow Distortion, " NACA RME57D05, June 12, 1957.

4.) Smith, Leroy H. Jr.
"Recovery Ratio-A Measure of the Loss Recovery Potential of Compressor Stages", ASME Paper No. 56-A-206 (Presented at Annual Meeting, New York, Nov. 25-30, 1956.

5.) Alford, J. S.
"Inlet Flow Distortion Index", paper presented at International Days of Aeronautical Sciences, Paris, France, May 1957.

6.) Rannie, W. D. and Marble, F. E.
"Unsteady Flows in Axial Turbomachines", paper presented at International Days of Aeronautical Sciences, Paris, France, May 1957.

7.) Alford, J. S.
"Inlet Duct-Engine Flow Compatibility", Institute of Aeronautical Sciences, Preprint No. 566, June 1955.

8.) Murphy, J. S. and Clutter, D. W.
"Investigation of the Effectiveness of a Windmill for Improving Flow Uniformity in a Duct", Report No. ES26393, Douglas Aircraft Co., Inc., El Segundo, Calif., Oct. 8, 1957.

9.) Von Karman, Theodore and Tsien, Hsue-Shen
"Lifting Line Theory for a Wing in Non-Uniform Flow", Quarterly of Applied Mathematics, Volume 3, No. 1, April 1945.

10.) Sears, W. R.
"Some Aspects of Non-Stationary Airfoil Theory and its Practical Application", Journal of the Aeronautical Sciences, Vol. 8, No. 3, 1941.

11.) Sears, W. R.
"Operational Methods in the Theory of Airfoils in Non-Uniform Motion", Journal of the Franklin Institute, Vol. 230, No. 1, 1940.

12.) Meyer, R. X.
"The Effects of Wakes on the Transient Pressure and Velocity Distributions in Turbomachines", ASME Paper No. 57-A-83, 1957.

13.) Kemp, N. H. and Sears, W. R.
"Aerodynamic Interference between Moving Blade Rows", Journal of the Aeronautical Sciences, Vol. 20, No. 9, 1953.

14.) Kemp, N. H. and Sears, W. R.
"The Unsteady Forces Due to Viscous Wakes in Turbomachines", Journal of the Aeronautical Sciences, Vol. 22, No. 7, 1955.

15.) Kemp, N. H.
"On the Lift and Circulation of Airfoils in some Unsteady Flow Problems", Journal of the Aeronautical Sciences, Vol. 19, No. 10, 1952.

16.) Goethert, Bernhard H.
"Some Selected Problems in Engine Altitude Testing", Arnold Engineering Development Center, U.S.A.F., Oct. 1958.

17.) Isaacs, Rufus
"Airfoil Theory for Flows of Variable Velocity", Journal of the Aeronautical Sciences, Vol. 12, No. 1, 1945.

18.) Sears, W. R.
"On Asymmetric Flow in an Axial Flow Compressor Stage", ASME paper No. 52-F-15, 1952.

19.) Turner, R. C., Ritchie, J. and Moss, C. E.
"The Effect of Inlet Circumferential Maldistribution on an Axial Compressor Stage", Aeronautical Research Council Reports and Memoranda, No. 3066, London, 1958.

20.) Woods, L. C.
"On Unsteady Flow through a Cascade of Airfoils", Proc. Royal Society (A), Vol. 228, 1955.

21.) Carter, Frank R.
"Circumferential Inlet Distortions in an Axial Flow Compressor", S.M. Thesis, Department of Aeronautical Engineering, M.I.T., May 1958.

22.) Yeh, Hsuan and Eisenhuth, J. J.
"The Unsteady Wake Interaction in Turbomachinery and its Effect on Cavitation", ASME paper No. 58-A-114, July 1958.

23.) Lane, Frank, and Friedman, Manfred
"Theoretical Investigation of Subsonic Oscillatory Blade-Row Aerodynamics", NACA TN 4136, Feb. 1958.

24.) Shinbaum, Marvin S.
"Circumferential Distortion of the Inlet Flow in an Axial Compressor", S.M. Thesis, Department of Aeronautical Engineering, M.I.T., May 1959.

25.) Horlock, J. H.
"Instrumentation used in Measurement of the Three-Dimensional Flow in an Axial Flow Compressor", Aeronautical Research Council Current Paper, No. 321, London, March 1955.

26.) Katz, R.
"Performance of Axial Compressors with Asymmetric Inlet Flows", Ph.D. Thesis, Calif. Inst. of Tech., 1958.

27.) Yeh, Hsuan
"The Sears Function in Unsteady Flows", Journal of the Aeronautical Sciences, July 1957.

28.) Mellor, George L. Jr.
"The Aerodynamic Performance of Axial Compressor Cascades with Application to Machine Design", Gas Turbine Laboratory Report No. 38, Feb. 1957.

29.) Herrig, L. J., Emery, J. C. and Erwin, J. R.
"Systematic Two-Dimensional Cascade Tests of NACA 65-Series Compressor Blades at Low Speeds", NACA RM L51G31, 1951.

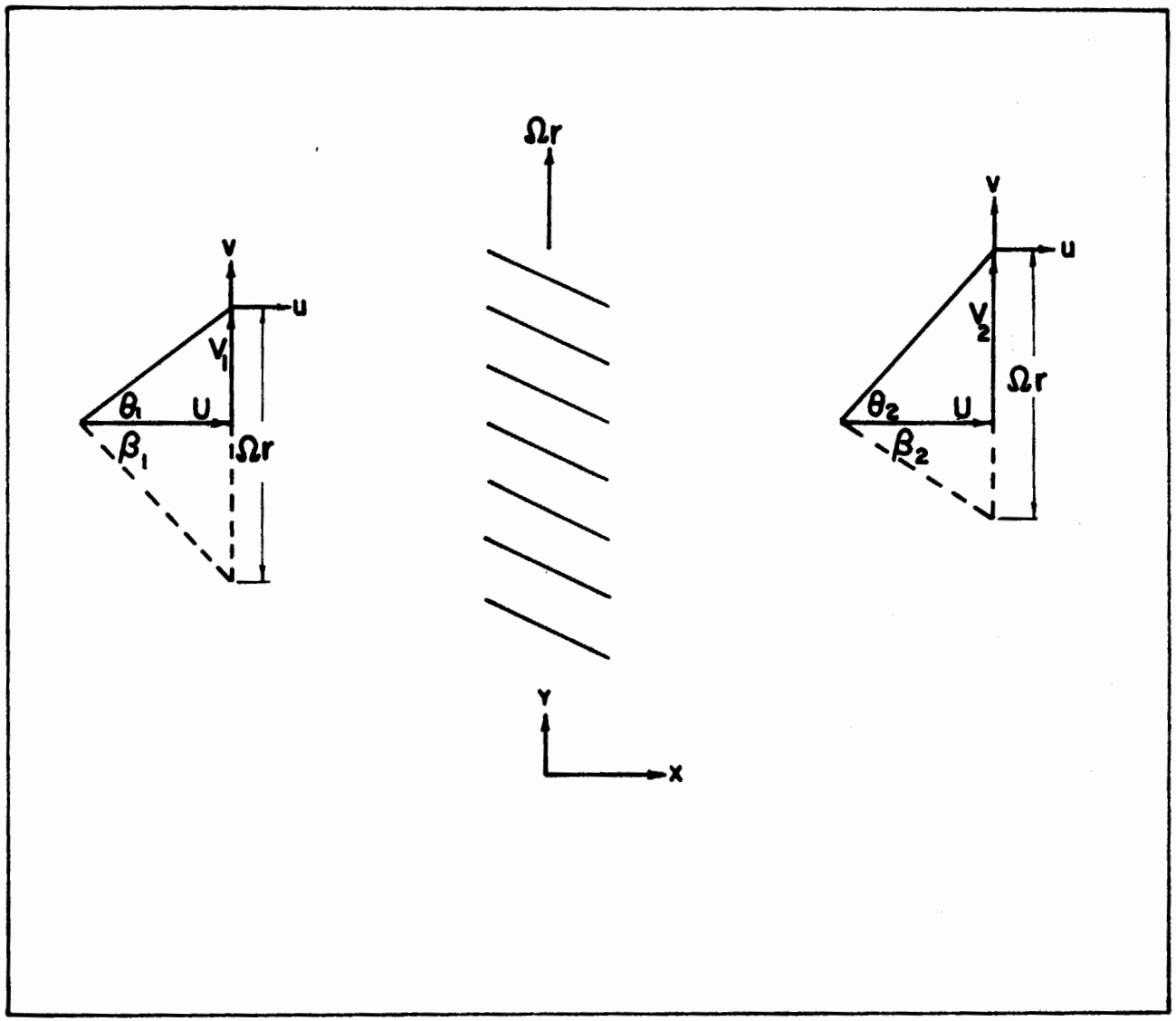

FIG. I COORDINATES AND NOTATION

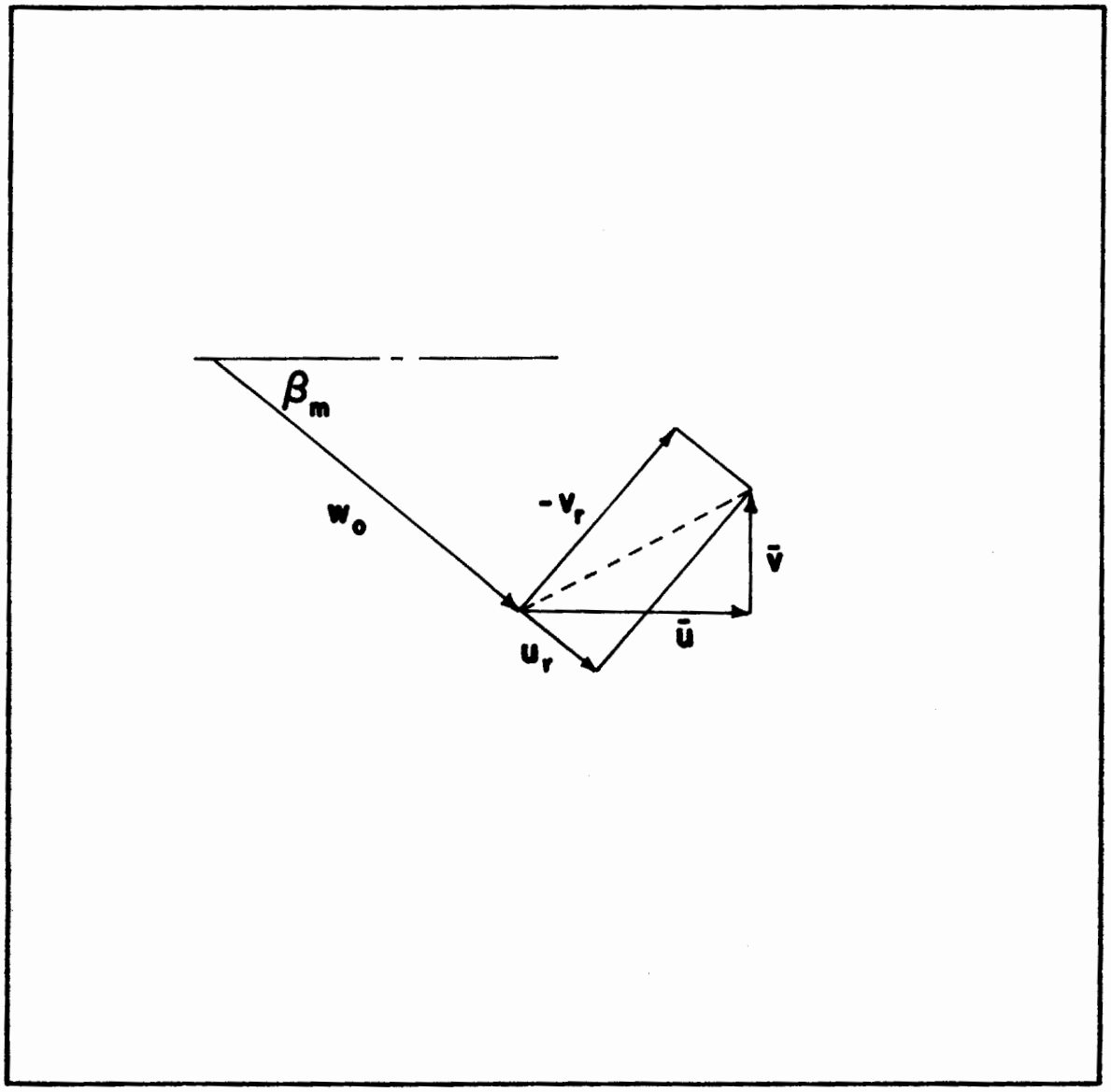

FIG. 2 DEFINITION OF u_r, v_r

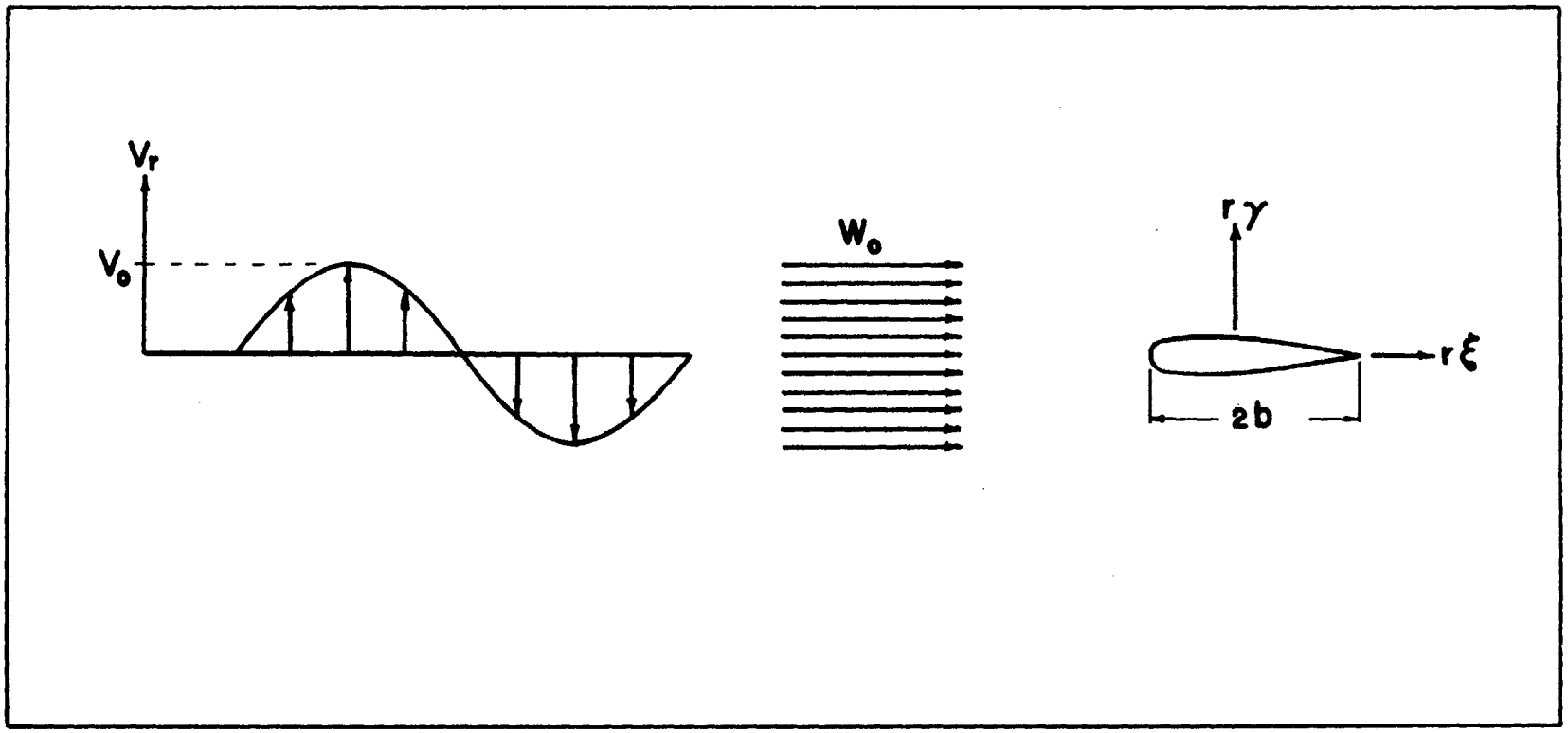

FIG.3 AIRFOIL IN A SINUSOIDAL UPWASH

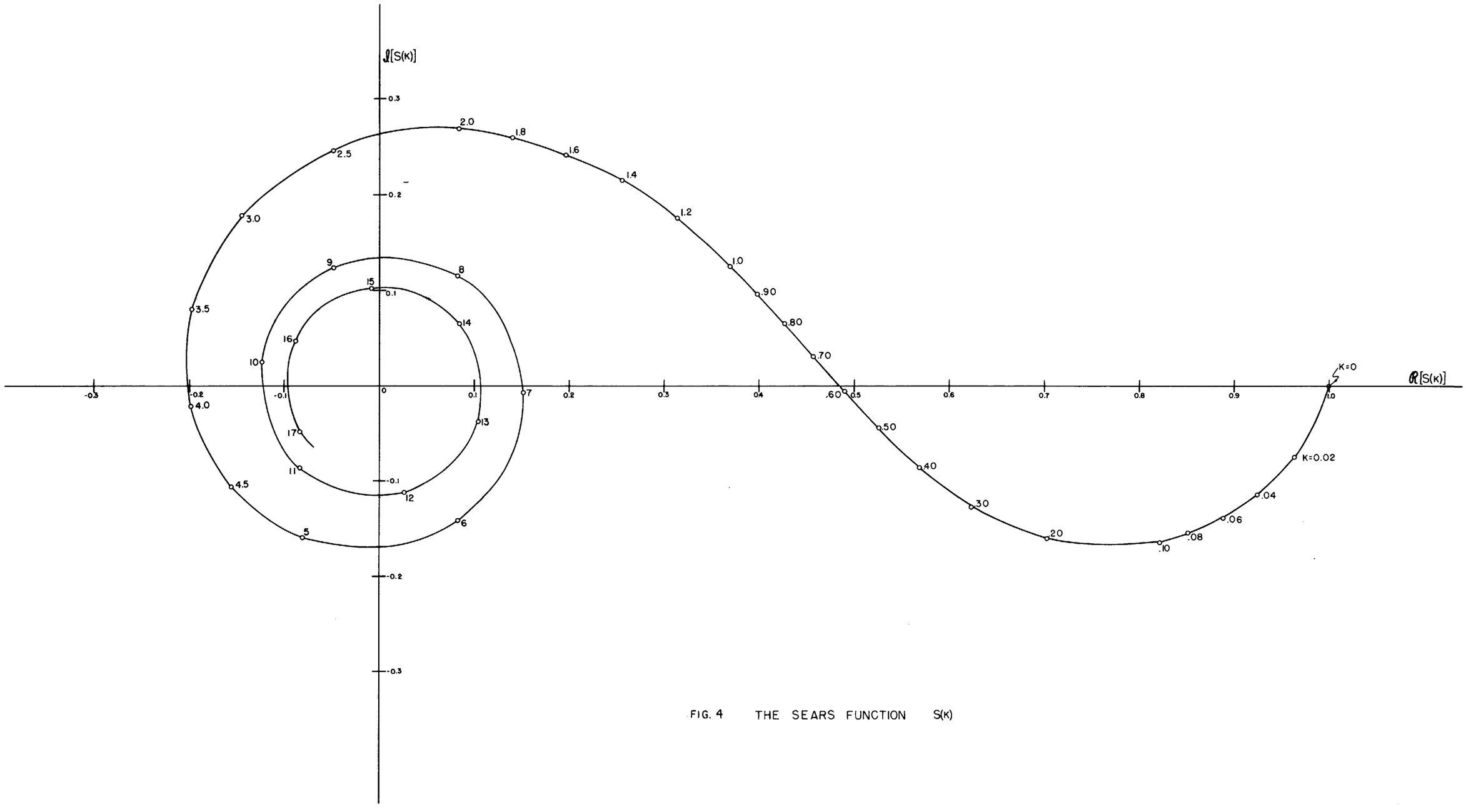

FIG. 4 THE SEARS FUNCTION S(K)

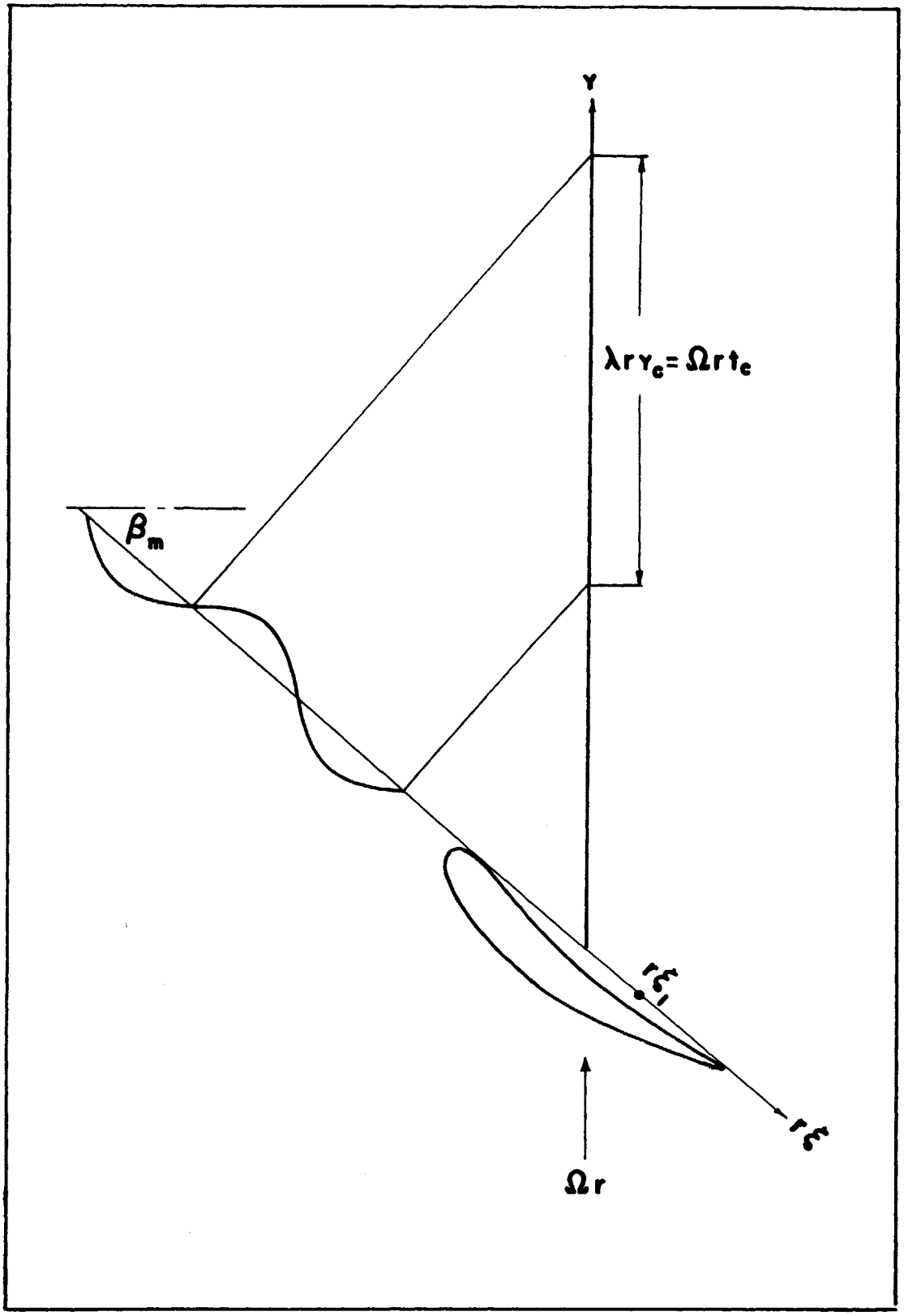

FIG.5 THE RELATIONSHIP BETWEEN Y, t, ξ

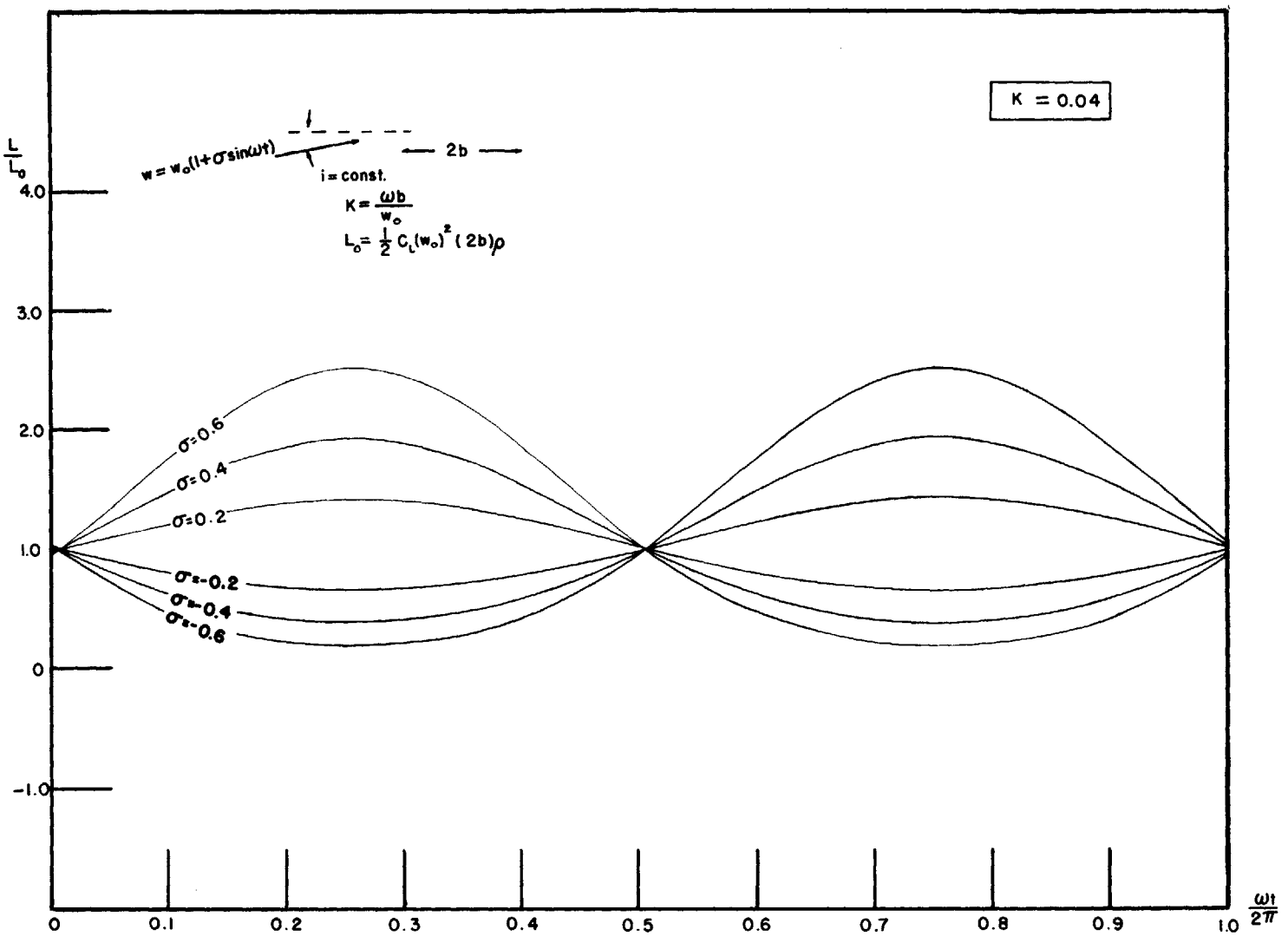

FIG. 6-1 BLADE LIFT FOR FLOWS OF VARIABLE VELOCITY

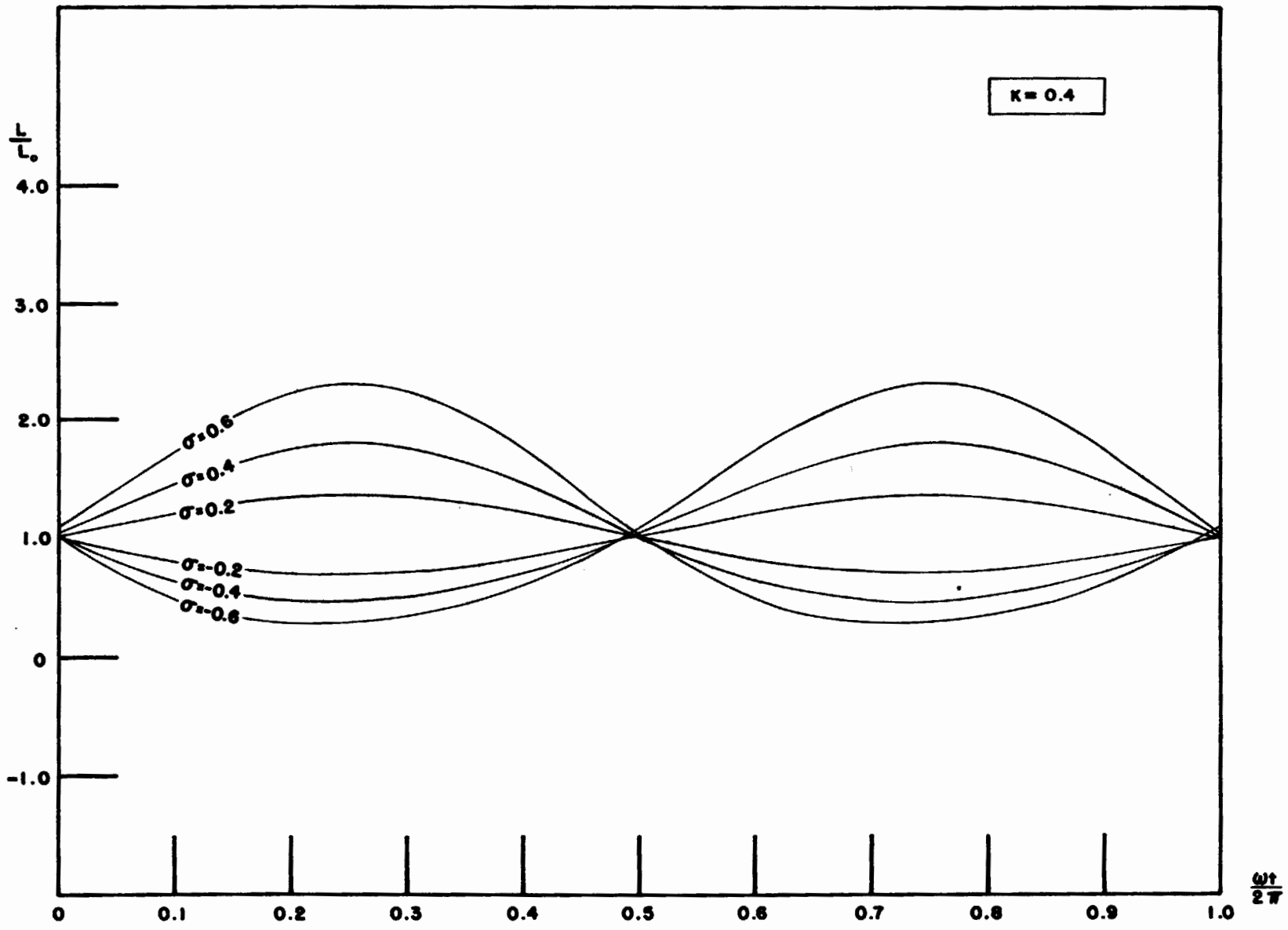
K= 0.4
L/L₀
4.0
3.0
2.0
1.0
0
-1.0
σ=0.6
σ=0.4
σ=0.2
σ=-0.2
σ=-0.4
σ=-0.6
0
0.1
0.2
0.3
0.4
0.5
0.6
0.7
0.8
0.9
1.0
ωt/2π

FIG. 6-2

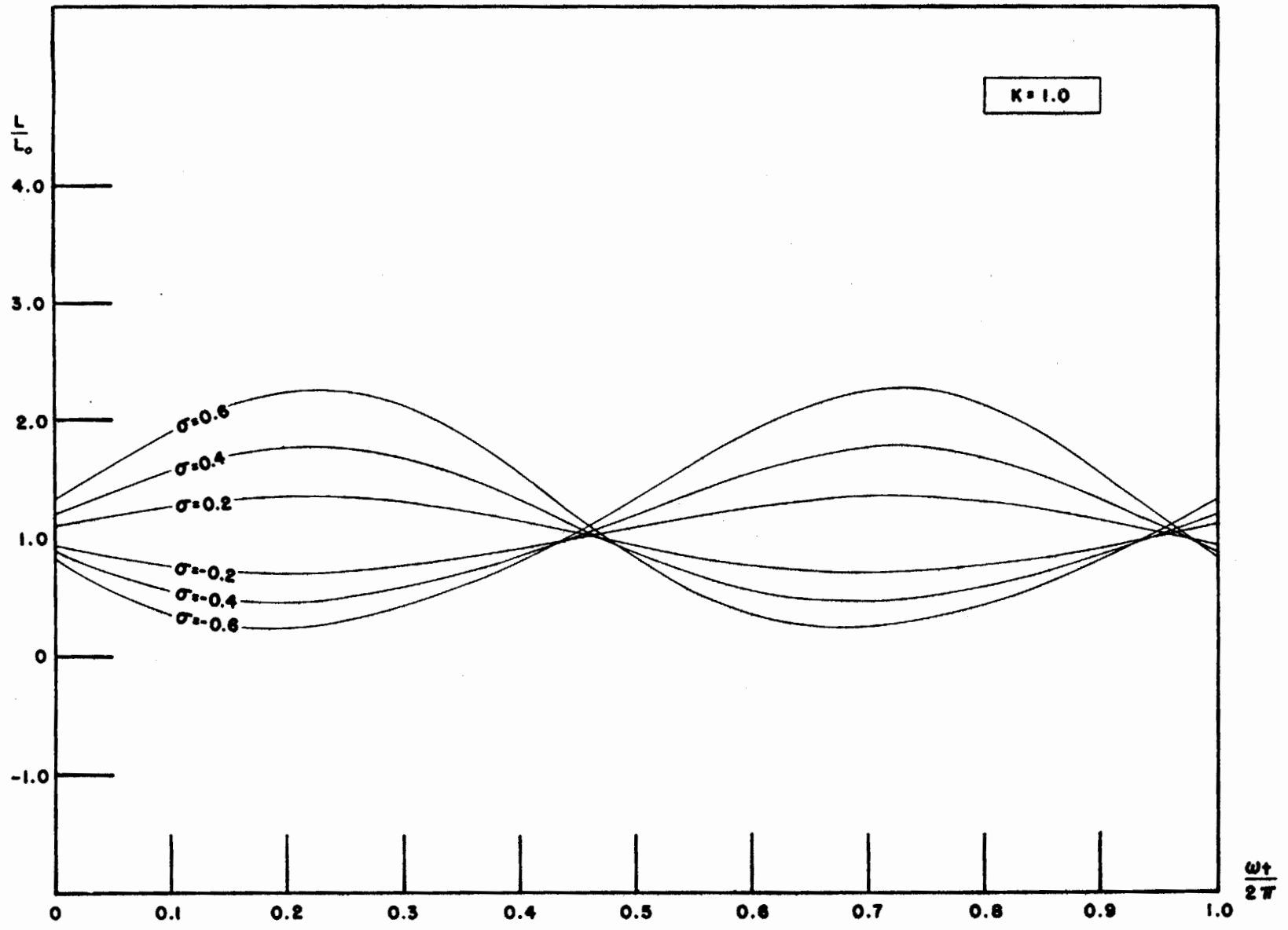
K = 1.0
L/L₀
4.0
3.0
2.0
1.0
0
-1.0
σ=0.6
σ=0.4
σ=0.2
σ=-0.2
σ=-0.4
σ=-0.6
0
0.1
0.2
0.3
0.4
0.5
0.6
0.7
0.8
0.9
1.0
ωt/2π

FIG. 6-3

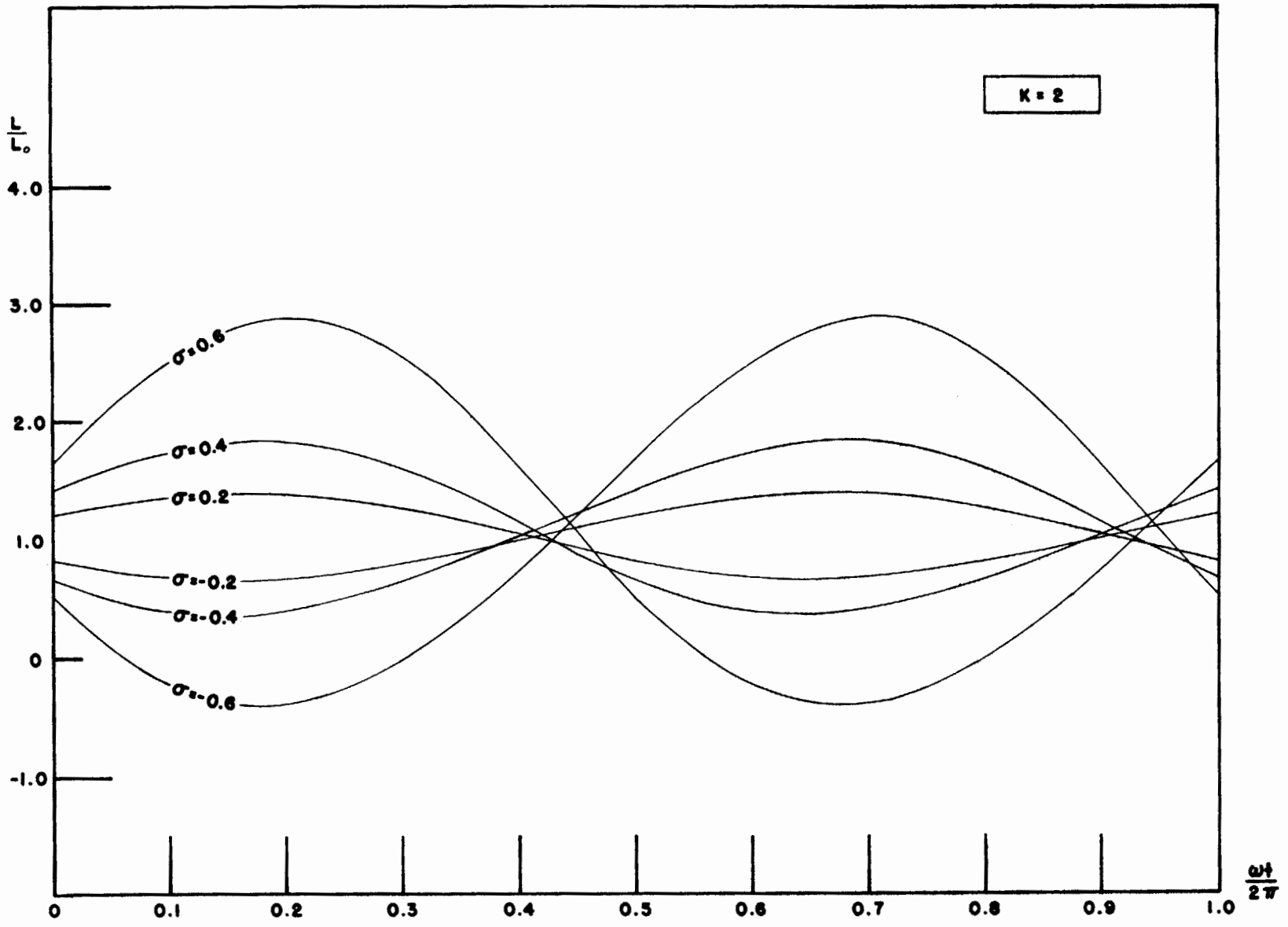
K = 2
L/L₀
4.0
3.0
2.0
1.0
0
-1.0
σ=0.6
σ=0.4
σ=0.2
σ=-0.2
σ=-0.4
σ=-0.6
0
0.1
0.2
0.3
0.4
0.5
0.6
0.7
0.8
0.9
1.0
ωt/2π

FIG. 6-4

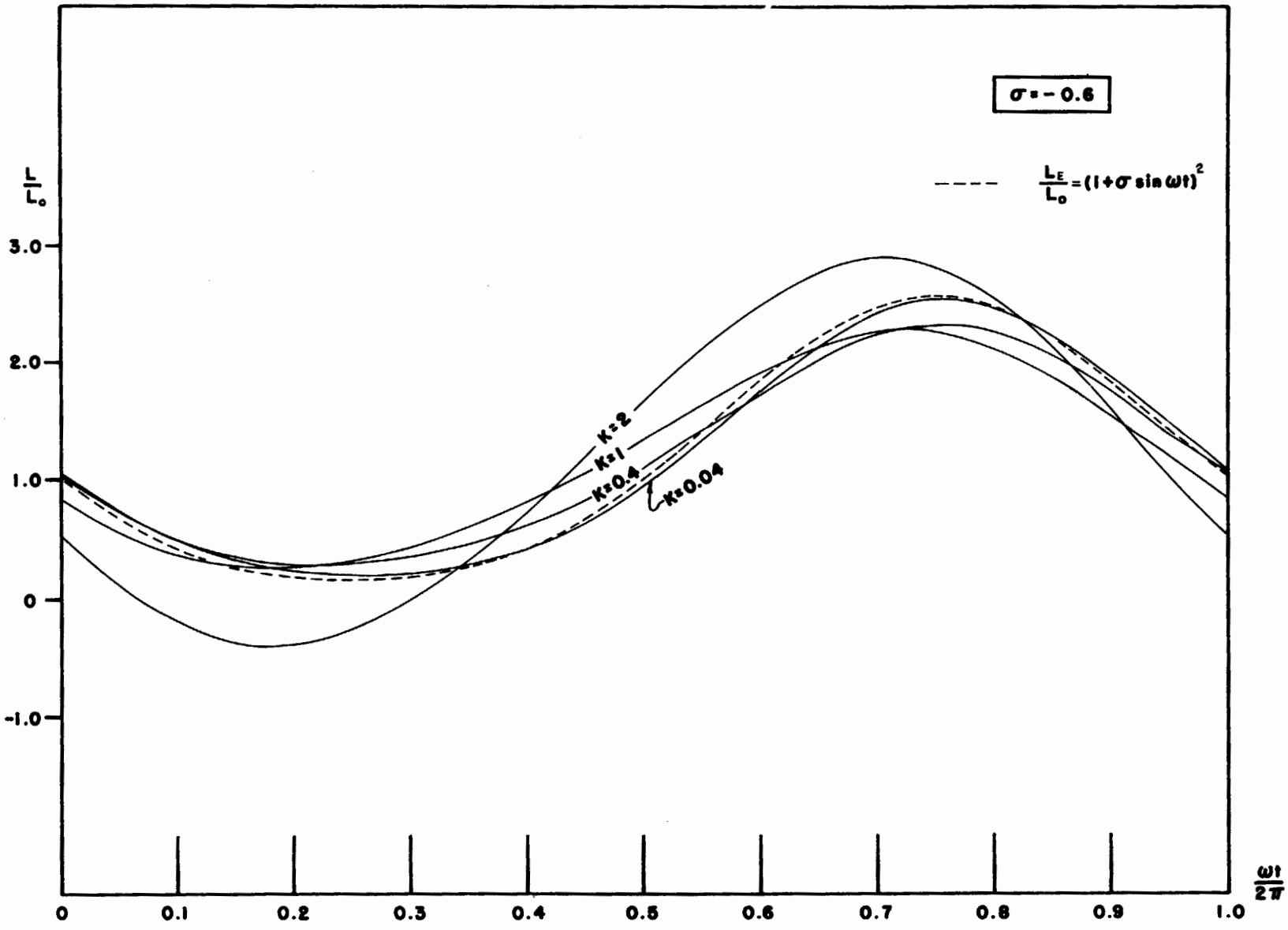
σ = - 0.6
L/L₀
L_E/L₀ = (1+σ sin ωt)²
3.0
2.0
1.0
0
-1.0
K=2
K=1
K=0.4
K=0.04
0
0.1
0.2
0.3
0.4
0.5
0.6
0.7
0.8
0.9
1.0
ωt/2π

FIG. 6-5

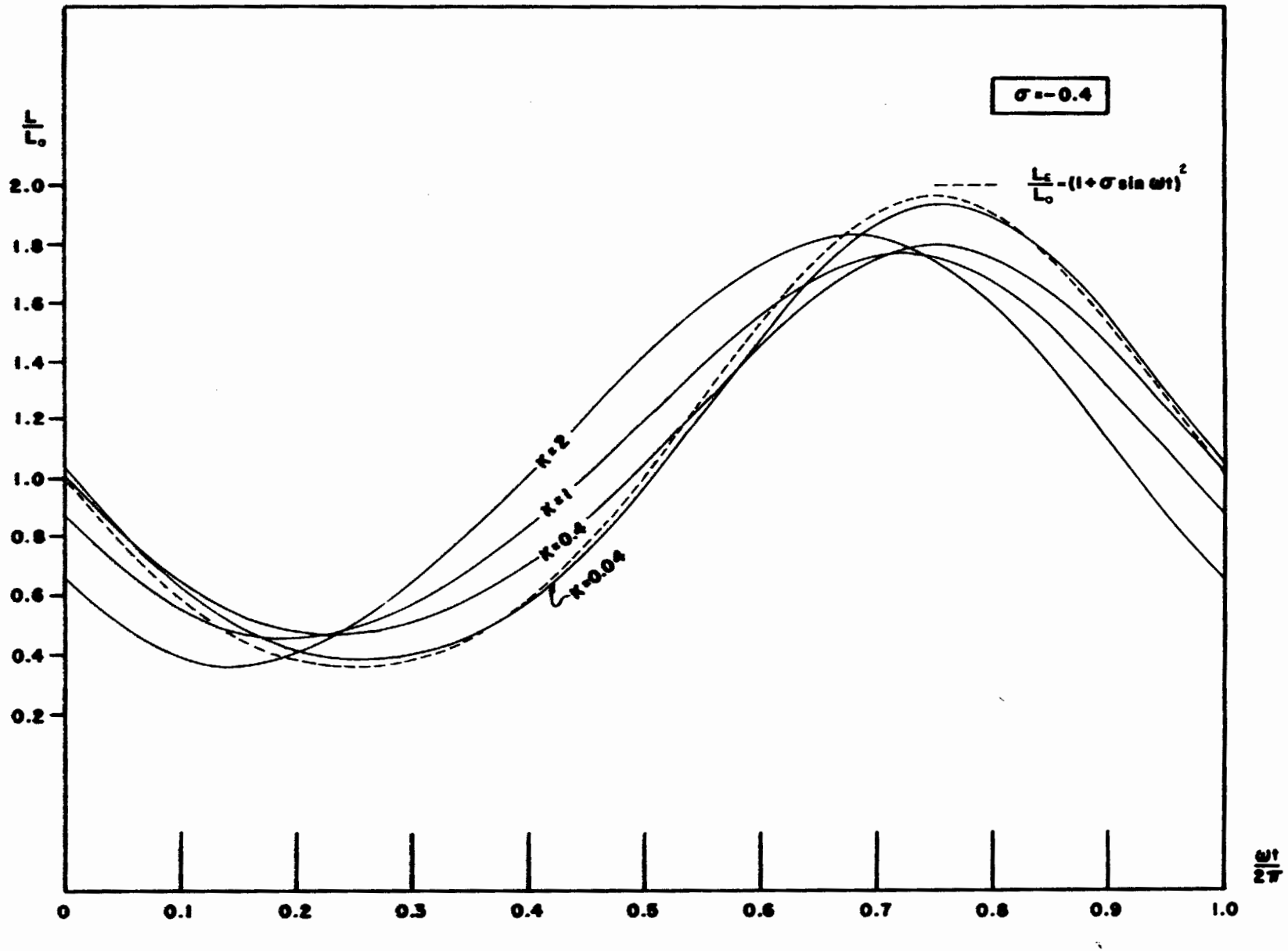
σ = -0.4
L/L₀
Lε/L₀ = (1 + σ sin ωt)²
K=2
K=1
K=0.4
K=0.04
2.0
1.8
1.6
1.4
1.2
1.0
0.8
0.6
0.4
0.2
0
0.1
0.2
0.3
0.4
0.5
0.6
0.7
0.8
0.9
1.0
ωt/2π

FIG. 6-6

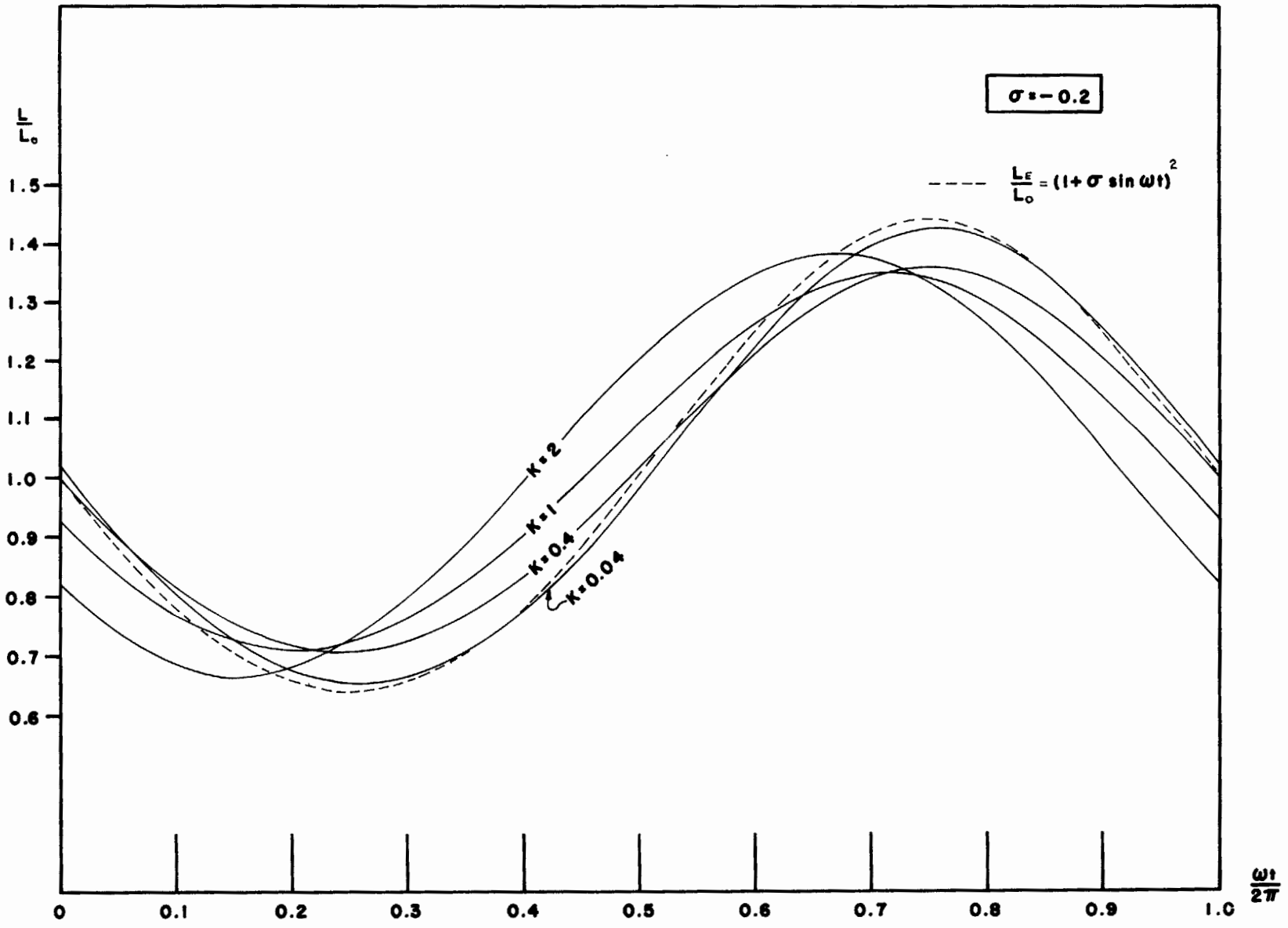
σ = −0.2
$\frac{L_\varepsilon}{L_o} = (1+\sigma \sin \omega t)^2$
$\frac{L}{L_o}$
1.5
1.4
1.3
1.2
1.1
1.0
0.9
0.8
0.7
0.6
K=2
K=1
K=0.4
K=0.04
0
0.1
0.2
0.3
0.4
0.5
0.6
0.7
0.8
0.9
1.0
$\frac{\omega t}{2\pi}$

FIG. 6-7

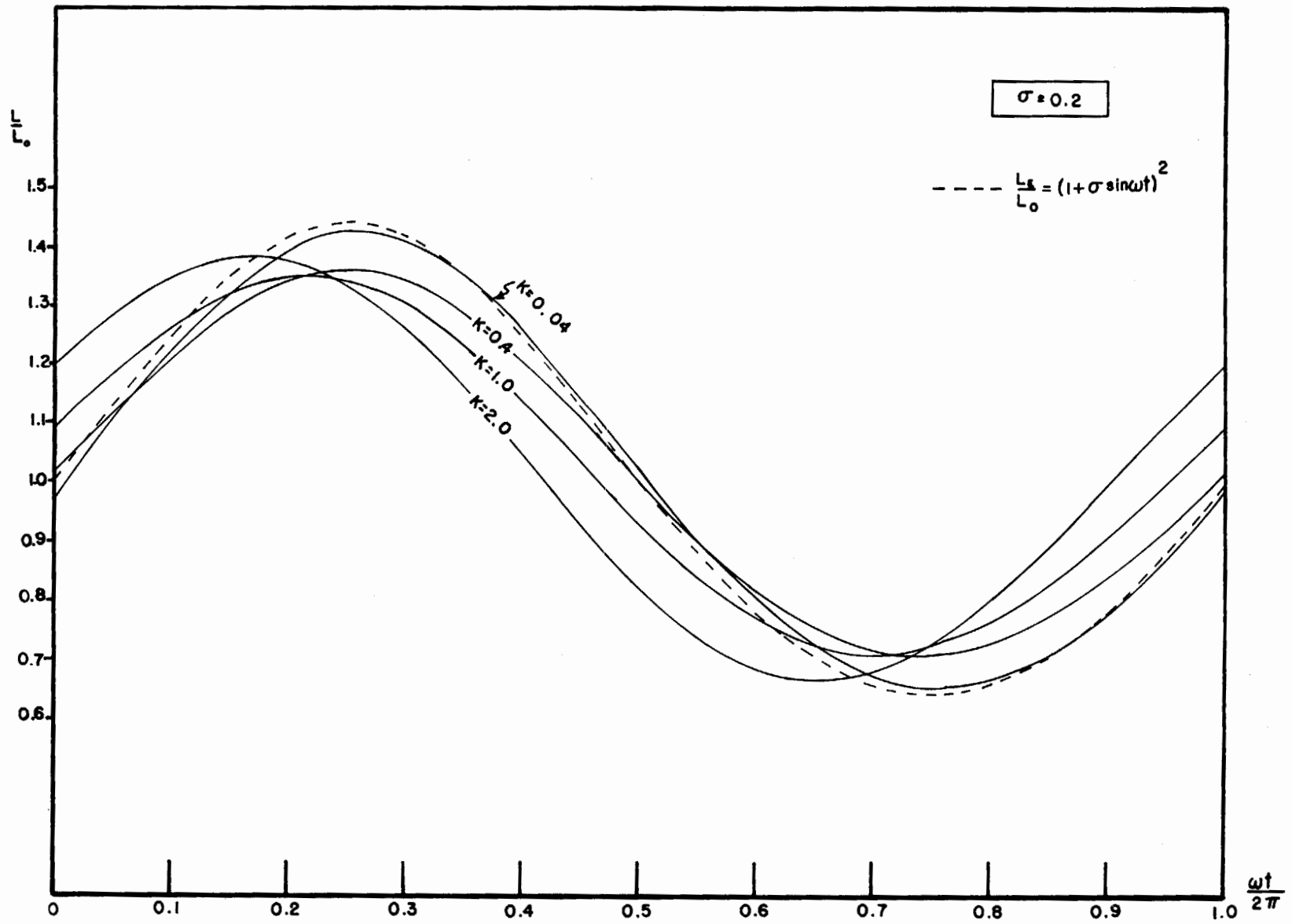
σ = 0.2
$\frac{L_s}{L_o} = (1+\sigma \sin\omega t)^2$
K=0.04
K=0.4
K=1.0
K=2.0
$\frac{L}{L_o}$
1.5
1.4
1.3
1.2
1.1
1.0
0.9
0.8
0.7
0.6
0
0.1
0.2
0.3
0.4
0.5
0.6
0.7
0.8
0.9
1.0
$\frac{\omega t}{2\pi}$

FIG. 6-8

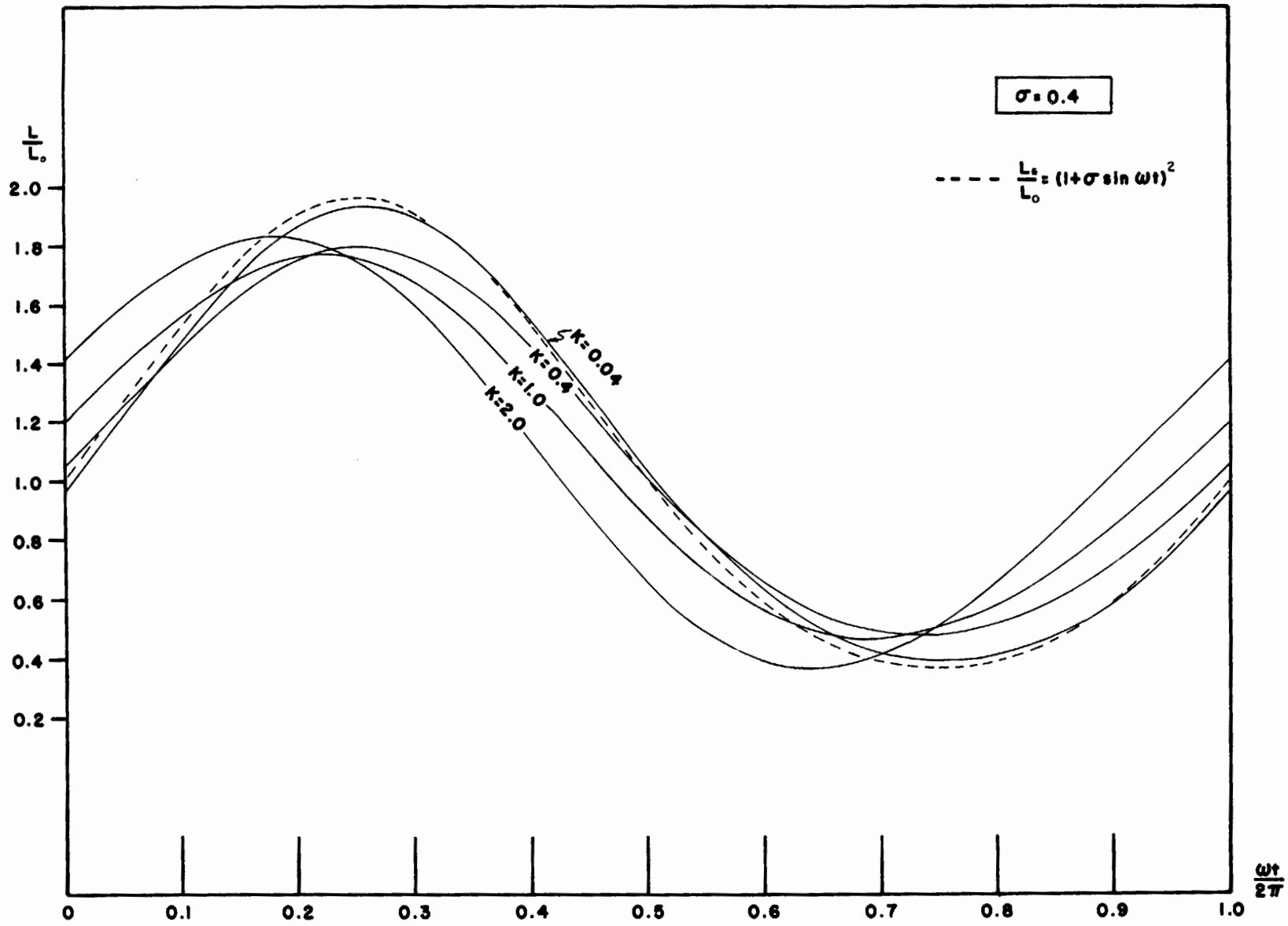
σ = 0.4
L/L₀ = (1+σ sin ωt)²
L/L₀
2.0
1.8
1.6
1.4
1.2
1.0
0.8
0.6
0.4
0.2
K=0.04
K=0.4
K=1.0
K=2.0
0
0.1
0.2
0.3
0.4
0.5
0.6
0.7
0.8
0.9
1.0
ωt/2π

FIG. 6-9

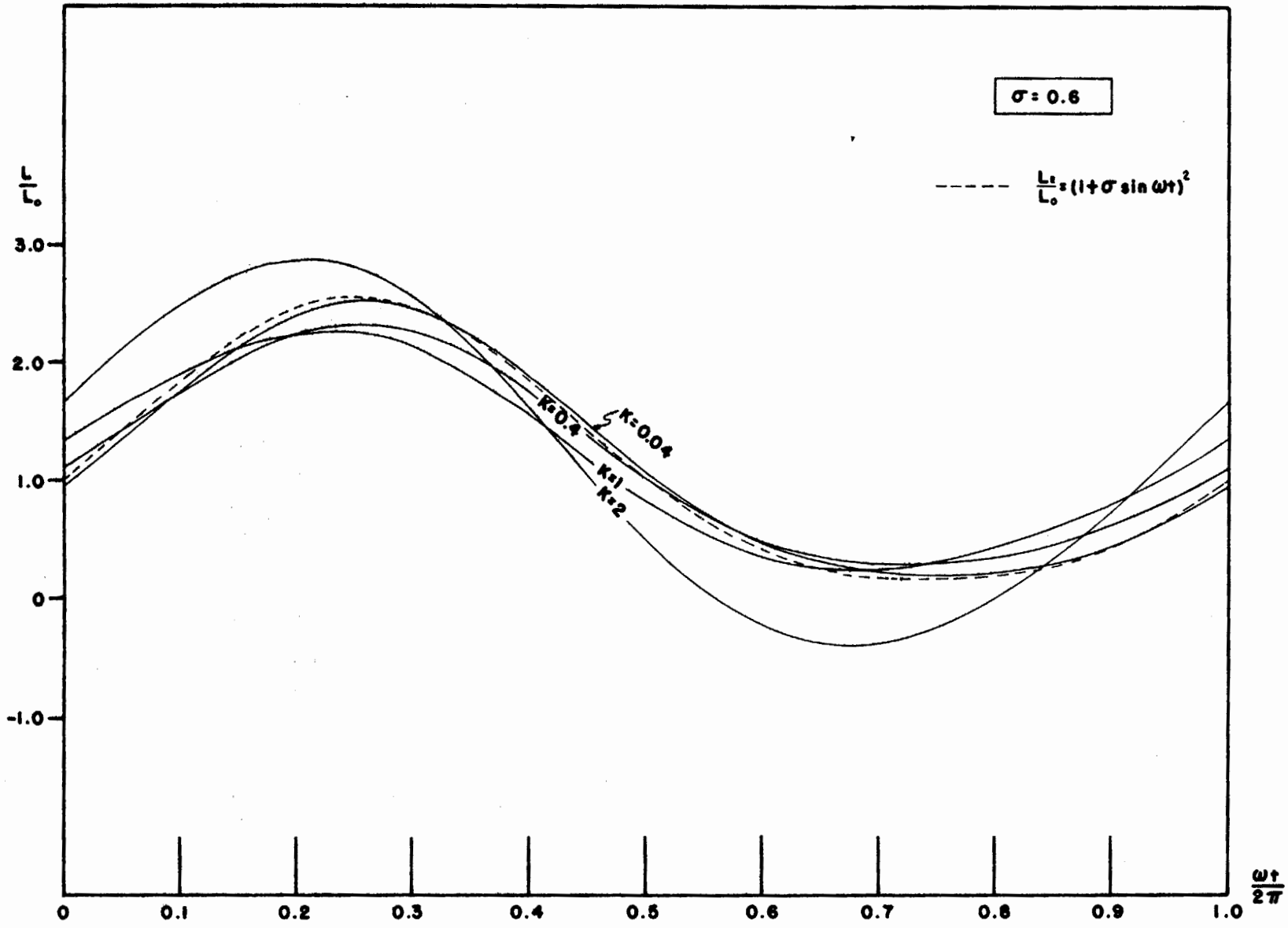
σ = 0.6
$\frac{L_t}{L_o} = (1+\sigma \sin \omega t)^2$
$\frac{L}{L_o}$
3.0
2.0
1.0
0
-1.0
K=0.04
K=0.4
K=1
K=2
0
0.1
0.2
0.3
0.4
0.5
0.6
0.7
0.8
0.9
1.0
$\frac{\omega t}{2\pi}$

FIG. 6-10

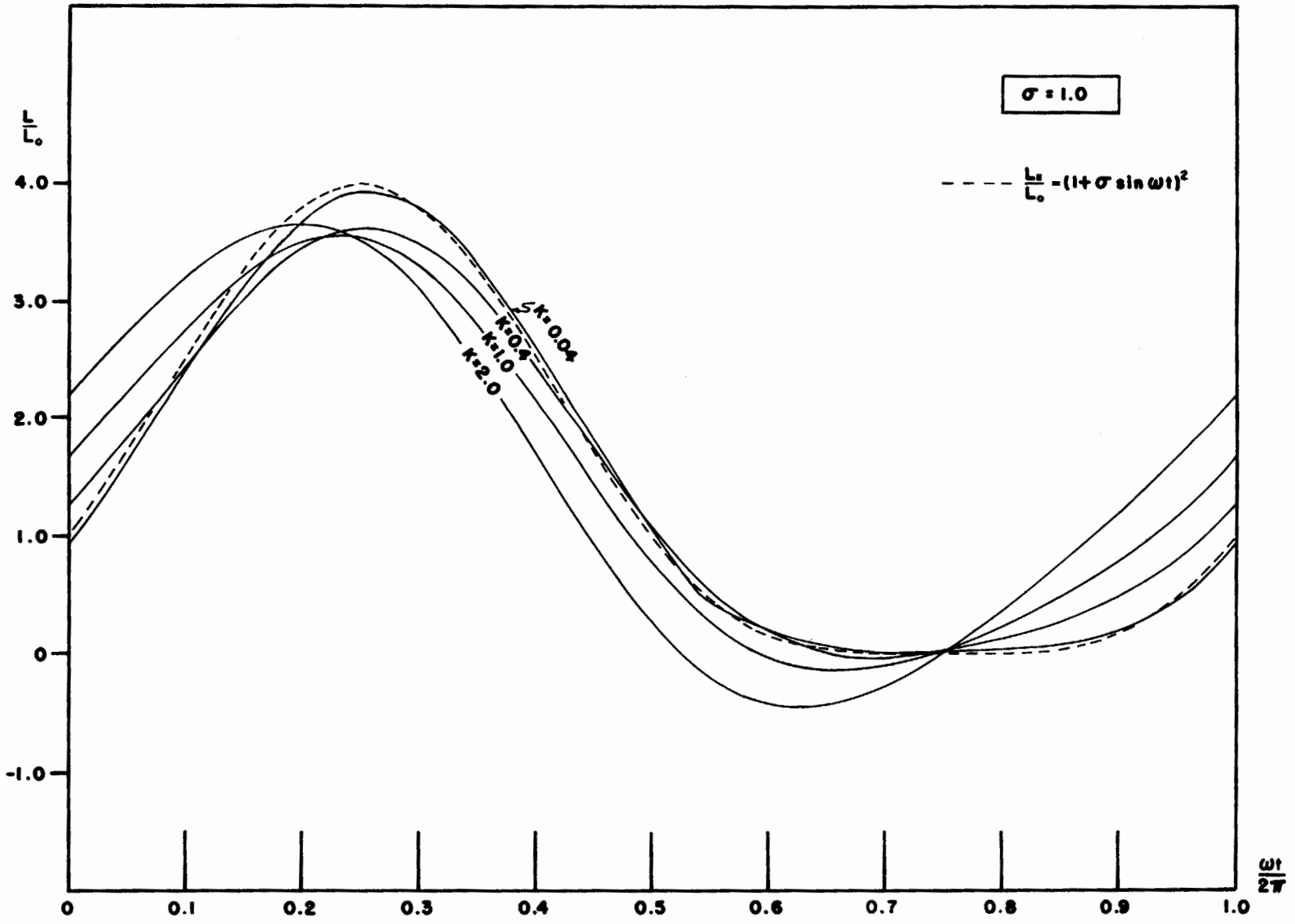
σ = 1.0
$\frac{L_s}{L_o} = (1+\sigma \sin \omega t)^2$
K=0.04
K=0.4
K=1.0
K=2.0
$\frac{L}{L_o}$
4.0
3.0
2.0
1.0
0
-1.0
0
0.1
0.2
0.3
0.4
0.5
0.6
0.7
0.8
0.9
1.0
$\frac{\omega t}{2\pi}$

FIG. 6-11

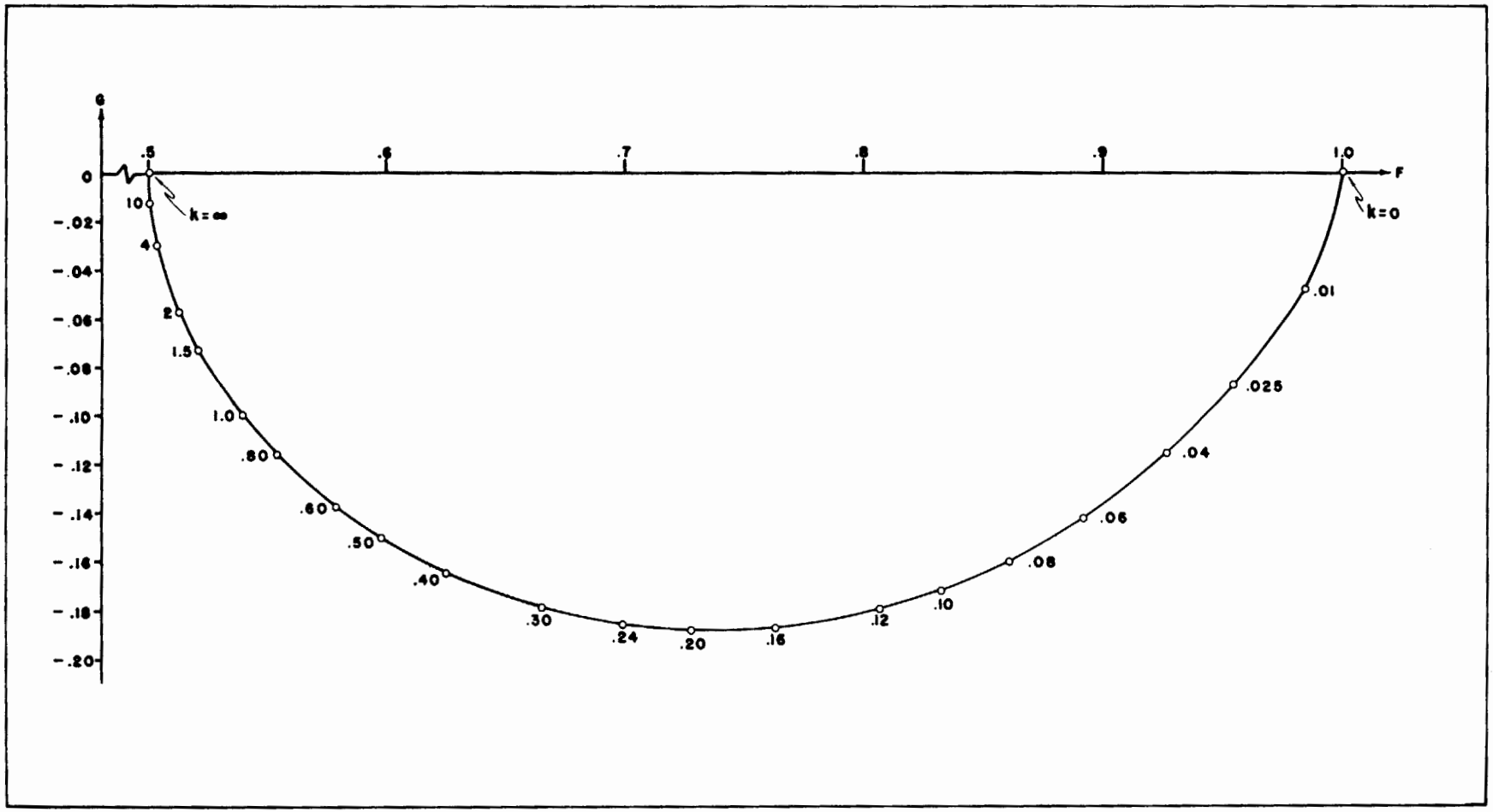

FIG. 7 THE THEODORSEN FUNCTION $C(k) = F(k) + iG(k)$

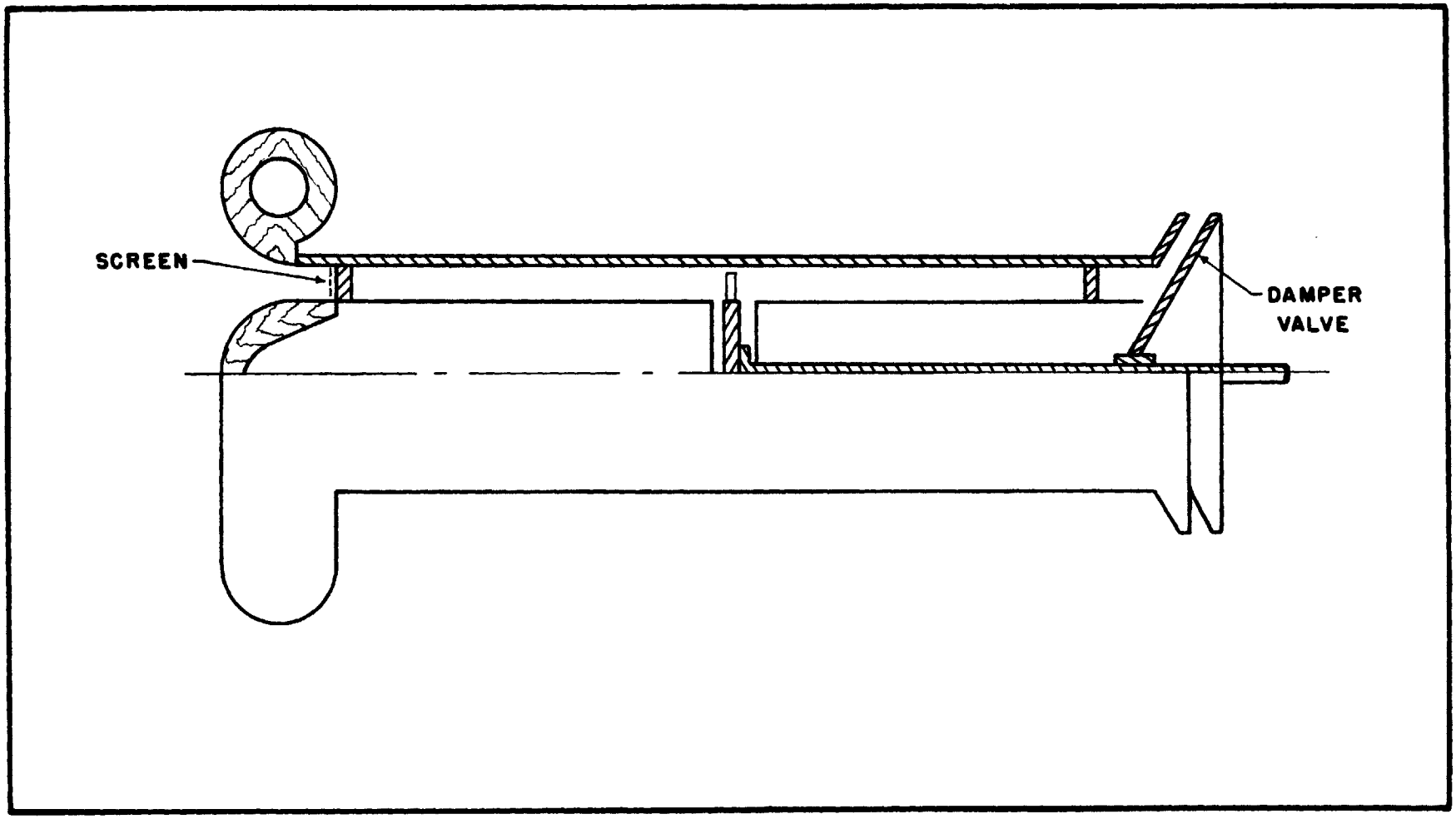

FIG. 8 SECTION VIEW OF COMPRESSOR

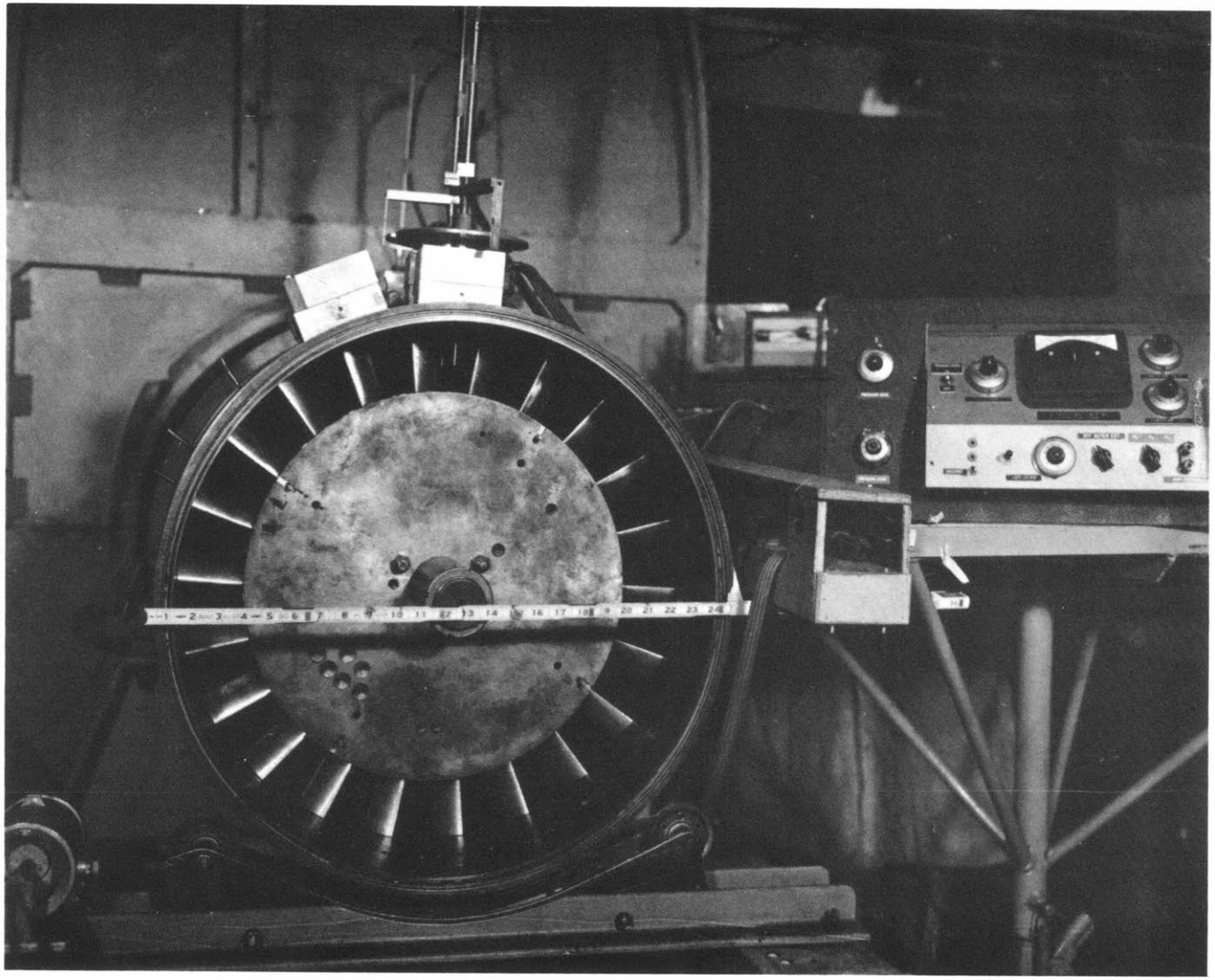

FIG. 9 VIEW OF ROTOR (2b/S=0.525) WITH CASING REMOVED

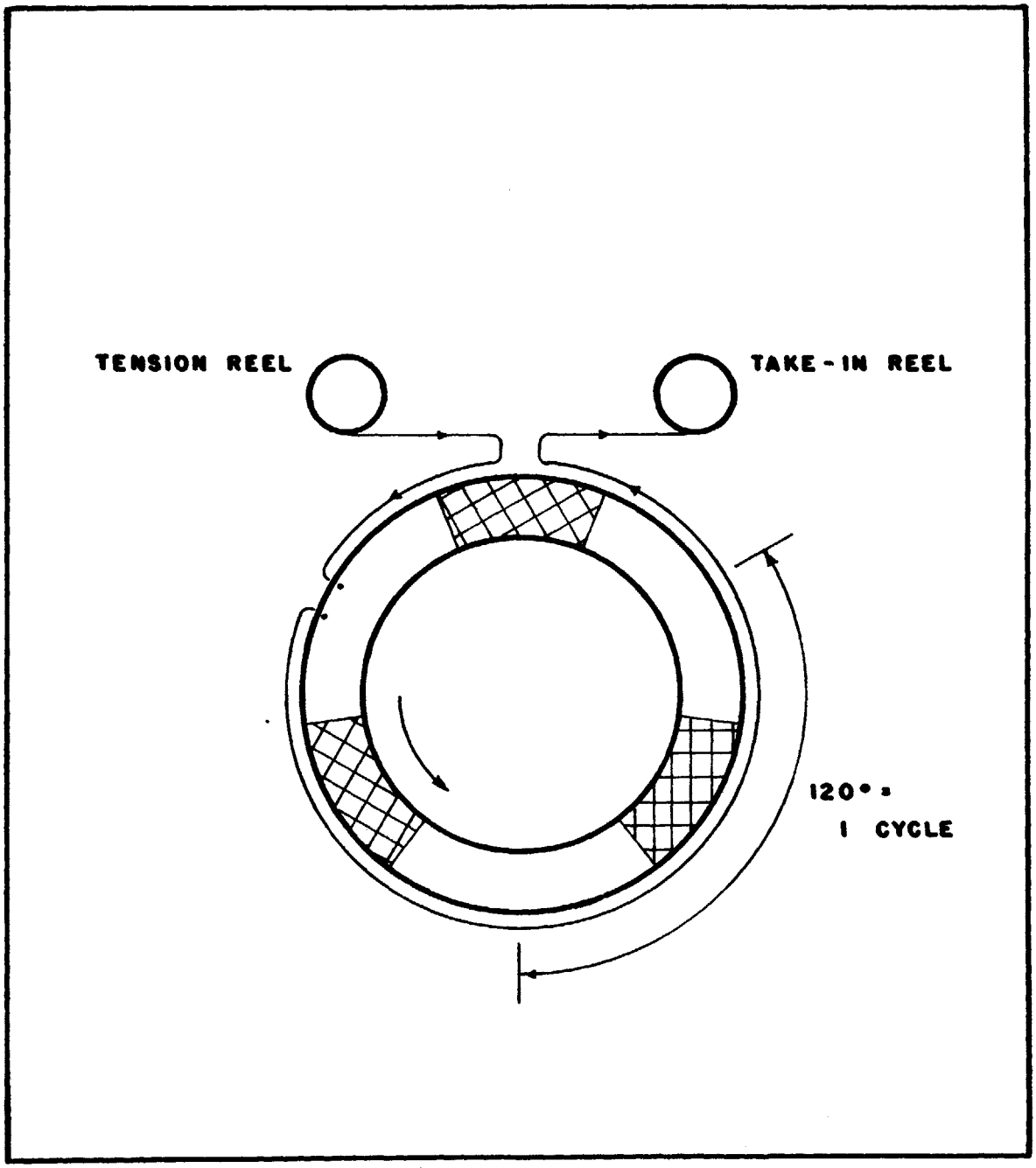

FIG. 10 REEL AND CORD ARRANGEMENT

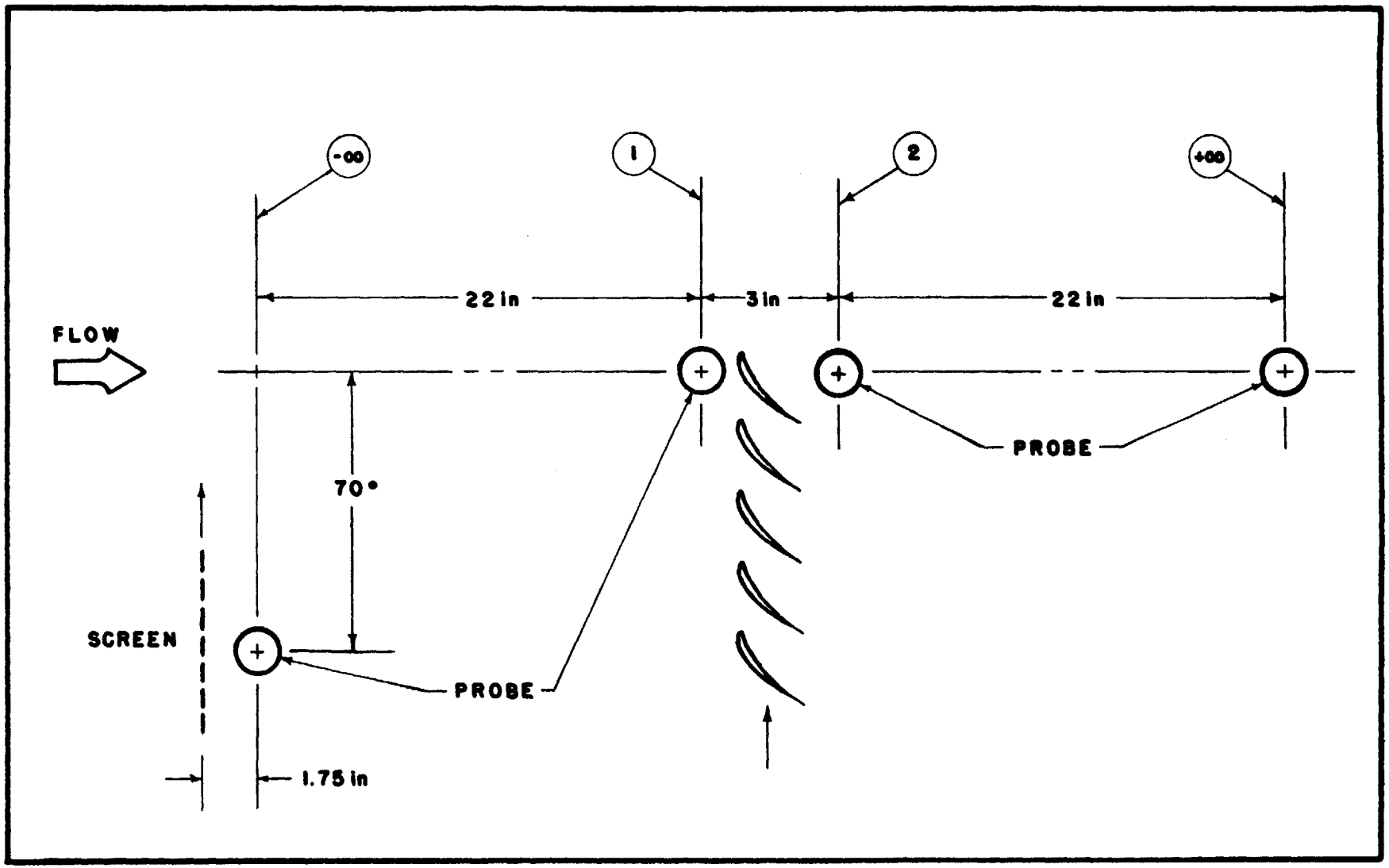

FIG. 11 LOCATION OF MEASUREMENT STATIONS AND SCREEN

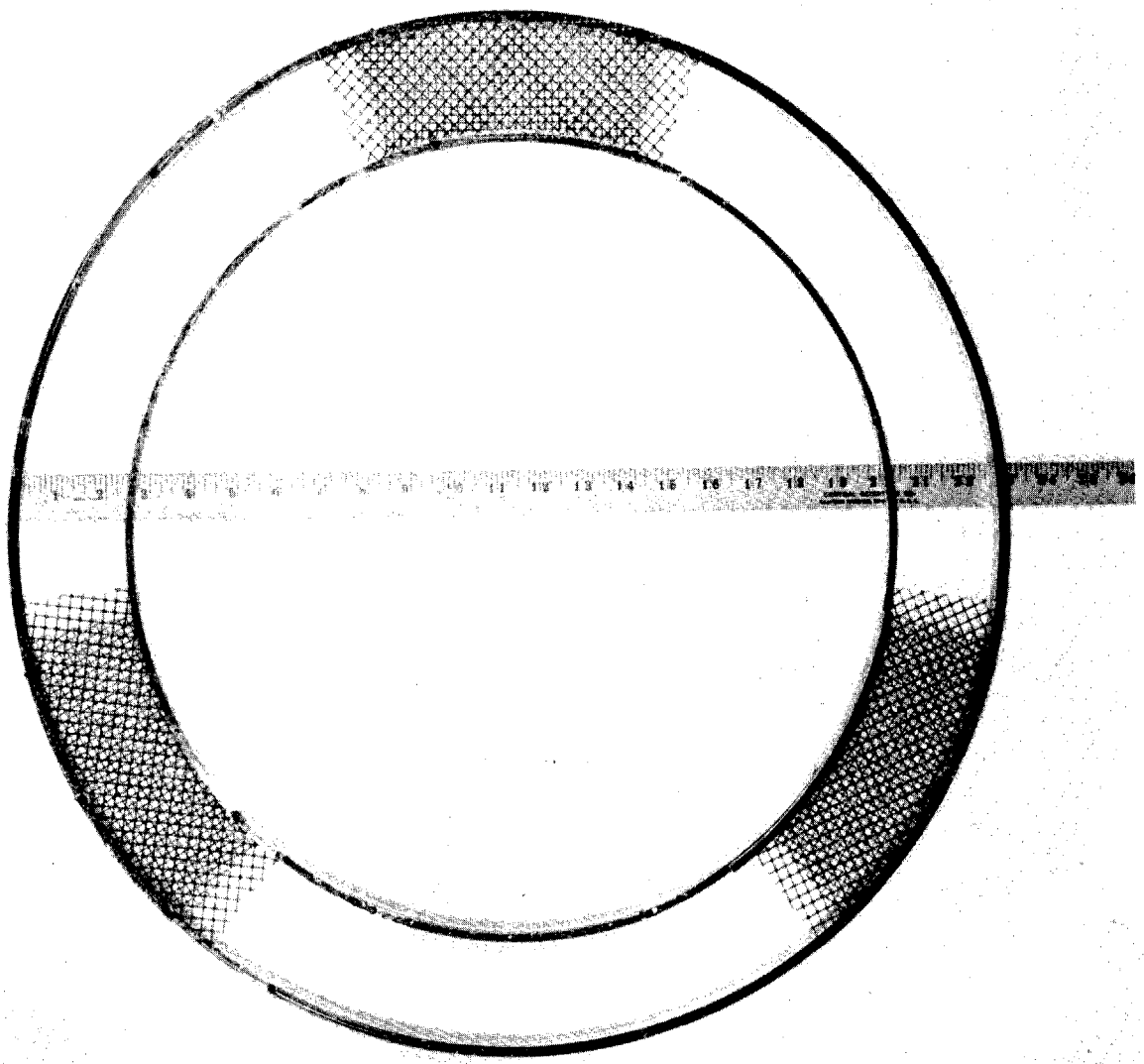

FIG. 12 DISTORTION SCREENS AND FRAME

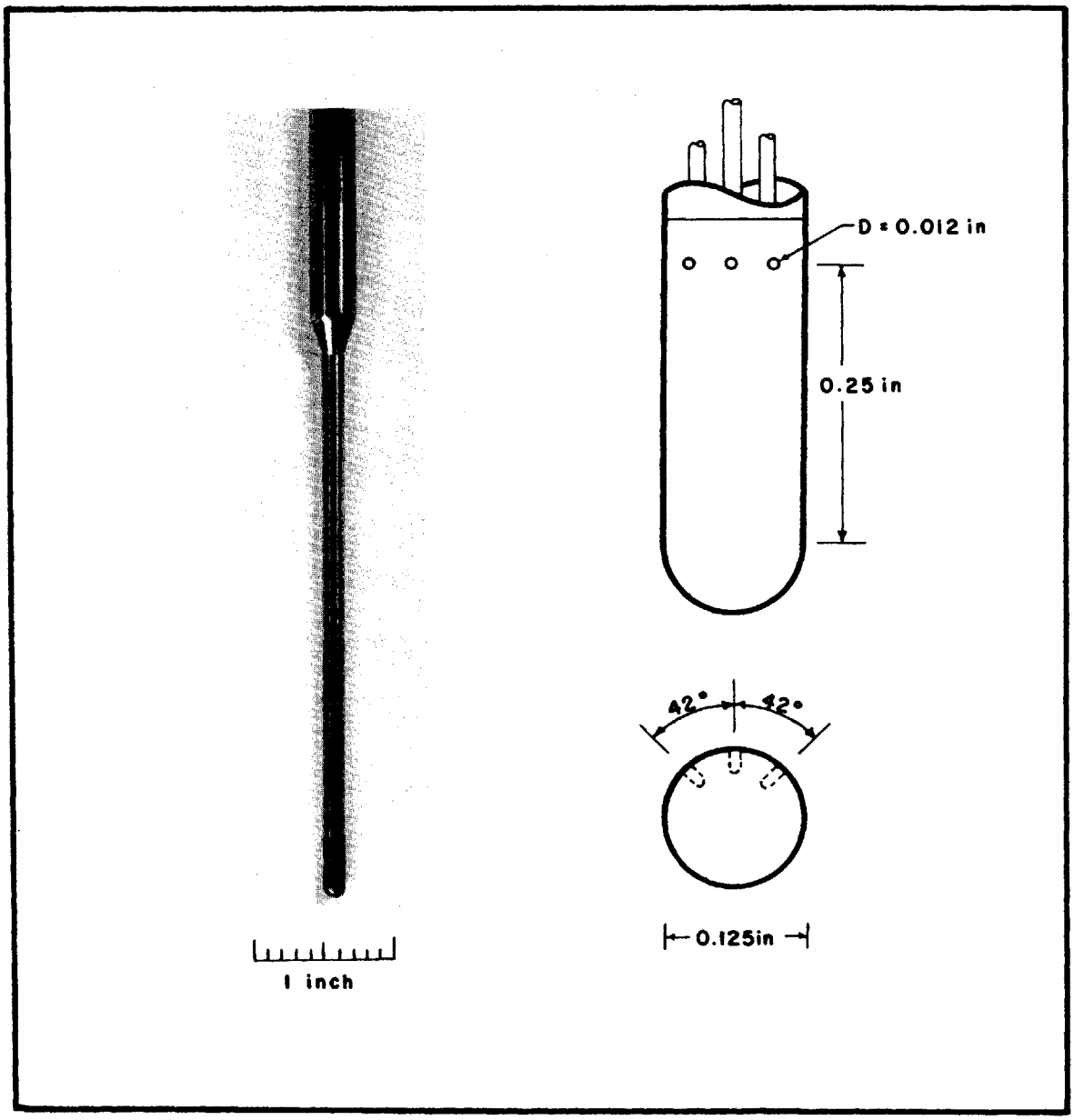

FIG. 13 THREE-HOLE FECHEIMER TUBE AND DETAILS

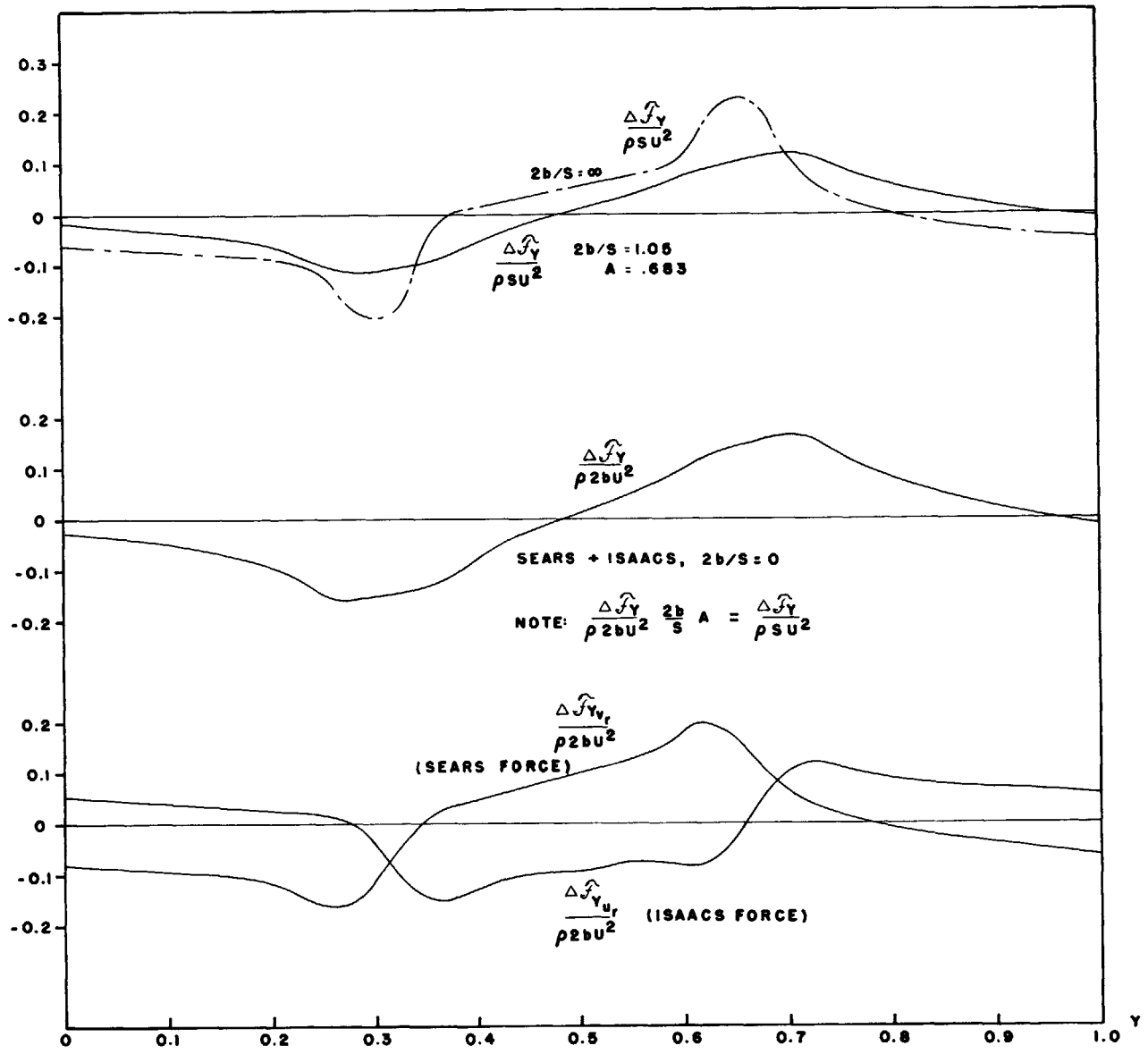

FIG. 14-1 THE PERTURBATION IN Y COMPONENT FORCE ON THE BLADE.

$2b/S = 1.05, U/\Omega r = .562, i_m = 9.3°$

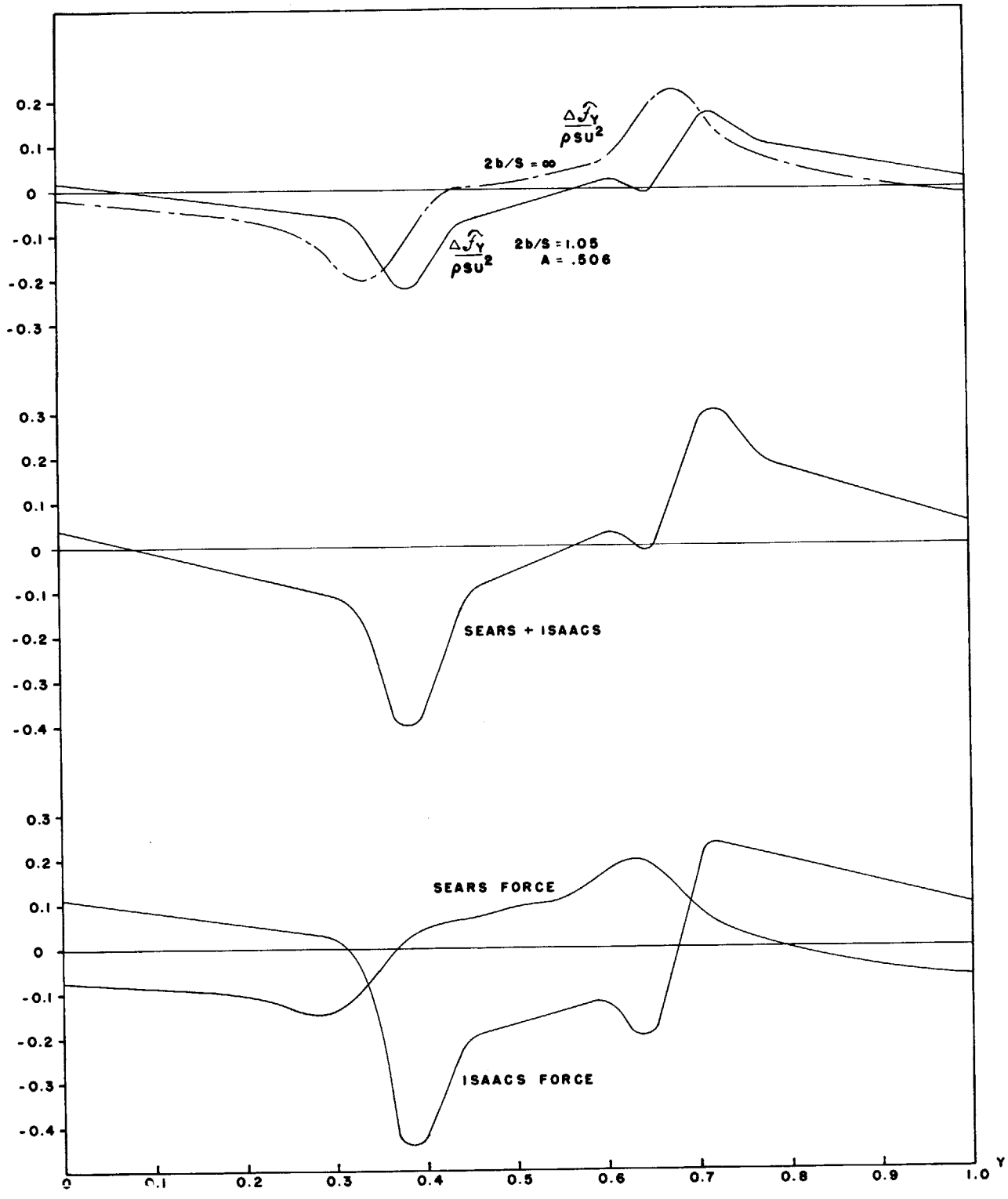

FIG. 14-2 $2b/S = 1.05,\ U/\Omega r = .460,\ i_m = 15.3°$

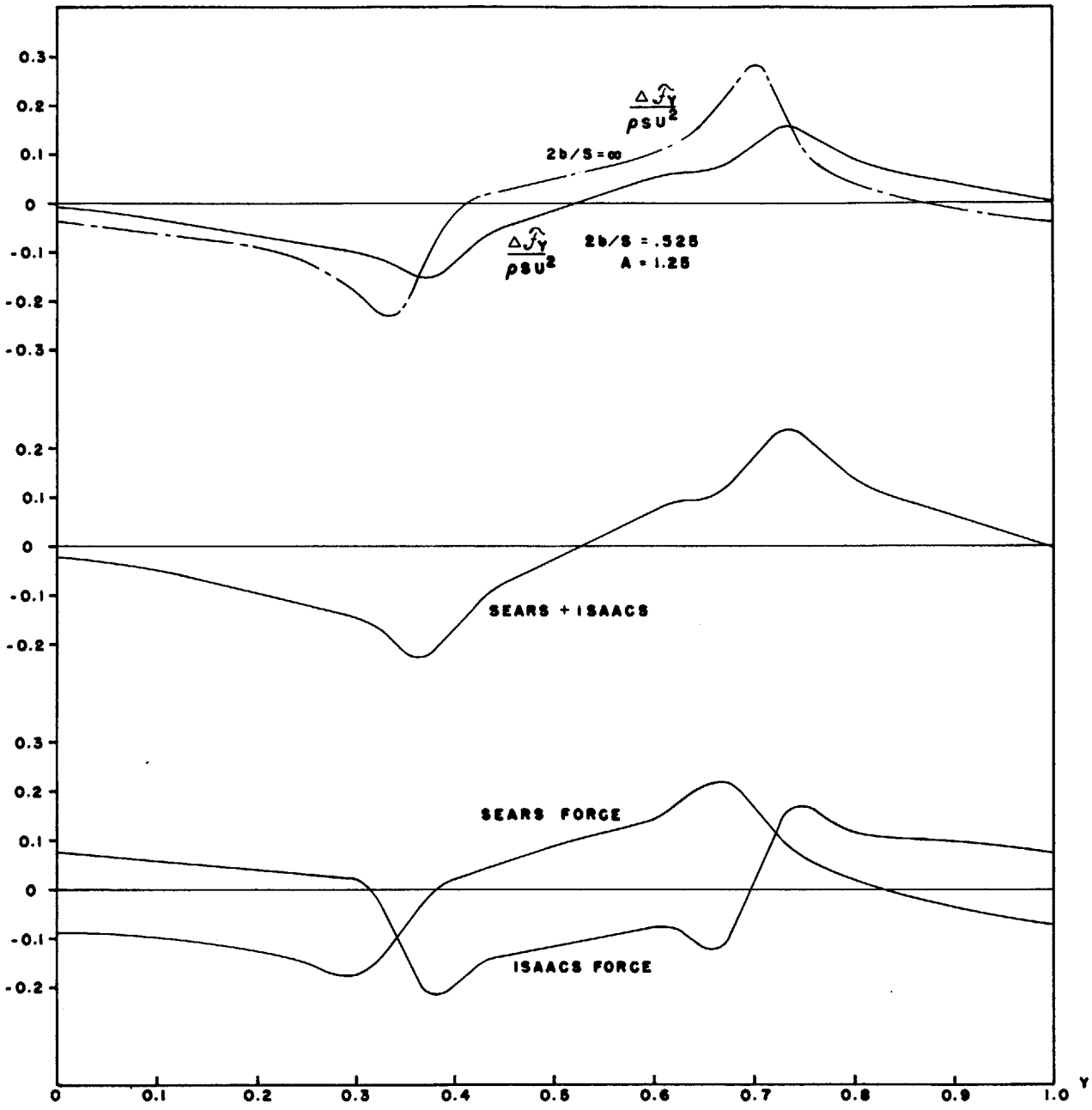

FIG. 14-3 $2b/S = .525,\ U/\Omega r = .514,\ i_m = 8.8°$

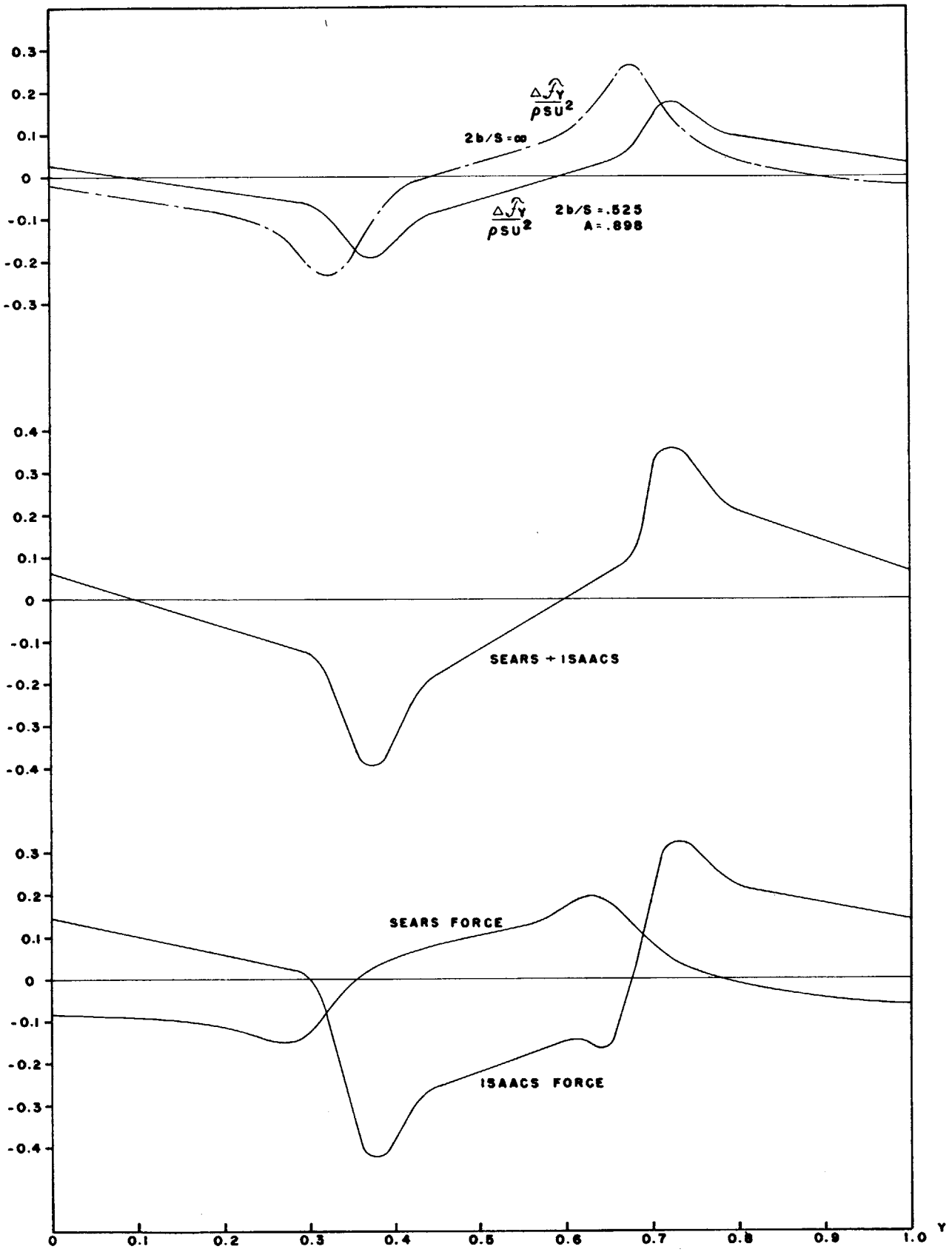

FIG. 14-4 $2b/S = .525,\ U/\Omega r = .391,\ i_m = 16.1°$

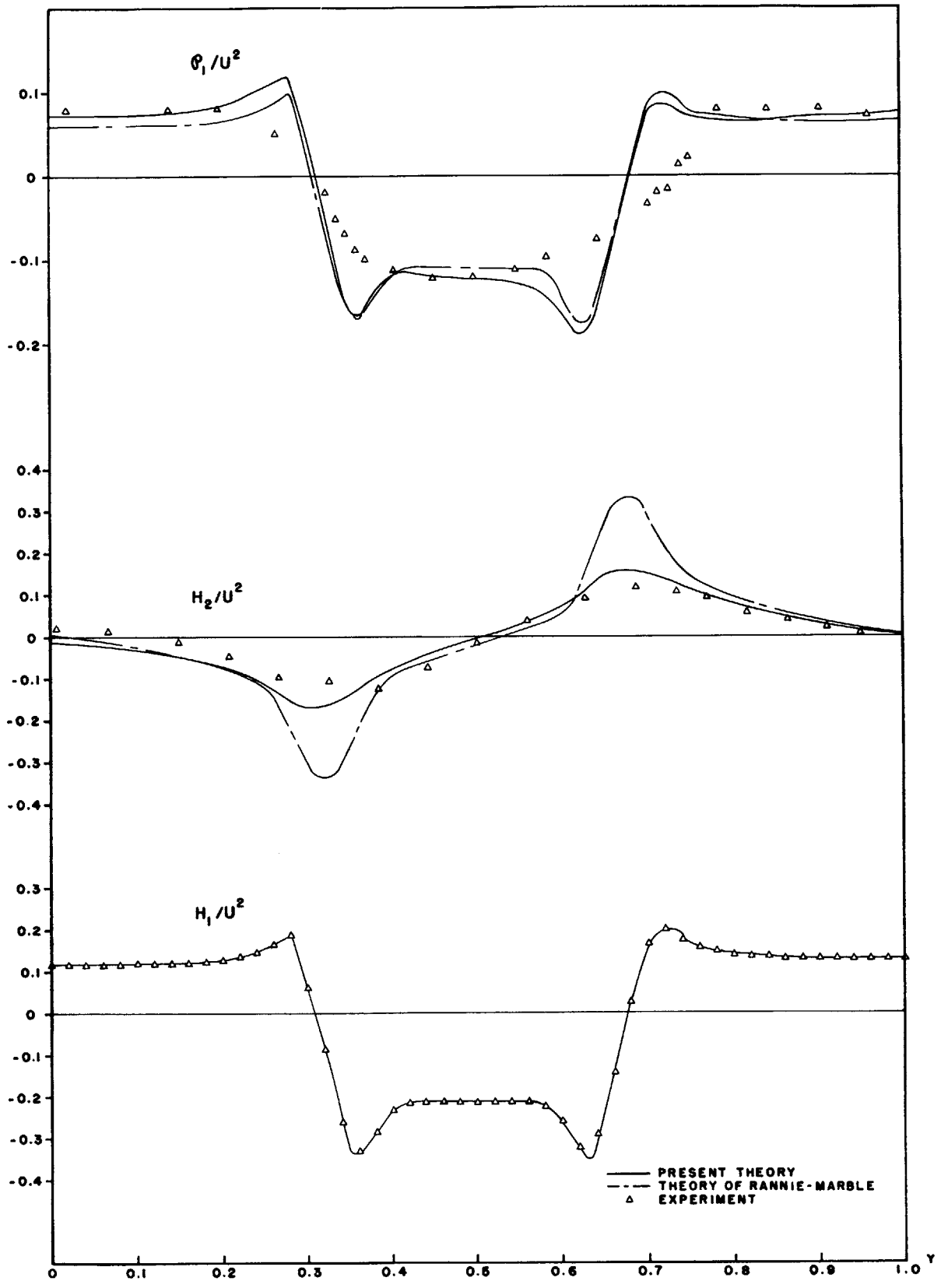

FIG. 15-1 PERTURBATIONS UPSTREAM AND DOWNSTREAM, THEORY AND EXPERIMENT. $2b/S = 1.05$, $U/\Omega r = .562$

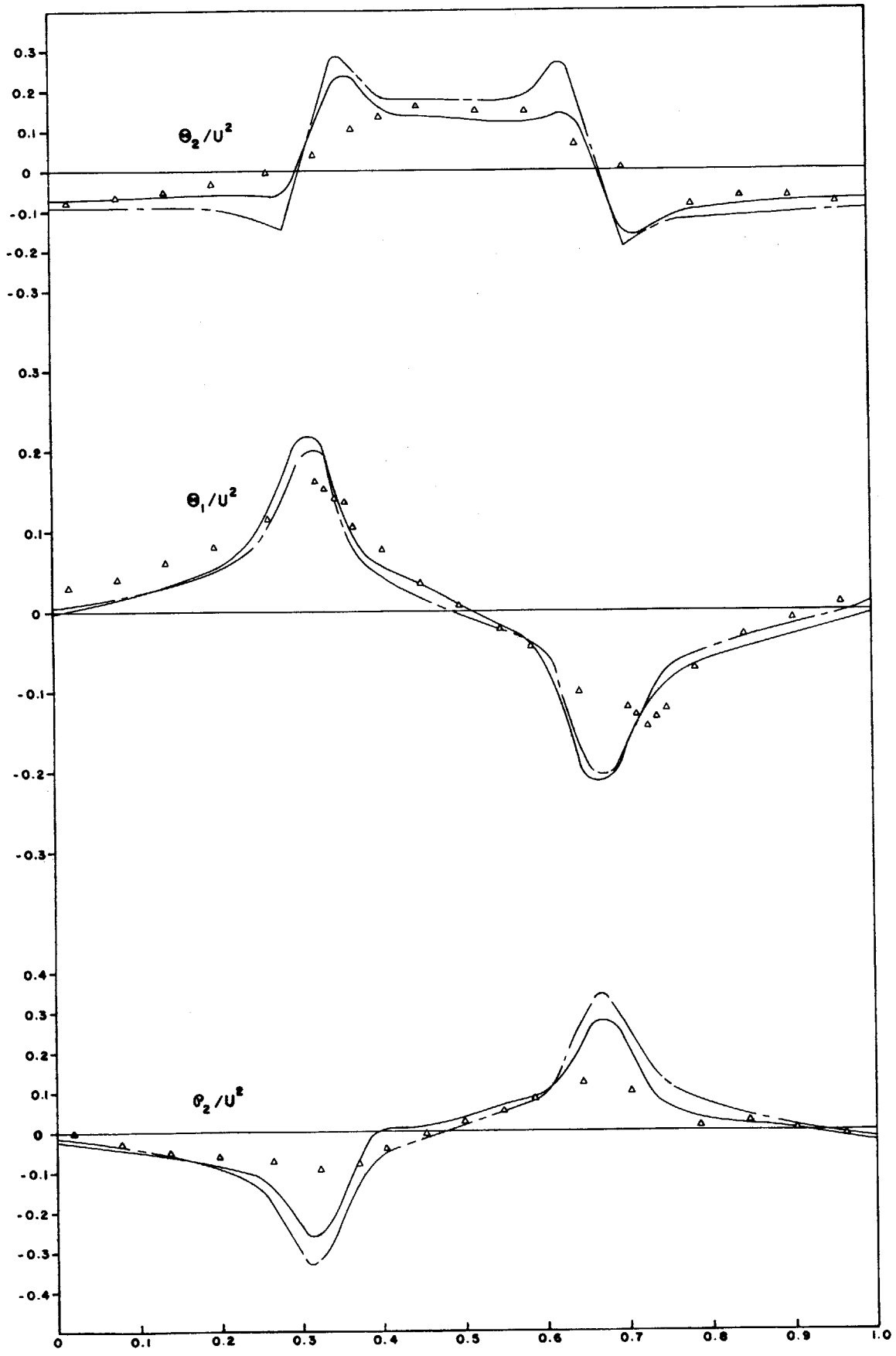

FIG. 15-1 CONTD.

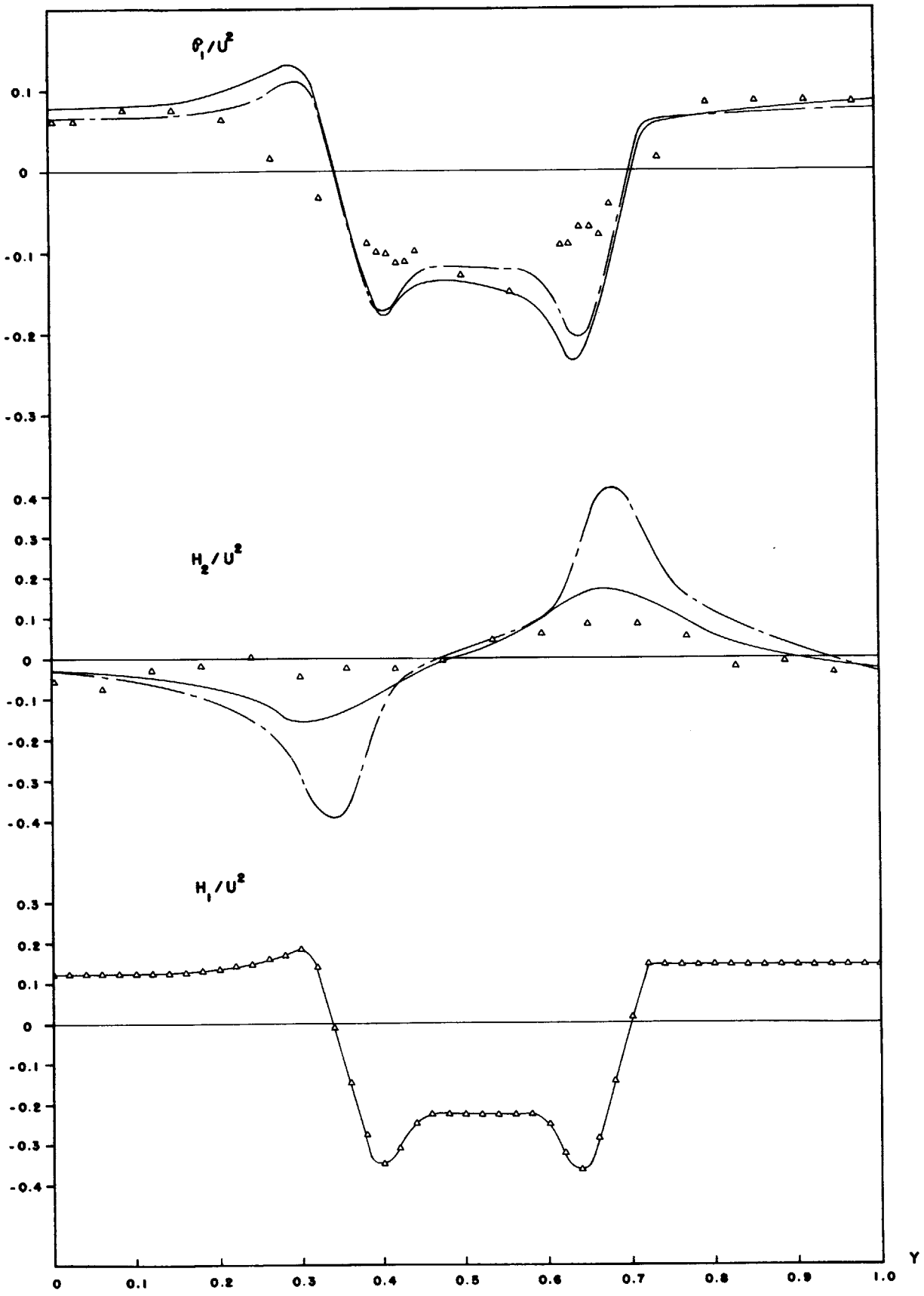

FIG. 15-2 $2b/S = 1.05$, $U/\Omega r = .460$

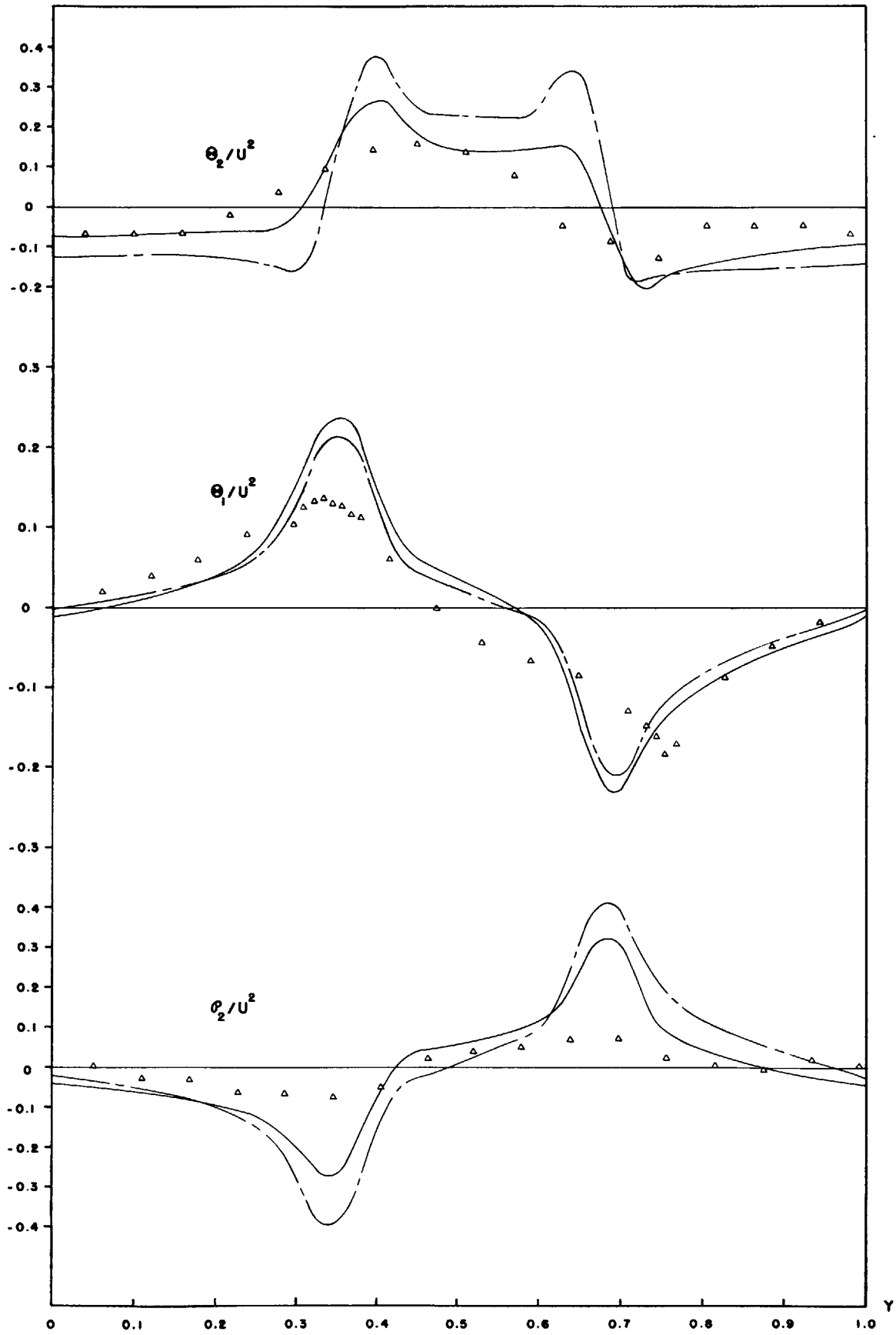

FIG. 15-2 CONTD.

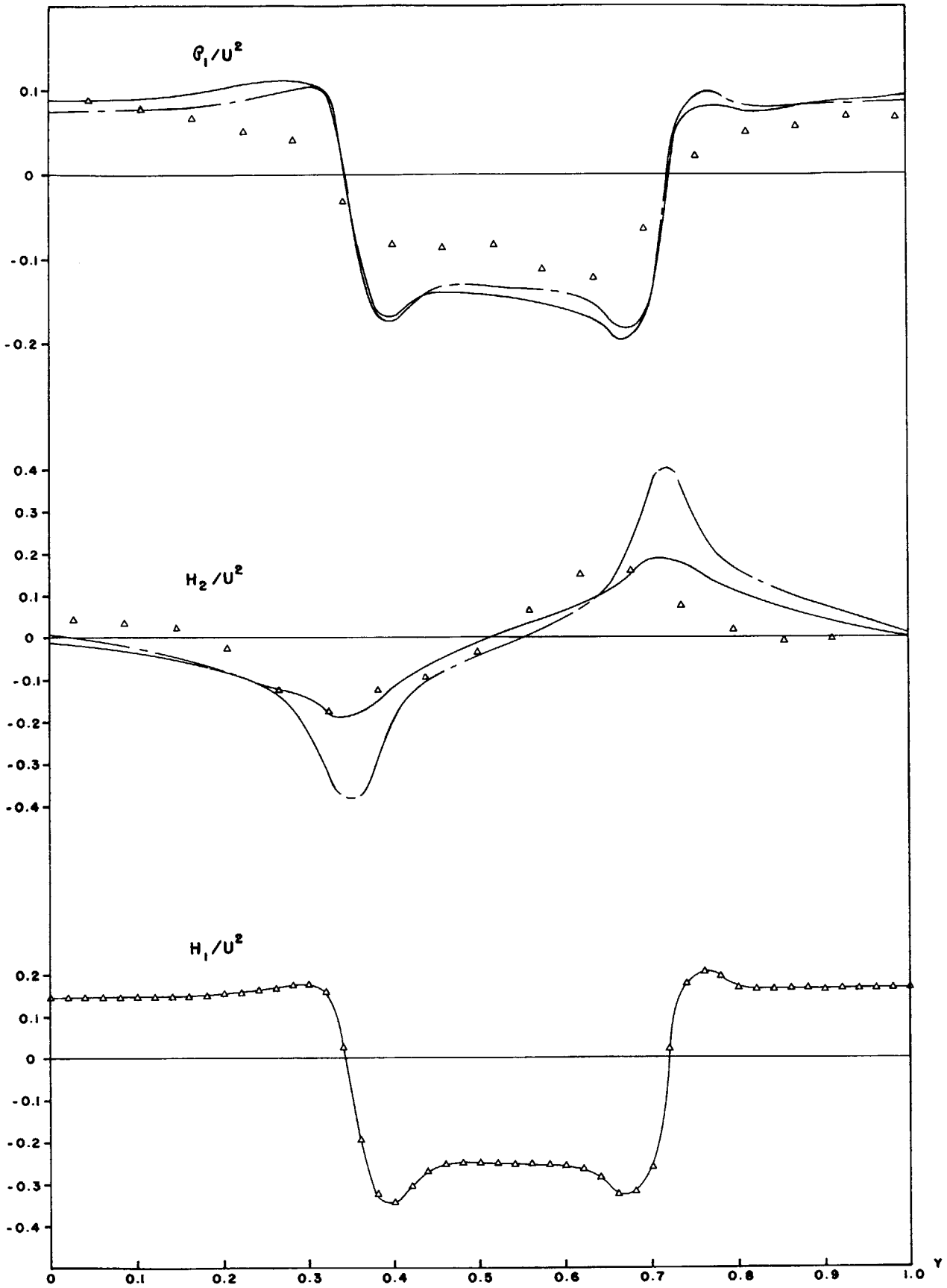

FIG. 15-3 $2b/S = .525$, $U/\Omega r = .514$

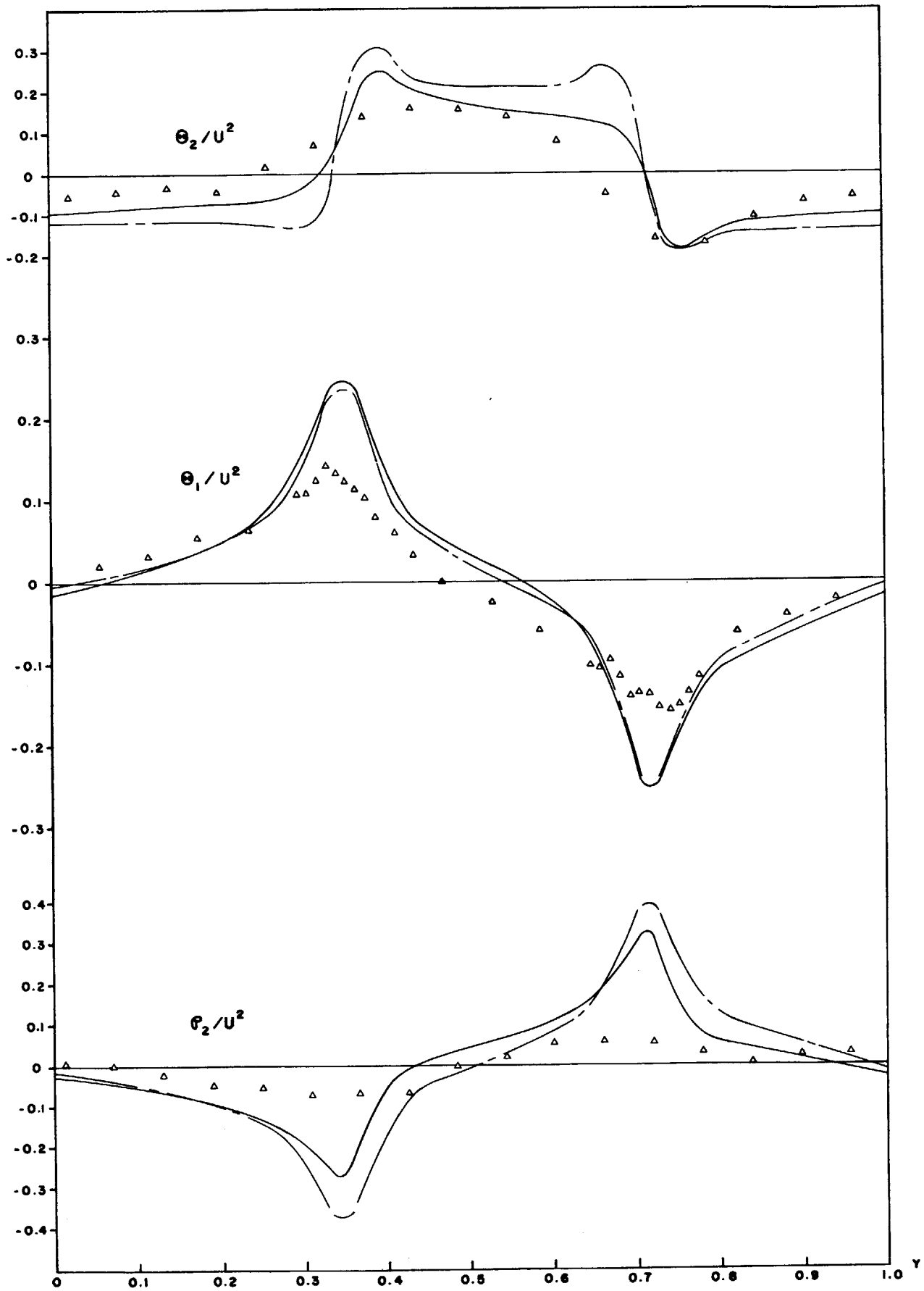

FIG. 15-3 CONTD.

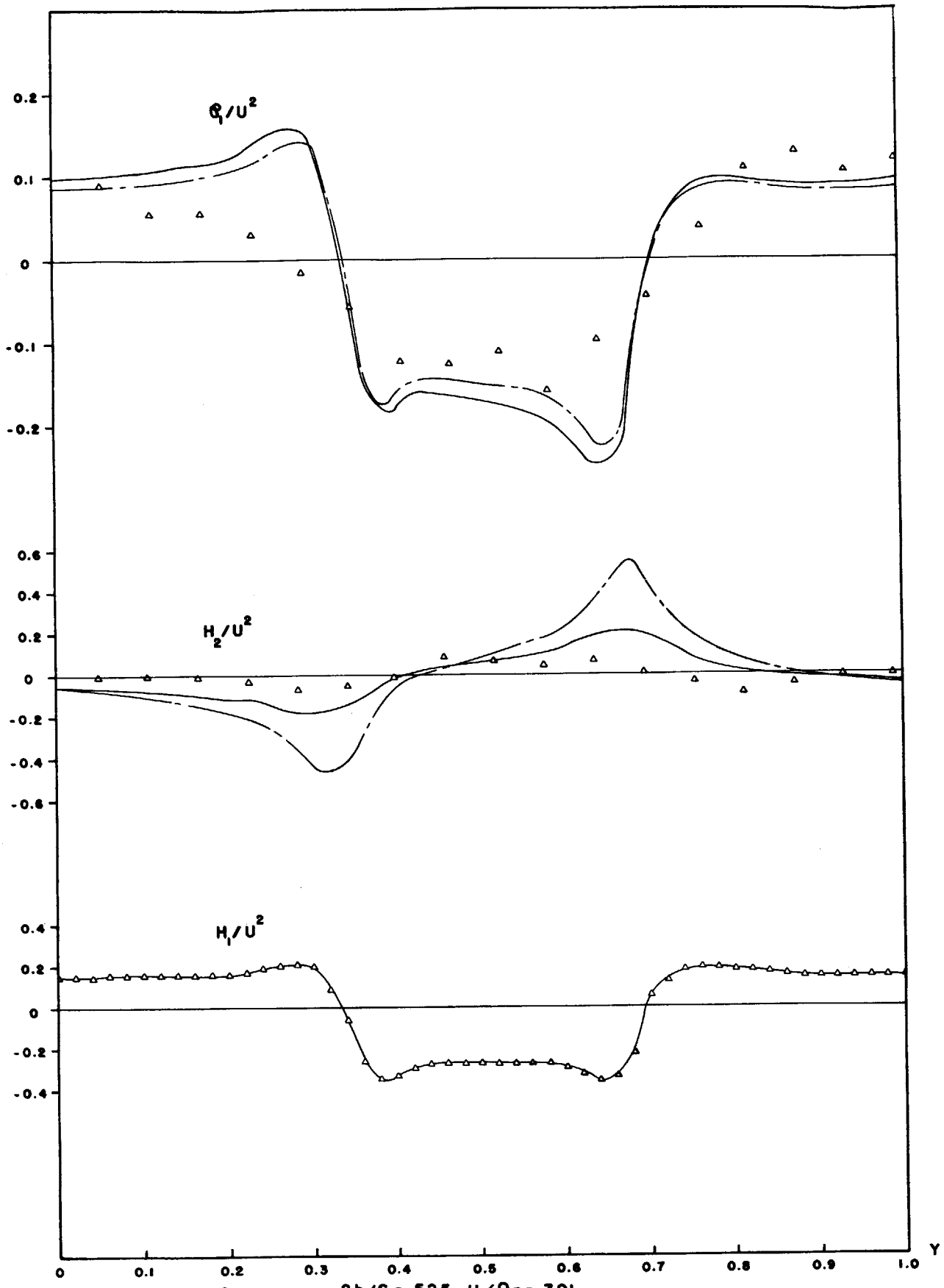

FIG. 15-4 $2b/S = .525,\ U/\Omega r = .391$

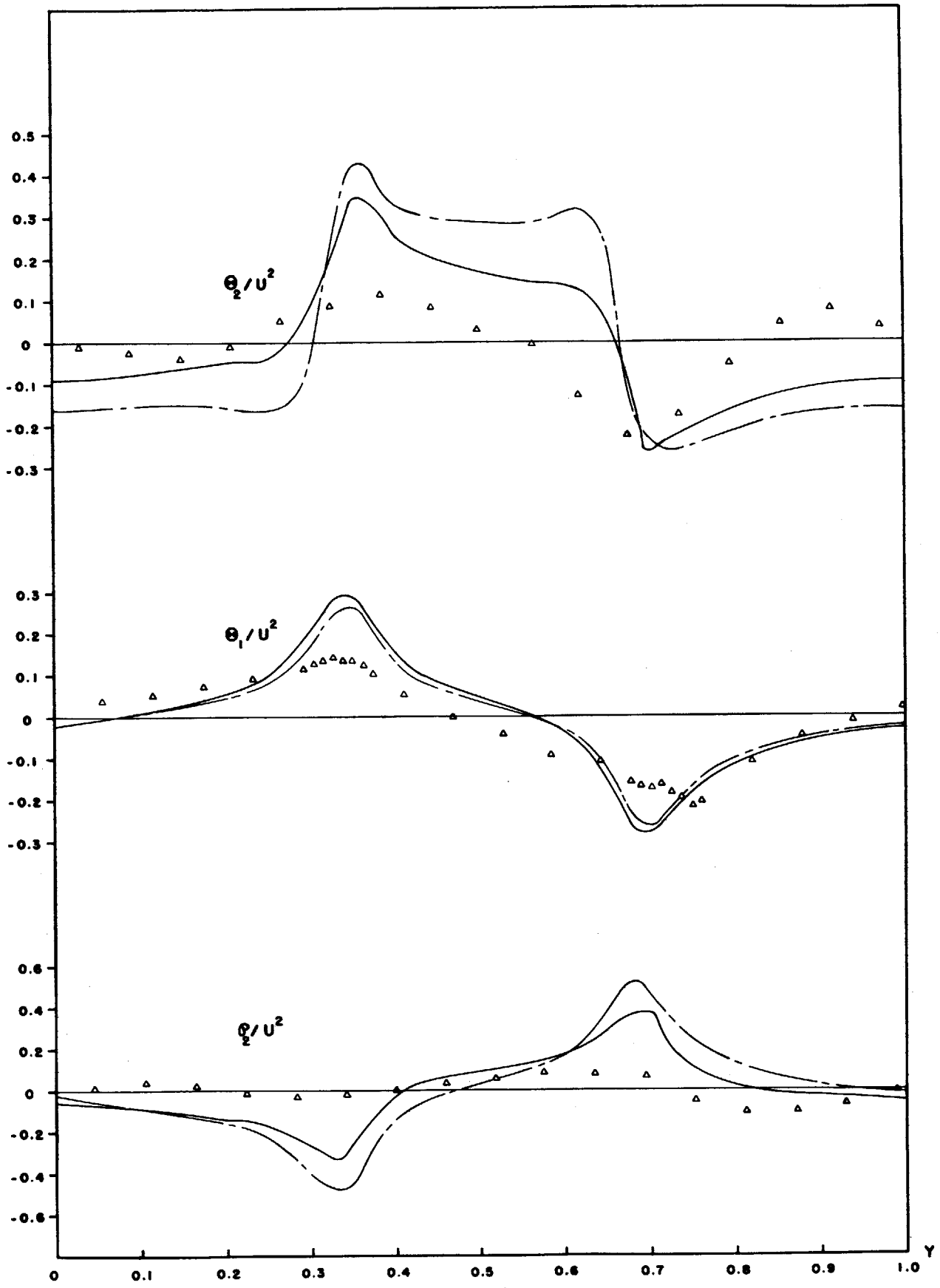

FIG. 15-4 CONTD.

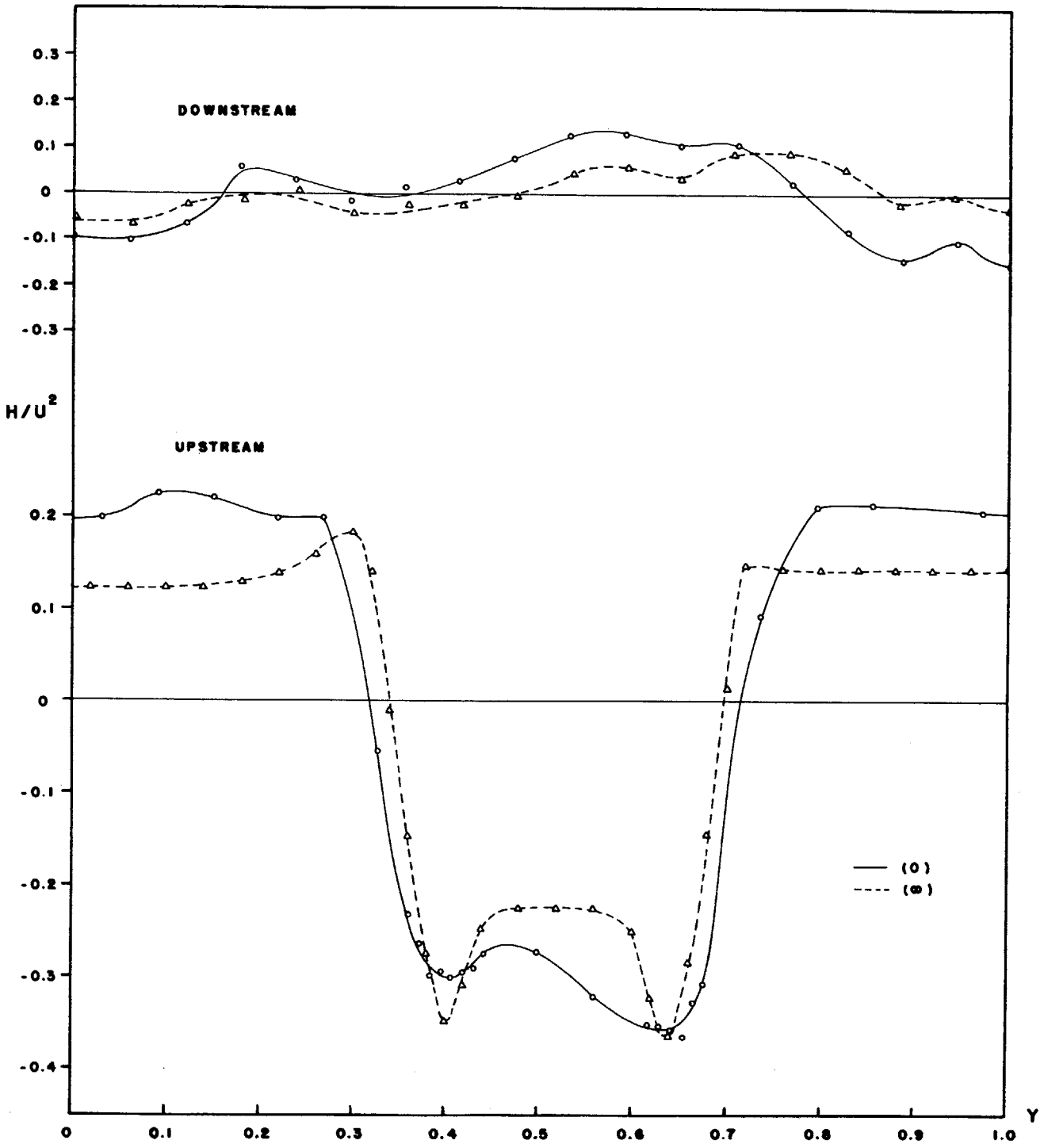

FIG. 16 COMPARISON OF EXPERIMENTAL $H_{-\infty}/U^2$ AND H_{-0}/U^2 (UPSTREAM); H_{+0}/U^2 AND $H_{+\infty}/U^2$ (DOWNSTREAM)

$2b/S = 1.05$, $U/\Omega r = .460$

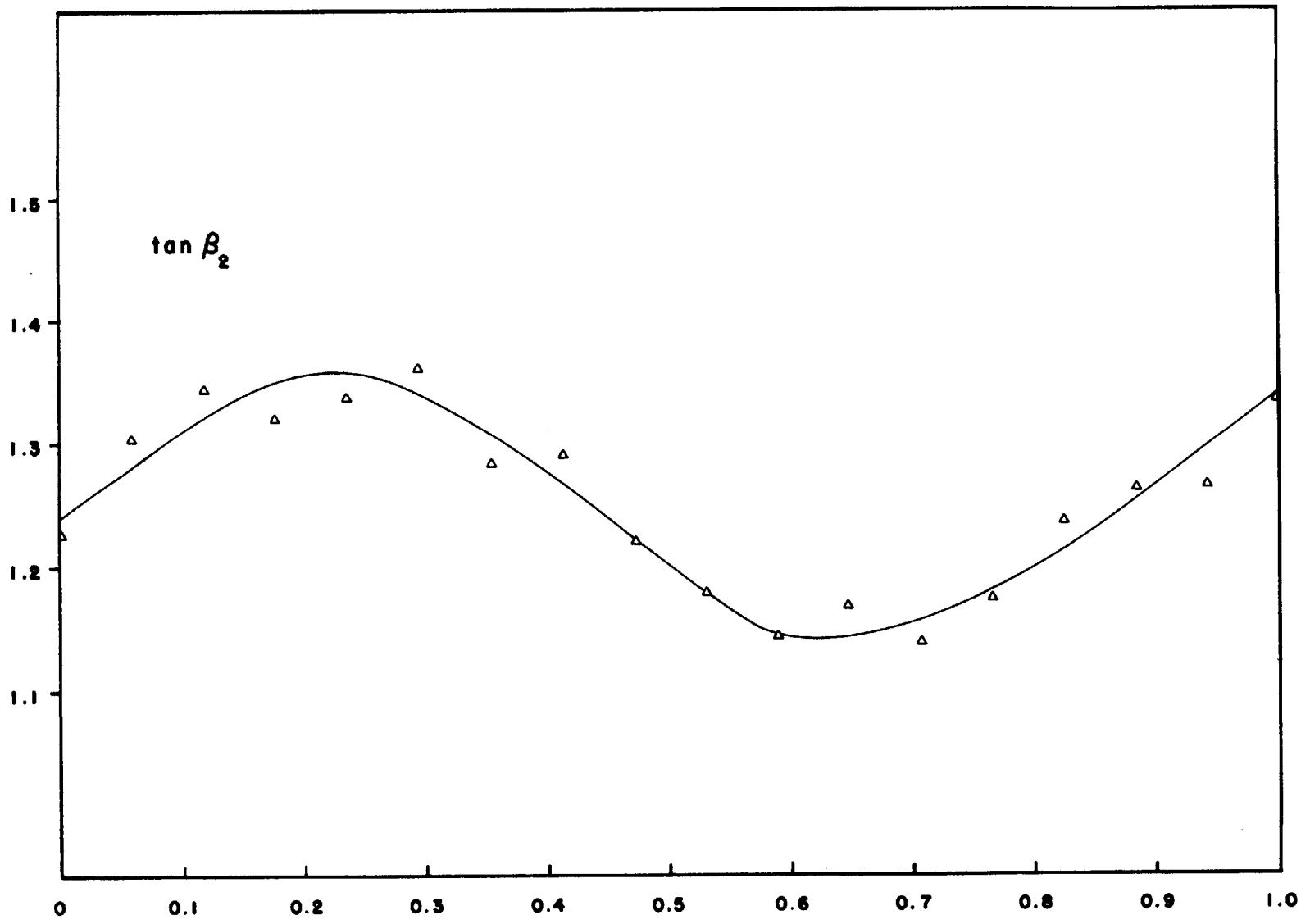

FIG. 17 VARIATION IN $\tan\beta_2$ WITH Y ($2b/S = 1.05, U/\Omega r = .460$)

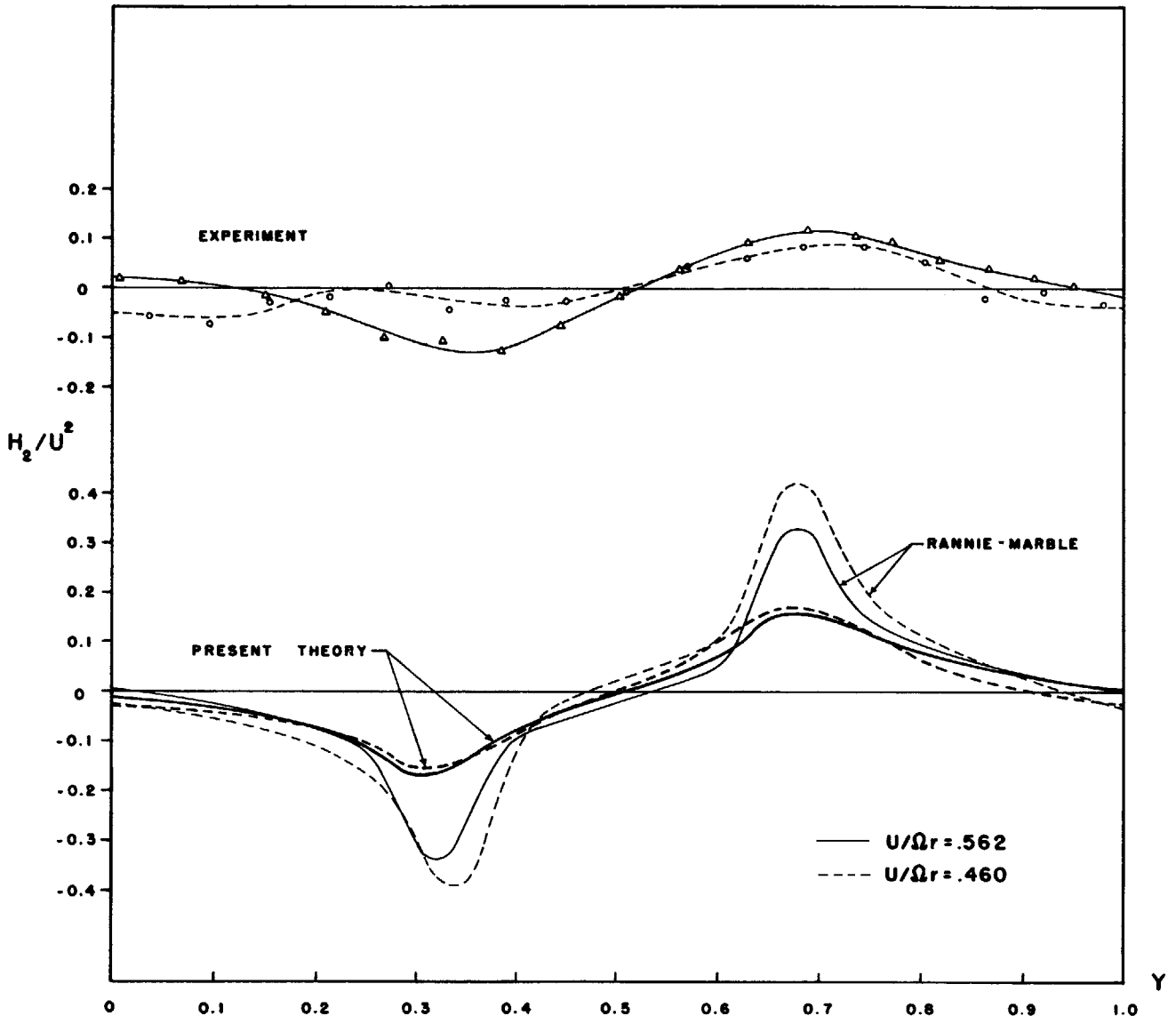

FIG.18 EFFECT OF FLOW RATE ON ATTENUATION, THEORY AND EXPERIMENT. 2b/S = 1.05

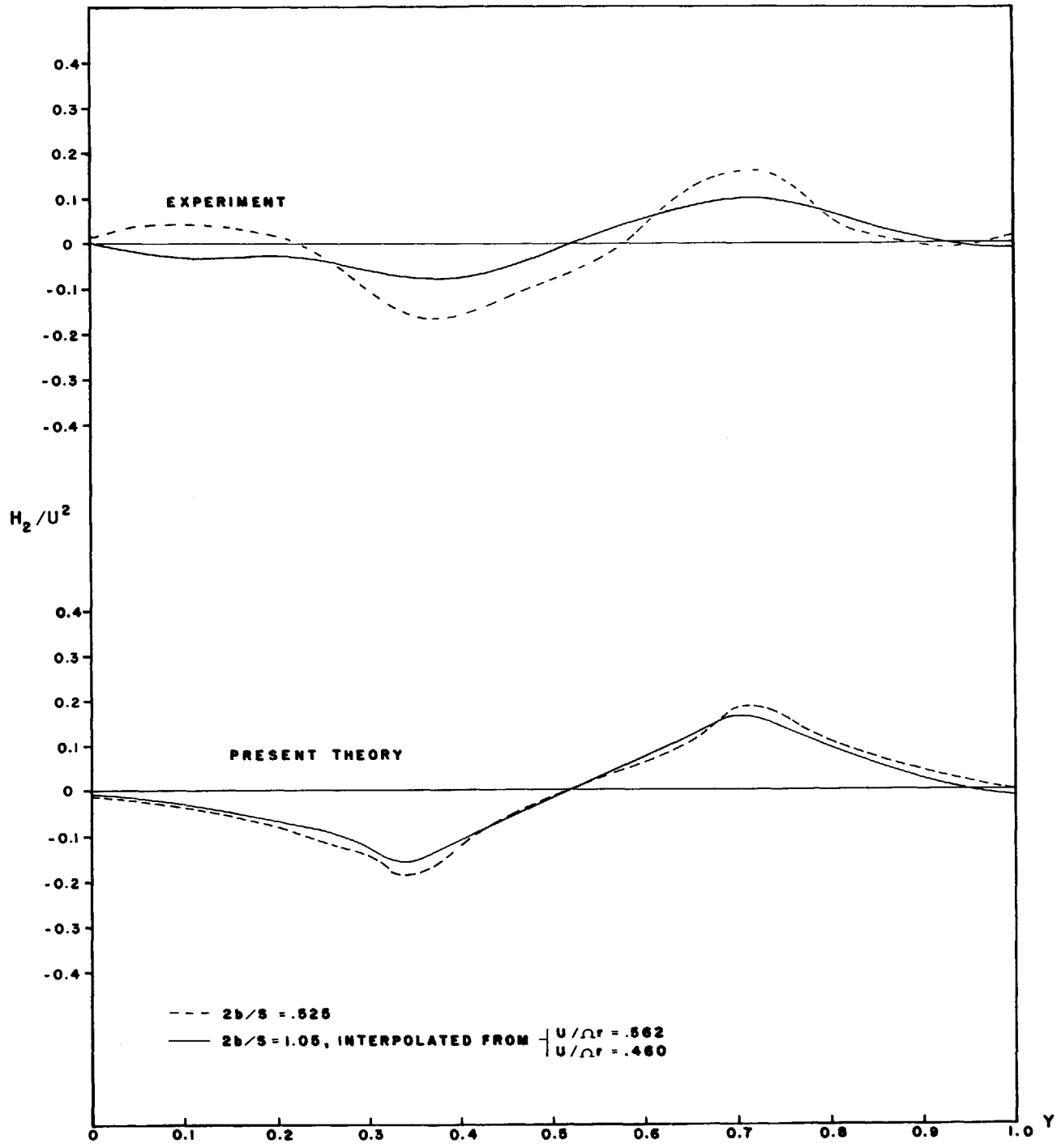

FIG.19 EFFECT OF SOLIDITY ON ATTENUATION, THEORY AND EXPERIMENT, $U/\Omega r = .514$

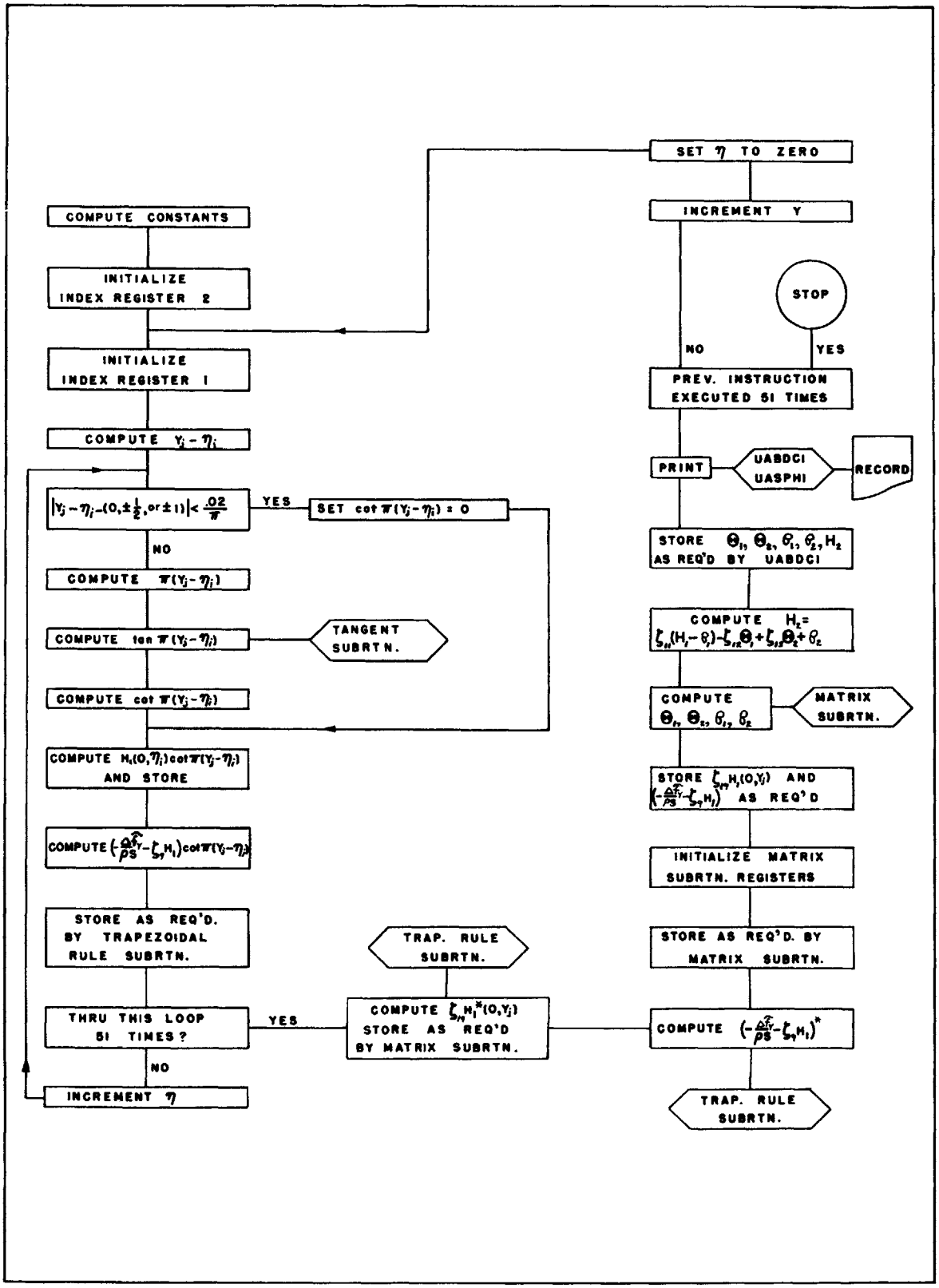

FIG.20 BLOCK DIAGRAM OF THE COMPUTATION, PRESENT THEORY

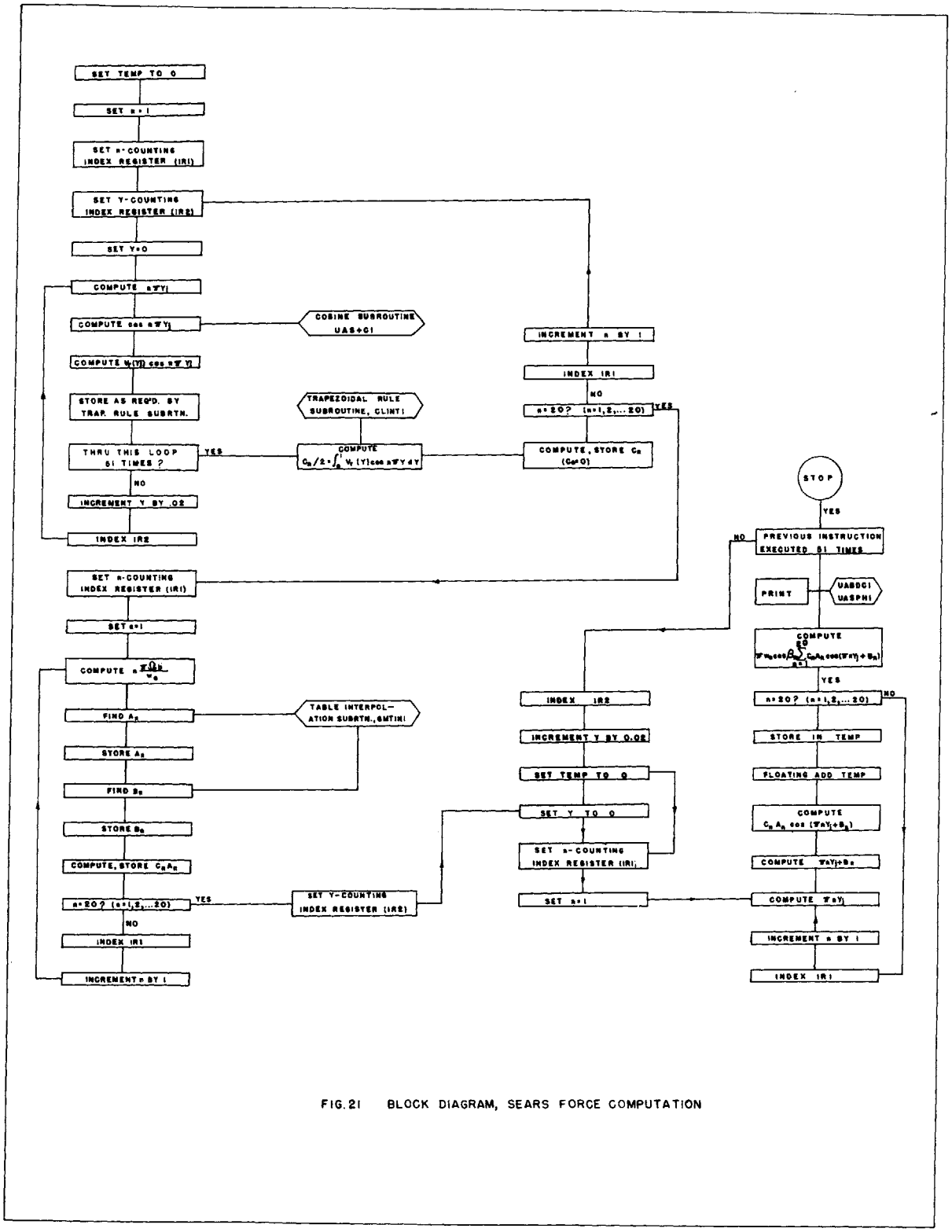

FIG. 21 BLOCK DIAGRAM, SEARS FORCE COMPUTATION

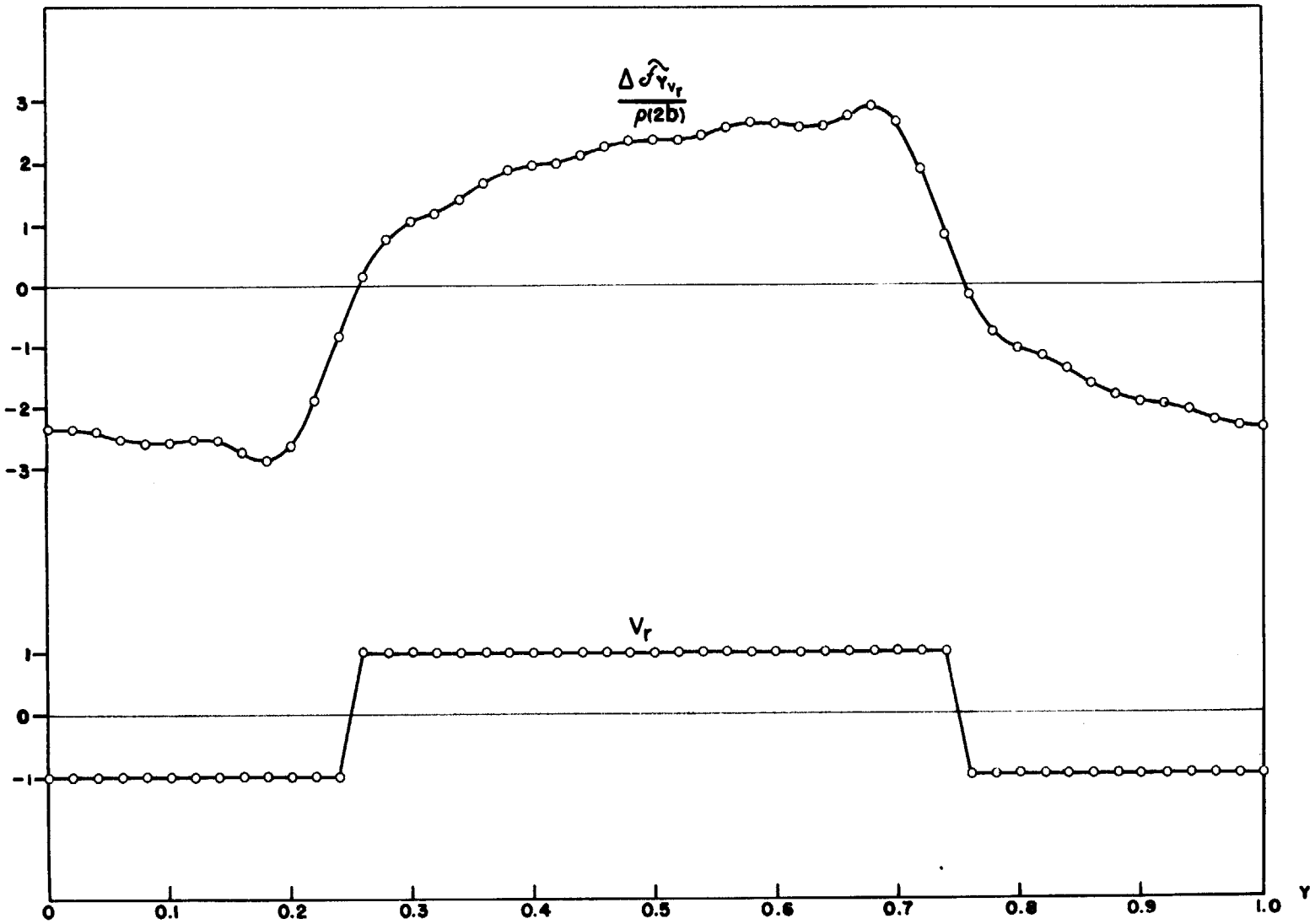

FIG. 22 TEST SOLUTION, COMPUTATION OF THE SEARS FORCE; $\Pi W_0 \cos\beta_m = \Pi$, $K_r = \frac{\Pi \Omega b}{W_0} = 0.1$

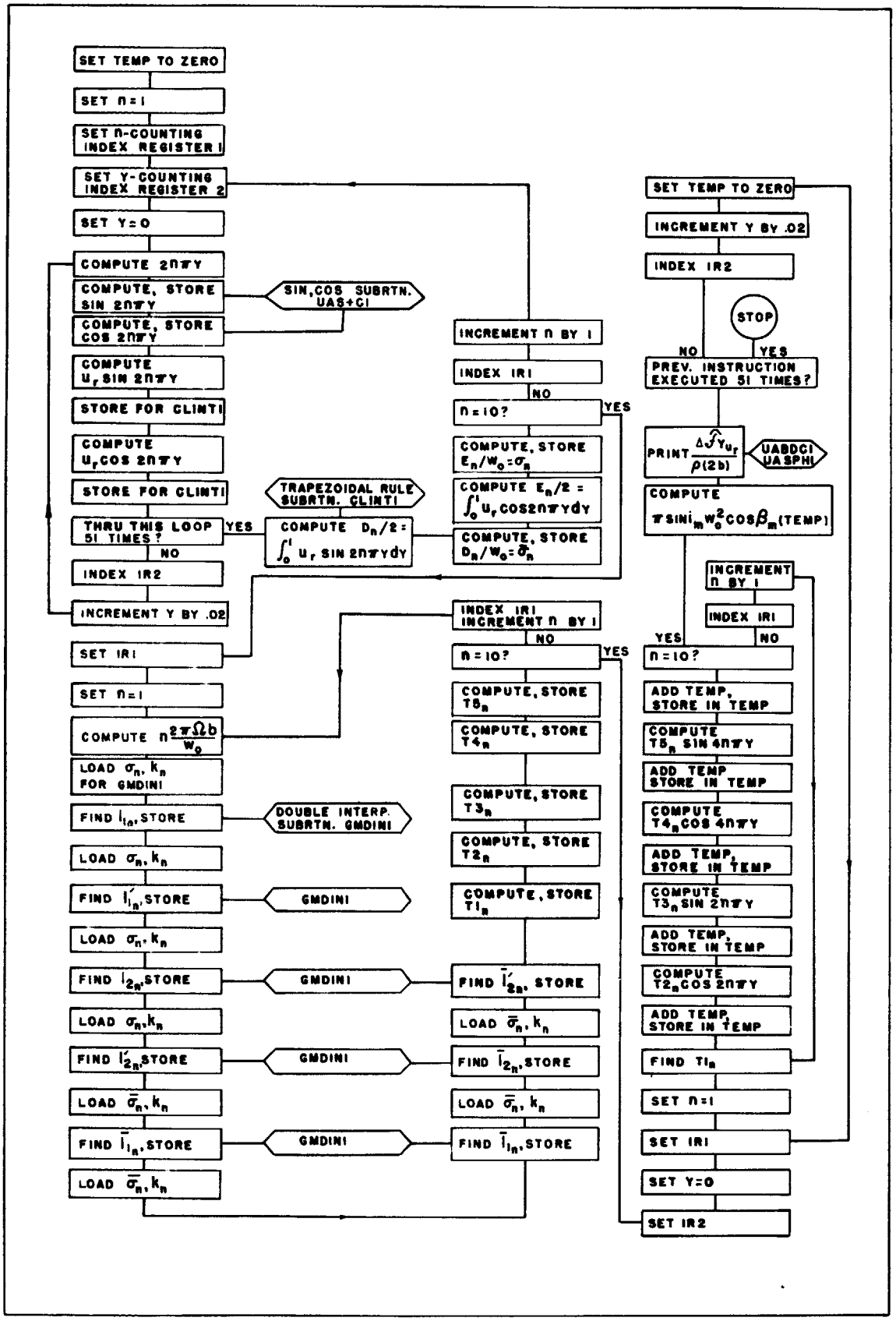

FIG.23 BLOCK DIAGRAM, ISAACS FORCE COMPUTATION

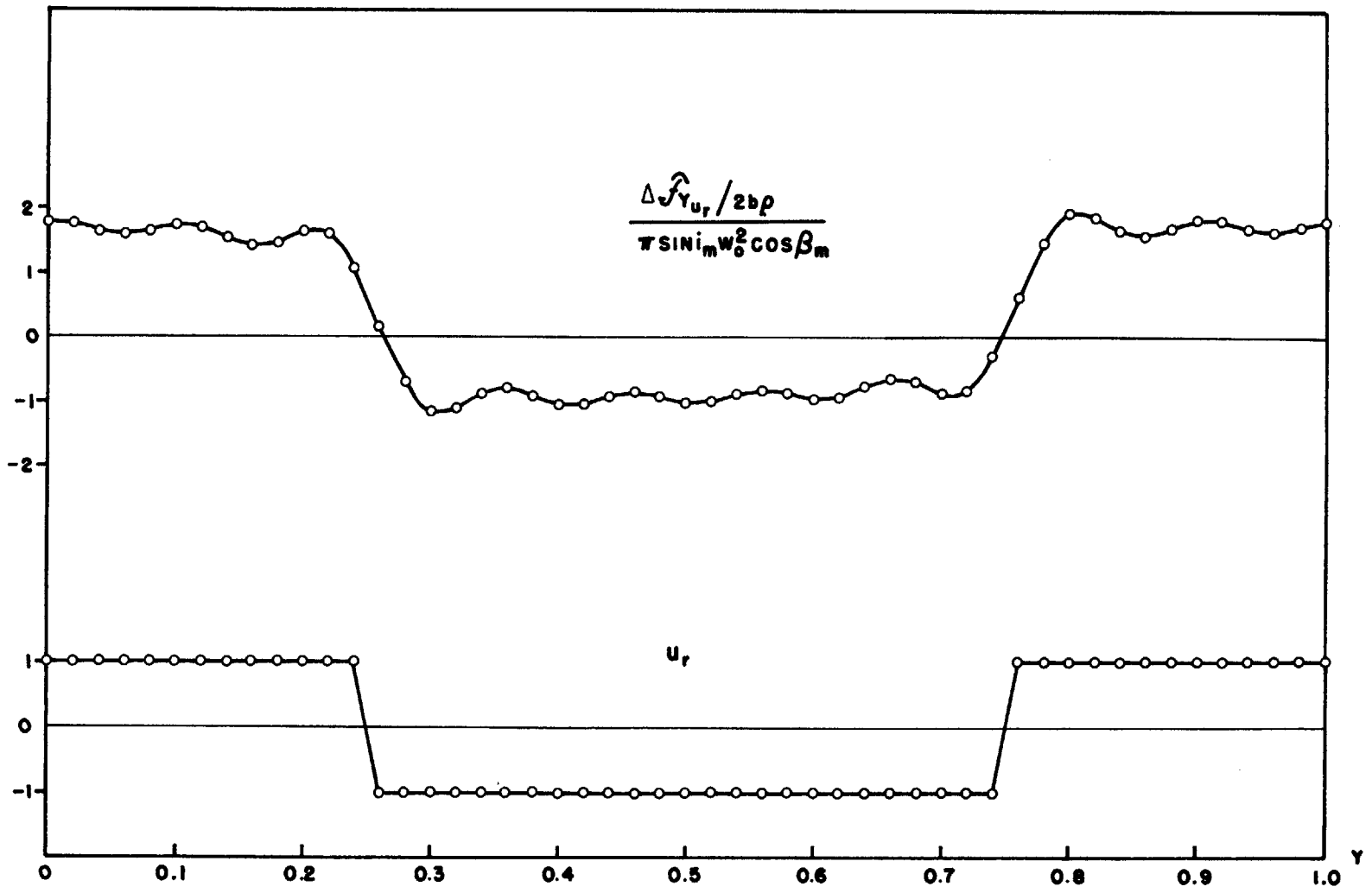

FIG.24 TEST SOLUTION, ISAACS FORCE COMPUTATION; $2\pi\Omega b/w_0 = 0.2$, $2/W_0 = \sqrt{2}$, $\pi \sin i_m w_0^2 \cos\beta_m = 1.0$

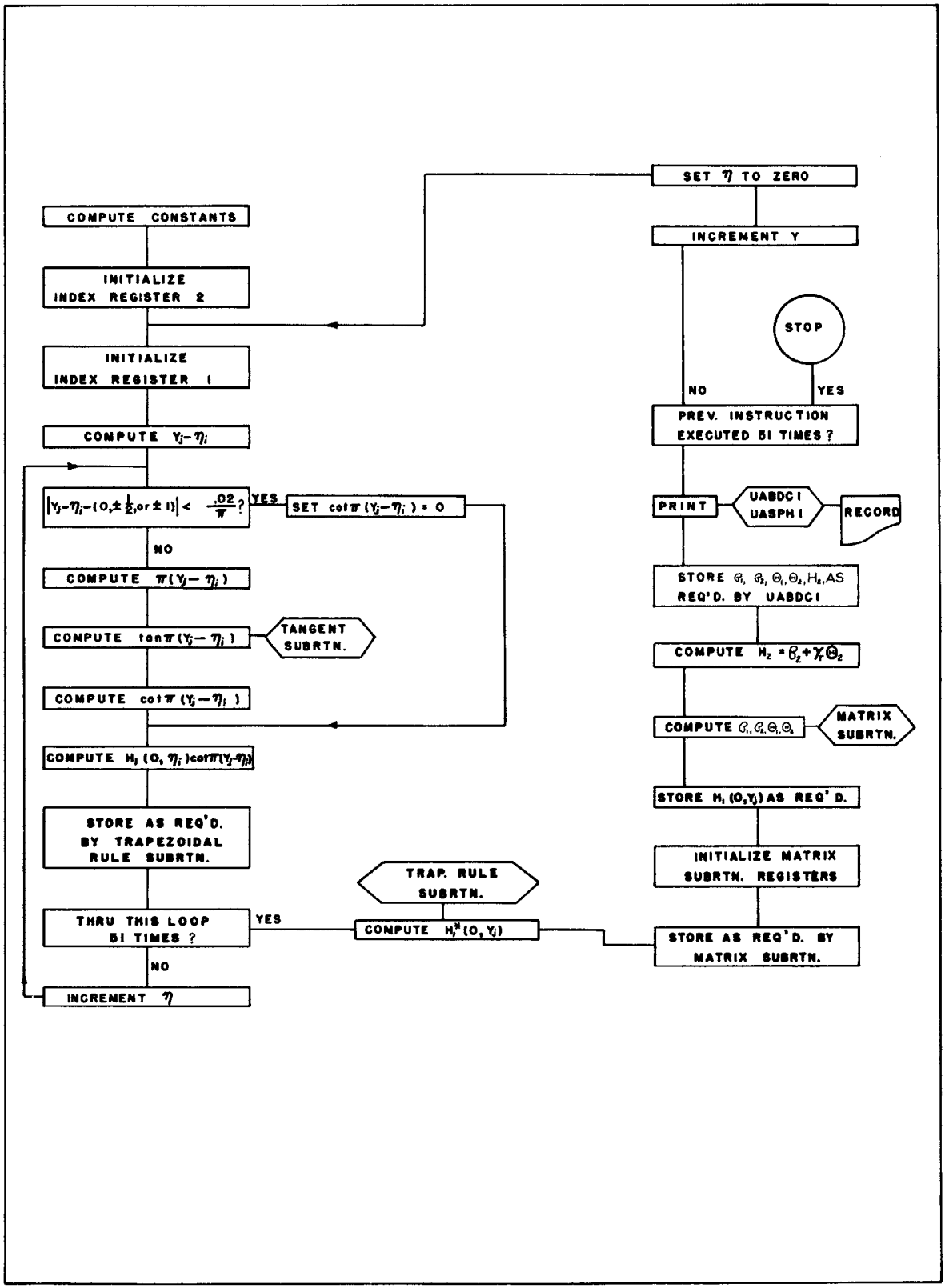

FIG. 25 BLOCK DIAGRAM OF THE COMPUTATION, THEORY OF RANNIE-MARBLE

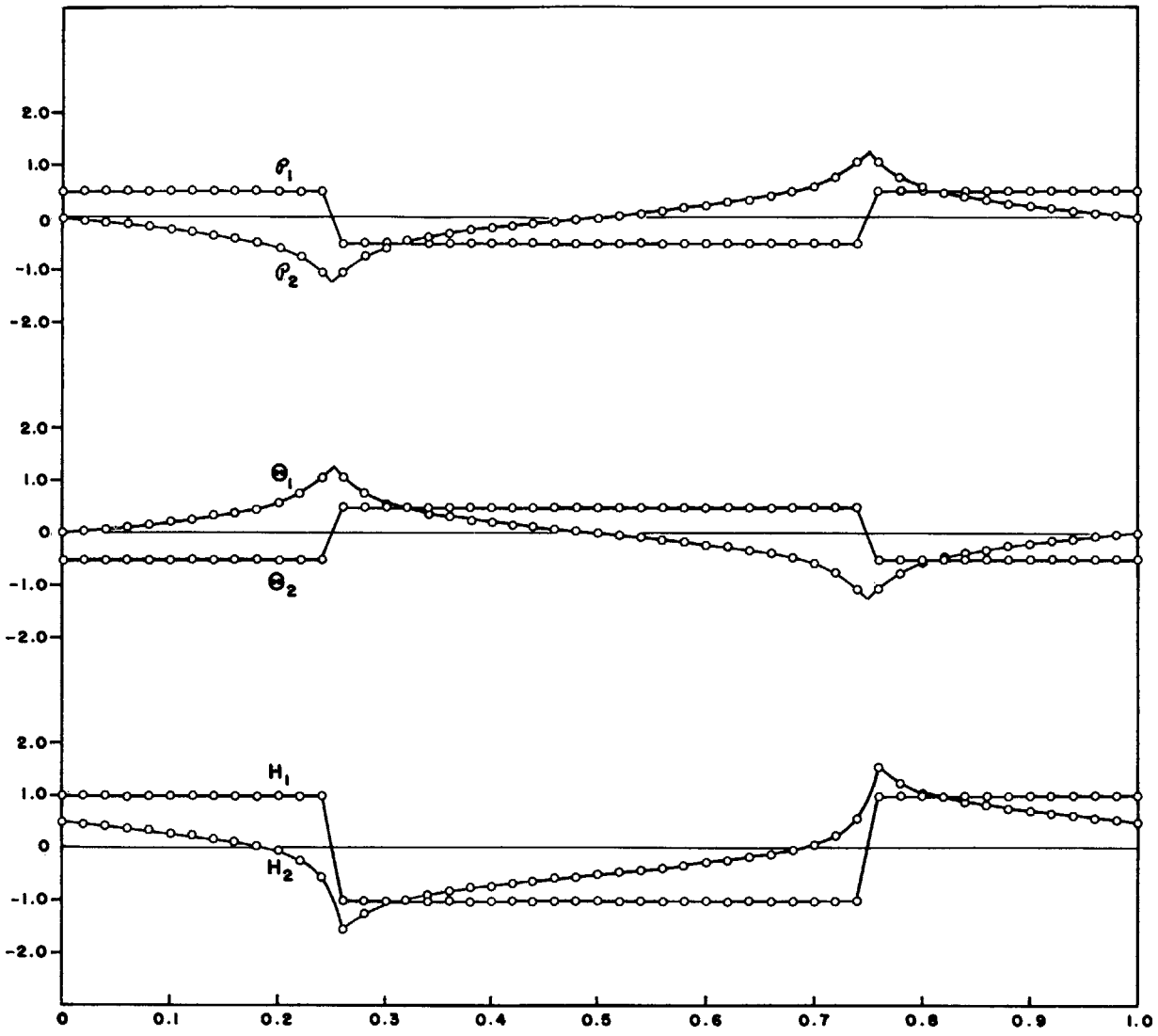

FIG. 26 TEST SOLUTION, THEORY OF RANNIE-MARBLE. SQUARE WAVE INLET DISTORTION, FREE WHEELING ROTOR. $U = \Omega r = 1$, $V_1 = V_2 = 0$.
NOTE THAT $\rho_{-\infty} = \rho_{+\infty} \equiv 0$, $\Theta_{-\infty} = \Theta_{+\infty} \equiv 0$, $H_{-\infty} = H_1$, $H_{+\infty} = H_2$